THE GLIDING FEDERATION OF AUSTRALIA INC

C4/1-13 THE GATEWAY, BROADMEADOWS, VIC 3047

PHONE +61 (0) 3 9359 1613, FAX +61 (0) 3 9359 9865. ABN: 82 433 264 489

PA-25 PAWNEE FRONT SPAR STRESS ANALYSIS AIRW-D0026

TABLE OF CONTENTS

REV	DEVELOPED BY:	REVIEWED BY:	COMPLIANCE VERIFICATION BY:	APPROVED BY:
1	A.C. Smith 6 Sep 2025			

1. REFERENCES

1.1 Pawnee C Operators Handbook, Piper Aircraft Corporation

1.2 Wing and Lift Truss Loads and Analysis, Piper Aircraft Corporation

1.3 Airplane Flight Manual Model PA-25-235, 12 Oct 1962

1.4 Department of Transport, Federal Aviation Administration, Type Certificate Data Sheet 2A8 Revision 23, 14 July 2021

1.5 Software: AeroFoil Version 4.0 https://aerofoilengineering.com/

1.6 Excel Spreadsheet *"Pawnee Shear and Bending Calculator 5_05 Piper.xlsx"*

1.7 Civil Air Regulations Part 3 – Airplane Airworthiness; Normal, Utility and Acrobatic Categories, 15 May 1956

1.8 Excel Spreadsheet "*Vortex Lattice.xlsx*"

1.9 NACA TN 219 "*The Comparison of Well-known and New Wing Sections Tested in the Variable Density Wind Tunnel"* May 1925

1.10 MIL-C-5651D Cord, Elastic, Exerciser and Shock Absorber, For Aeronautical Use, 2 March 1977

1.11 NACA Report 663, Wind Tunnel Investigation of an NACA 23012 Airfoil with Various Arrangements of Slotted Flaps

1.12 Excel Spreadsheet *"Pawnee Shear and Bending Calculator 5_0 - Landing.xlsx"*

1.13 Excel Spreadsheet *"Pawnee Shear and Bending Calculator 5_0 - Taxi.xlsx"*

1.14 TN-250401 Pawnee Spar Bending, P. Brooks

2. INTRODUCTION

2.1 The Piper PA-25 Pawnee was first designed in the early 1950's as an agricultural aircraft. Prior to this most agricultural aircraft were converted from existing civil or military designs. Several versions of the Pawnee were made which increased engine power in later models.

2.2 The aircraft was popular with crop dusting / spraying operators in Australia in the 1960s and 1970s. The type was largely replaced in agricultural work in the 1980s by the larger and more powerful Air Tractor.

2.3 Pawnees became increasingly popular as aerotow aircraft at gliding clubs in the mid 1980's as they became available in the second-hand aircraft market. Without the agricultural equipment or weight of fertiliser / pesticide, the type has an excellent power to weight ratio which results in a very good climb rate whilst towing a glider. It is highly suitable for operations off unsealed airstrips and paddocks.

2.4 Piper ceased production of the Pawnee in 1981. On 15 April 1988, Piper Aircraft sold the design to Latino Americana de Aviación S.A (Lavia SA) in Argentina. This resulted in Lavia SA being the Type Certificate Holder and responsible for maintaining the ongoing airworthiness of the type

2.5 The Airworthiness regulator of Argentina (ANAC) issued Airworthiness Directive 2024-05-01 for the Piper PA-25 Pawnee. This Airworthiness Directive requires inspections for corrosion and cracking in the spars.

2.6 This report investigates the stresses of the front spar during agricultural and aerotow operations for several configurations including two seat Pawnees and Pawnees with fuel tanks fitted in the wings. The Excel spreadsheet at Reference 1.6 was created to calculate the shear and bending of the front and rear spars. This report details how the spreadsheet calculates the stresses for the upper and lower spar caps of the front and rear spars respectively.

3. AIRCRAFT PARAMETERS

3.1 The parameters are at Table 3-1 below:

Parameter	Value	Source
Wing Span	434 in	Reference 1.1
Wing Area	183 ft^2	Reference 1.1
Root Chord	63 in	Reference 1.1
Aspect Ratio AR	7.161	Calculated
Dihedral	7 degrees	Reference 1.1
Empty Weight	1521 lb	Reference 1.1
Fuel Capacity	38 gal (231.4 lb)	Reference 1.1
Pilot Weight	100 kg (220.5 lb)	Assumed
Max Take Off Weight	2900 lb	Reference 1.1
Max Manoeuvre Speed V_A	108 kts	Reference 1.3
Never Exceed Speed V_{NE}	135 kts	Reference 1.3
Design Speed V_D	150 kts	Calculated from V_{NE}

Table 3-1 Aircraft Parameters

3.2 **Wing Washout:** Reference 1.1 provides a wing rigging angle for the rib outboard of the aileron only. It does not provide a rigging angle for the wing root. Page II-3a of Reference1.2 shows that the original washout was 3 degrees, but this was amended to 2.5 degrees.

3.3 **Airfoil:** The coordinate system for the USA35B airfoil is slightly unusual in that the trailing edge is not at the 1,0 co-ordinate. This results in the airfoil having an effective 1.5 degree angle of attack with the airfoil reference plane at zero angle of attack.

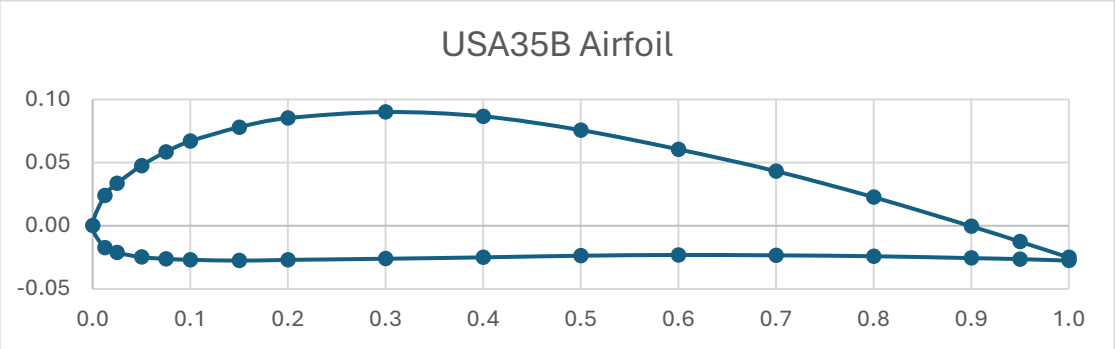

Figure 3-1 Airfoil Co-ordinates

The rigging angle for the rib outboard of the aileron is specified in Reference 1.1. A 30 inch level is placed on the underside of the rib outboard of the aileron with a 0.25 inch space at the front spar. This results in an additional 1 degree of incidence of the airfoil reference plane at that wing position with the fuselage level.

4. DESIGN REQUIREMENTS

4.1 Reference 1.4 states the Piper PA-25 Pawnee was designed to meet the airworthiness requirements of Reference1.7.

4.2 **Manoeuvring Load Factor:** Section 3.186 of Reference1.7 gives the positive limit load factor as:

$$n = 2.1 + \frac{24{,}000}{W + 10{,}000}$$
$$= 3.96$$

With the exception that n need not be greater than 3.8 and shall not be less than 2.5.

Reference 1.3 gives: Maximum positive load factor n = 3.8, and Maximum negative load factor n = 0.

Section 3.186 of Reference1.7 gives the positive limit load factor as "not less than -0.4 times the positive load factor". This gives -0.4 x 3.8 = -1.52.

However, Reference 1.2 defines "Cond E" as n = -1.48.

The following will be used:

Maximum positive load factor n = 3.8,

Maximum negative load factor n = -1.48.

4.3 **Gust Load Factor:** Section 3.188 of Reference1.7 gives the gust load factors as:

$$n = 1 + \frac{\mathrm{KUVm}}{575(W/S)}$$

Where $\mathrm{K} = \frac{1}{2}(W/S)^{1/4}$

For operations at maximum take-off weight:

$$\mathrm{K} = \frac{1}{2}\left(2900/183\right)^{1/4}$$
$$= 0.9976$$

The lift curve slope m is estimated by:

$$m = \frac{a_0}{\left(1 + \frac{a_0}{\pi AR}\right)}$$
$$= 4.9114\ per\ rad = 0.08572\ per\ deg$$

For Max Manoeuvre Speed V_A = 108 kts = 182.3 ft/sec and Gust U = 30 ft/sec:

$$n = 1 \pm \frac{0.9976 \times 30 \times 182.3 \times 4.9114}{575(2900/183)}$$

$$= 1 \pm 2.940$$

For Design Speed V_D = 150 kts = 253.17 ft/sec and Gust U = 15 ft/sec:

$$n = 1 \pm \frac{0.9976 \times 15 \times 253.17 \times 4.9114}{575(2900/183)}$$

$$= 1 \pm 2.042$$

4.4 **Flight Envelope:** The flight envelope is shown below at Figure 4-1. The negative $C_{L\ Max}$ of the wing is estimated to be -0.52.

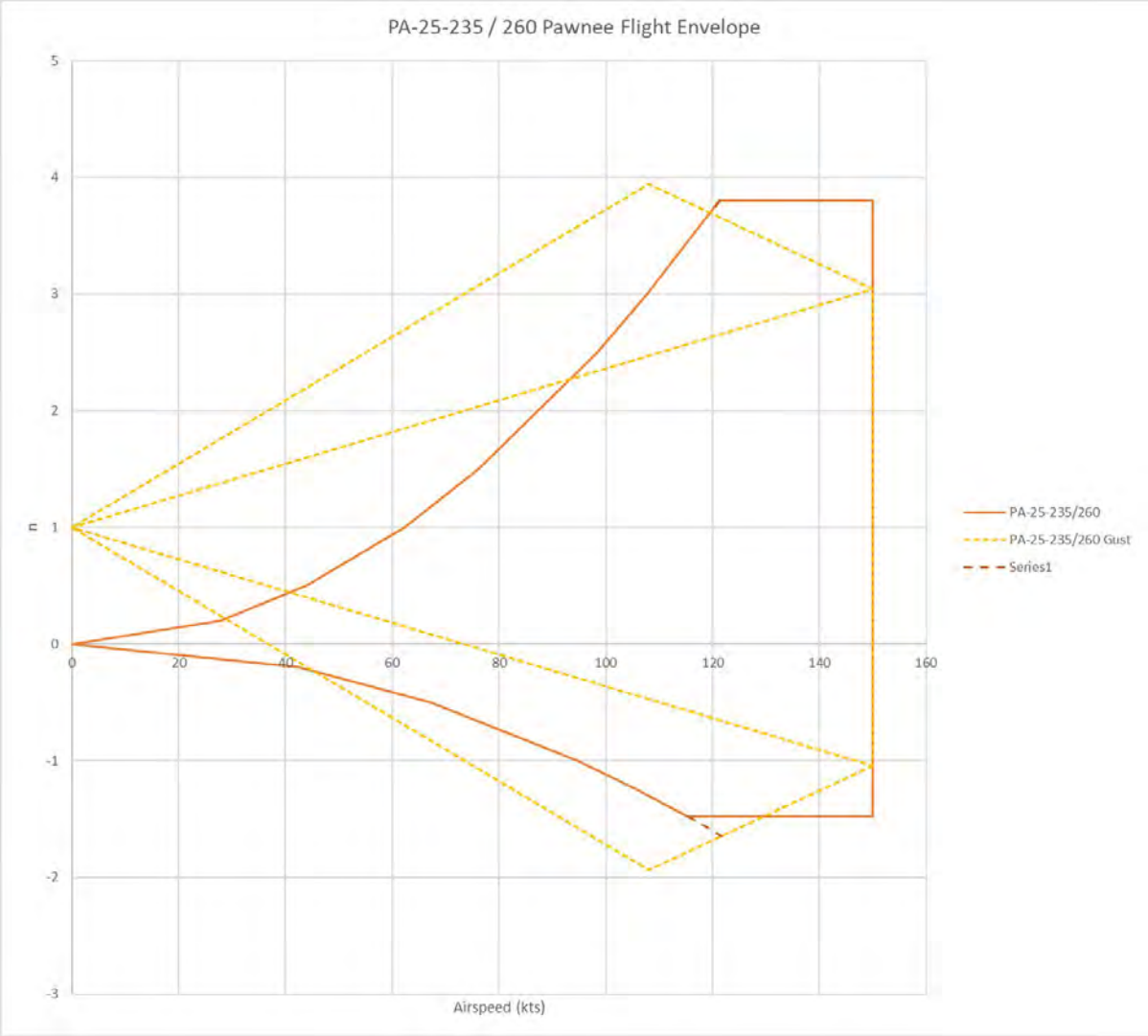

Figure 4-1 Flight Envelope for PA-25-235 and PA-25-260 at 2900 lb

5. FRONT AND REAR SPAR LOAD DISTRIBUTION

5.1 **Lift and Pitching Moment:** The ribs were modelled as a beam with two simple supports at the front and rear spars respectively. The front spar is 9 inches aft of the leading edge at 14.3% chord. The rear spar is 40 inches aft of the leading edge at 63.5% chord. The air loads are applied at 25% chord.

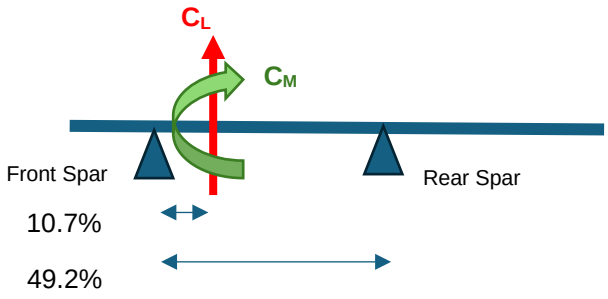

Figure 5-1 Air Loads Relative to Spar Locations

The rear spar load from lift is given by:

$$Spar_{rear} = \frac{L \times 0.107}{.492} = 21.75\%$$

The front spar load from lift is given by

$$Spar_{front} = 1 - 0.2175 = 78.25\%$$

Page II-34 of Reference 1.2 used 20.5% for the rear spar and 79.5 % for the front spar based on loads around the aerodynamic centre.

The pitching moment is reacted out equally between the front and rear spars.

5.2 The front spar and rear spar lift percentages are set at cells B83 and B84 respectively.

5.3 **Drag:** Drag loads produce a moment which is reacted out as a couple between the front and rear spars via internal bracing wires. Drag produces a tension in the front spar and a compression in the rear spar. Similar to the pitching moment, the drag moment is reacted equally between the front and rear spar.

5.4 At high angles of attack, the lift load vector is rotated and starts to produce a thrust component relative to the airfoil reference line. This counters the drag and produces a compression in the front spar and a tension in the rear spar. Similar to the drag moment, the thrust moment from lift is reacted equally between the front and rear spar. The methodology is described at Section 6.59 below.

6. LOAD CALCULATION METHOD

6.1 Reference 1.6 utilises data from worksheet 'Input' in Rows 2 to 23. These inputs are then used to calculate the loads and stress in worksheet 'Rigid Wing'.

6.2 **Aspect Ratio:** The aircraft wing span and wing area are at Cells B2 and B3 respectively from Reference 1.1. This is used to calculate the average chord at Cell B4 and the aspect ratio at Cell B6.

6.3 **Mean Aerodynamic Chord.** The mean aerodynamic chord is estimated at 'Rigid Wing' cell AN8. This result is divided by 12 at 'Input' Cell B5 to give the result in feet.

6.4 **Lift Curve Slope:** The lift curve slope corrected for aspect ratio is calculated at Cell B7. This assumes an ideal lift curve slope of 0.109662 per degree and uses the aspect ratio calculated at Cell B6.

$$m = \frac{a_0}{\left(1 + \frac{a_0}{\pi AR}\right)}$$

$$= 4.9114\ per\ rad = 0.08572\ per\ deg$$

6.5 **Tail Arm:** The distance between the wing and tail ¼ chord positions is estimated to be 194.0 in. This is entered at Cell B9. It is subsequently used to calculate the tail load to balance the aircraft in flight.

6.6 **Wing ¼ Chord from Datum:** The datum is defined as 78 inches forward of the wing leading edge at page 2 of Reference 1.3. The Mean Aerodynamic Chord (MAC) is from Cell B5. The wing ¼ chord position is calculated as 78 + 0.25 x MAC at Cell B10.

6.7 **Fuel:** The fuel volume in gallons is entered at Cell I2. Cell K2 allows the weight of the fuel to be included in wing tanks if fitted. If 'N' is selected, the fuel is part of the fuselage weight.

6.8 If 'Y' is selected at Cell J2, the weight of the fuel is calculated at 'Rigid Wing' Cells AA32 to AE32. This is done by assuming the wing tanks is a rectangle inclined at the dihedral of the wing. The mass in each section of wing fuel tank is estimated in Sheet 'Wing Tank Fuel Level'.

6.9 **Empty Weight:** The empty weight is entered at Cell I5. This is assumed to be 1531 lb from Reference1.1. The actual empty weight can be entered for an individual aircraft if required.

6.10 **Pilot Weight:** The pilot weight is entered at Cell I6. Reference 1.7 does not specify a maximum design weight for restraint of the pilot and refers to the use of cockpit placards to specify maximum pilot weight. Reference 1.7 specifies a value of 170 lb (77 kg) for calculating the CG position. 170 lbs (77 kg) is also used in Reference 1.3 for calculating the CG position but does not specify a maximum pilot weight. For the purposes of calculations, a maximum pilot weight of 242.6 lb (110 kg) is assumed.

6.11 **Payload Weight:** The payload weight is entered in Cell I7 and is assumed to be in the fuselage hopper. The maximum payload allowed in the hopper is 1200 lb.

6.12 **Aircraft Centre of Gravity:** The spreadsheet assumes that the aircraft is operating at the forward CG limit as the additional load from the tail to balance the aircraft in flight produces the highest wing loads. Reference 1.2 does not show the inclusion of tail loads in calculating the wing lift. As a result, the results from Reference 1.6 will be slightly higher than those calculated by Piper.

6.13 The centre of gravity envelope from Reference 1.3 is shown on worksheet 'CG Range'. The forward CG limit for the weight of the aircraft is calculated at 'Input' Cell I14. The CG position relative to the ¼ chord is calculated at 'Input' Cell B11.

6.14 **Tail Load:** The tail load is calculated from the sum of the moment of the aircraft weight around the ¼ chord and the aircraft pitching moment calculated at Cell AK44. The total moment is then divided by the tail arm from Cell B9 to give the required tail down force to balance the aircraft. This process is iterative as the tail load increases the required lift from the wing which alters the pitching moment. Excel requires iteration to be enabled in the menu File => Options => Formulas => Enable Iterative Calculations.

6.15 **Lift Coefficient:** The aircraft lift coefficient C_L is calculated at Cell B16. This adds the tail load from Cell I19 onto the aircraft weight from Cell I8 times the total g load from Cell B23. This total is then divided by the dynamic pressure times the wing area.

6.16 **Aircraft AoA Zero Lift:** The angle of attack relative to the fuselage level line at which the wing produces zero lift is calculated at Cell B17. It is the sum of the angle for zero lift from the washout from paragraph 6.25, the zero lift angle of the airfoil from Sheet "USA35B Airfoil" and the incidence angle from the rigging from paragraph 3.2. Note that the Sheet "USA35B Airfoil" rotated the airfoil co-ordinates by 1.5 degrees so that the trailing edge was at the 1,0 co-ordinate.

6.17 **Aircraft AoA:** The aircraft AoA is estimated at Cell B18 using the calculated C_L, lift curve slope and zero lift angle.

6.18 **Gust Loads:** The gust speed (if required) is input at Cell B21. The response is calculated at Cell B22 using the equations from Section 4.3 above. Typically, the nominal g at Cell B20 is set to 1g and the gust speed entered at Cell B21. The total g is at Cell B23.

6.19 **Flight Loads:** The flight loads are calculated at worksheet 'Rigid Wing'. The calculation of flight loads uses a panel method where the wing is divided into chordwise strips (panels). The panel edges were selected to align with the major ribs of the wing. Some panel edges were positioned to align with key structural features such as the wing strut attachment. The use of zero width panels was for areas where point loads were used. This is similar to the methodology employed in Reference 1.2.

6.20 The panels are shown at 'Rigid Wing' Rows 4 and 5. Row 4 shows the panel start position. Row 5 shows the panel centroid position.

6.21 **Panel Chord:** The panel chord is calculated at 'Rigid Wing' Row 6 for the centre of the panel. The wingtip is assumed to be slightly elliptical with an eccentricity of 1.175 based on chord data from page II-5 of Reference 1.2. Cells AE6 to AL6 calculate the chord for an elliptical tip at the panel centre.

6.22 **Panel Area:** The surface area of the panel is calculated at 'Rigid Wing' Row 7 using the panel chord and width. This is estimated as the chord from Row 6 times the panel width. This overestimates the area of the elliptical wingtip by a small amount.

6.23 **Wing Area:** The total wing area is calculated at 'Rigid Wing' Cell AN7 by doubling the sum of cells C7 to AL7. This produced a total of 183.05 ft^2 compared to the published value of 183 ft^2. This is most likely due to the estimation of the area of the panels at the elliptical wingtips. The wing area from Cell AN7 was used throughout the spreadsheet to maintain consistency.

6.24 **Lift Loads:** Lift loads were separated into lift due to the wing washout and lift due to the wing planform (additional lift).

6.25 Wing lift due to washout was calculated using a vortex lattice program encoded in an Excel spreadsheet at Reference 1.8. This produced a spanwise lift distribution with a zero lift angle of attack of -1.31 degrees as shown in Figure 6-1 below.

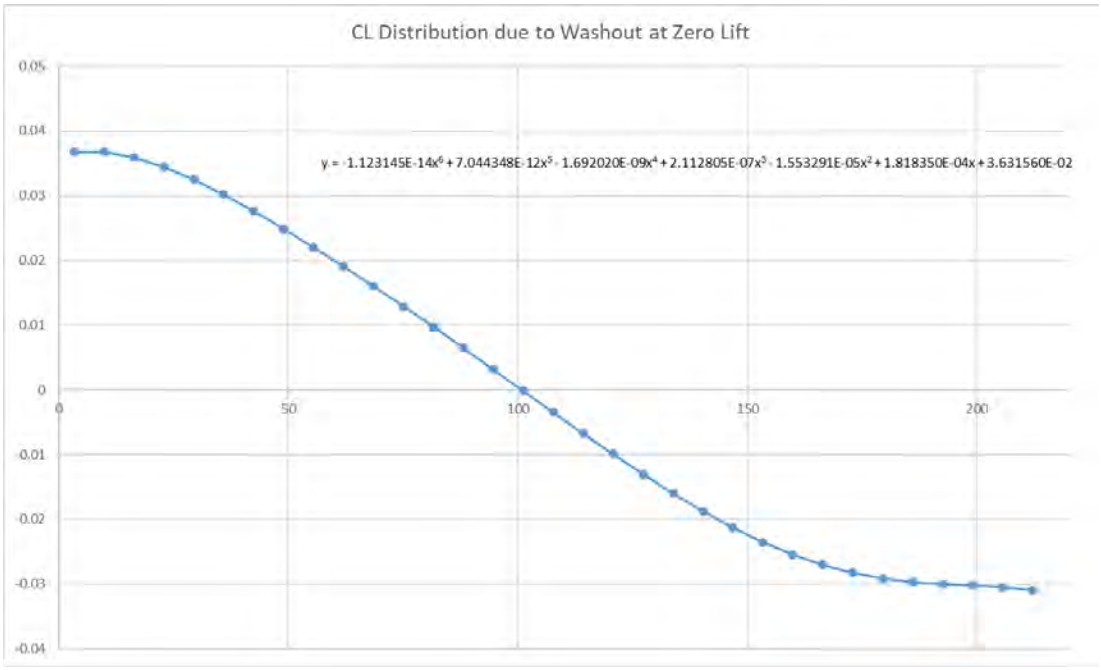

Figure 6-1 C_L Distribution at Zero Lift

6.26 A polynomial curve fit was used in order to calculate the local lift coefficient at zero lift for the midspan of each panel. The curve fit is shown on worksheet titled 'Vortex Lift Dist'. The wing local incidence is shown on worksheet 'Rigid Wing' at Row 13. Row 14 calculates the C_L at zero lift at the panel centroid using the curve fit.

6.27 Wing lift due to the planform (additional lift) was also calculated using the vortex lattice program at Reference 1.8 without washout applied. The angle of attack was adjusted until the average lift coefficient was 1.0. A polynomial curve fit was used in order to calculate the local lift coefficient at the midspan of each panel. The curve fit is shown below at Figure 6-2 and at worksheet titled 'Vortex Lift Dist'.

6.28 Also shown in Figure 6-2 is the C_L distribution used by Piper at Reference 1.2 for comparison. Reference 1.2 does not state how the C_L distribution was generated. In general, the vortex lattice is similar to the distribution by used Piper with the exception of the elliptical wingtip region. The Piper result gives increased bending at the outer wing which increases the load on the strut and the tension in the wing from the strut to the root. The Piper result produces reduced bending at the inner wing between the strut to the root.

6.29 The verification of the spreadsheet carried out at Reference 1.14 shows that the wing outboard of the strut assembly is not torsionally stiff. At higher aerodynamic loads the wingtip will twist nose up and increase the angle of attack. This would result in greater wing tip lift, but a small reduction in the lift inboard to compensate. It is possible that Piper included some consideration of the outer wing flexibility in their C_L distribution.

6.30 The Piper CL distribution was used in Reference 1.6 to maintain consistency with the certification of the aircraft.

6.31 The planform C_L for an overall wing C_L =1 for each panel is shown at 'Rigid Wing' Row 10 calculated from the curve fit from the Pipier distribution. Row 11 multiplies the local C_L by the panel area. Cell AN11 is double the sum of cells C11 to AL11, divided by the wing area at Cell AN7 giving the overall wing C_L. Cell AN11 should be very close to 1. This is a check for reasonable accuracy of the curve fit.

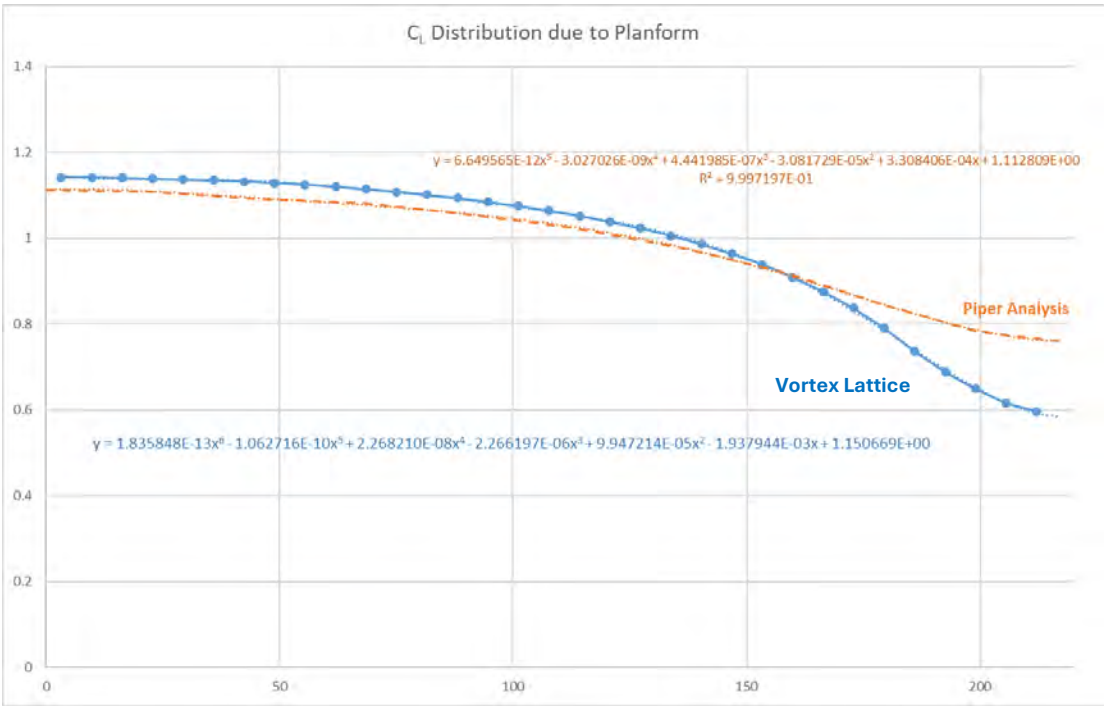

Figure 6-2 C_L Distribution Due to Planform for C_L =1.0

6.32 The effects of propwash over the inboard section of the wing or the effects of the fuselage was not considered.

6.33 The aircraft C_L is calculated for the aircrafts weight, g load, speed and tail load at 'Input' B16. For the 'Rigid Wing' worksheet, the spreadsheet multiplies the panel lift due to planform (additional lift) by the calculated aircraft C_L and adds the panel zero lift distribution at Row 14 to give the total panel C_L at Row 16.

6.34 Row 17 multiplies the C_L from Row 16 by the dynamic pressure and the panel area to give the lift from each panel. Row 18 calculates the lift applied to the wing normal to the dihedral by dividing the lift at Row 17 by the Cosine of the dihedral angle.

6.35 **Pitching Moment**: The airfoil pitching moment coefficient C_M was derived from Reference 1.5. As calculating pitching moment using panel methods is notoriously problematic, the pitching moment results were adjusted to match the value of -0.076 at zero lift to match Reference 1.2. The value at Reference 1.2 is about the aerodynamic centre. However, the calculated aerodynamic centre from Reference 1.5 is extremely close to the ¼ chord. This is to be expected as many of the early airfoils were deliberately designed around having an aerodynamic centre at the ¼ chord and having a relatively constant pitching moment coefficient across a wide angle of attack range. Reference 1.2 uses a constant value of the pitching moment coefficient regardless of the angle of attack.

6.36 Pitching moments are notoriously difficult to calculate from computer modelling and wind tunnel data is often required. There is no available wind tunnel data for the USA35B airfoil. Reference 1.9 gives wind tunnel data for a low aspect ratio wing using the USA35B airfoil. This agrees with the zero-lift pitching moment from Reference 1.2. However, as the angle of attack increases, the effects of the wing tip vortex become apparent.

6.37 A polynomial curve was fitted to the adjusted data from Reference 1.5 as shown in Figure 6-3 below. The spreadsheet calculates the local pitching moment from the lift coefficient of the panel at 'Rigid Wing' Row 20.

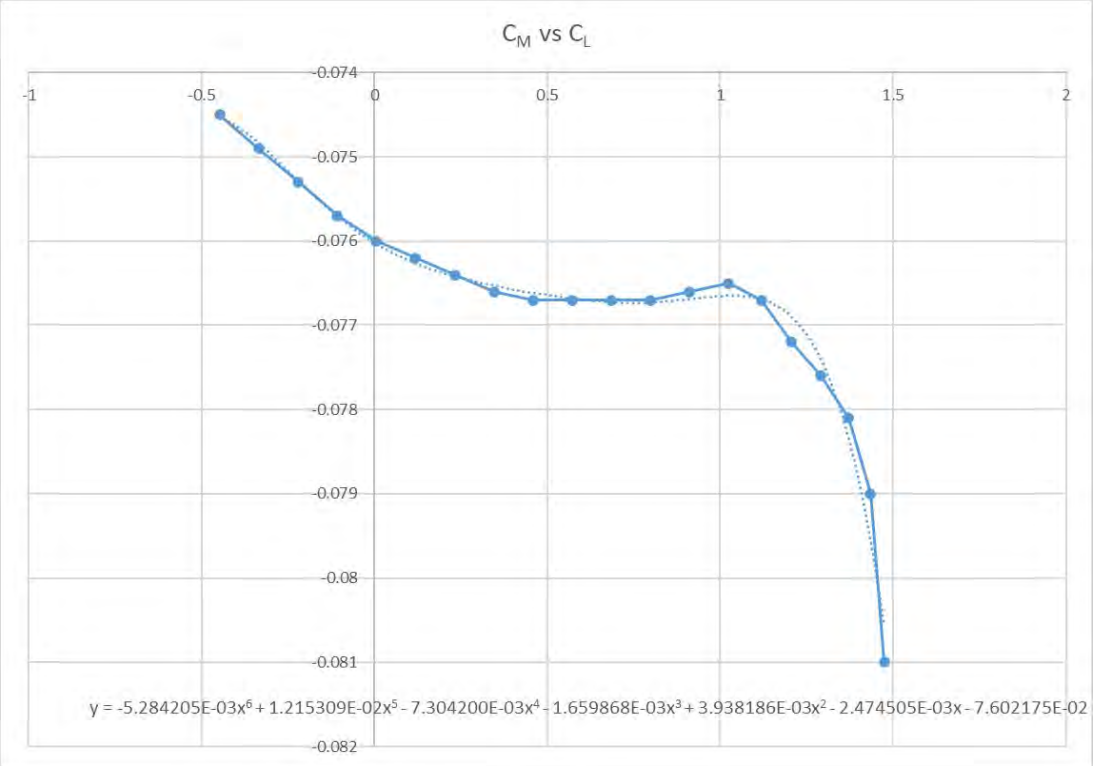

Figure 6-3 Pitching Moment versus Lift Coefficient

6.38 **Drag Coefficient**: The airfoil drag coefficient C_D was derived from Reference 1.5. A polynomial curve was fitted to the data on the 'USA35B Airfoil' worksheet as shown below in Figure 6-4. The spreadsheet calculates the panel drag coefficient from the panel lift coefficient of the panel using the curve fit at 'Rigid Wing' Row 24.

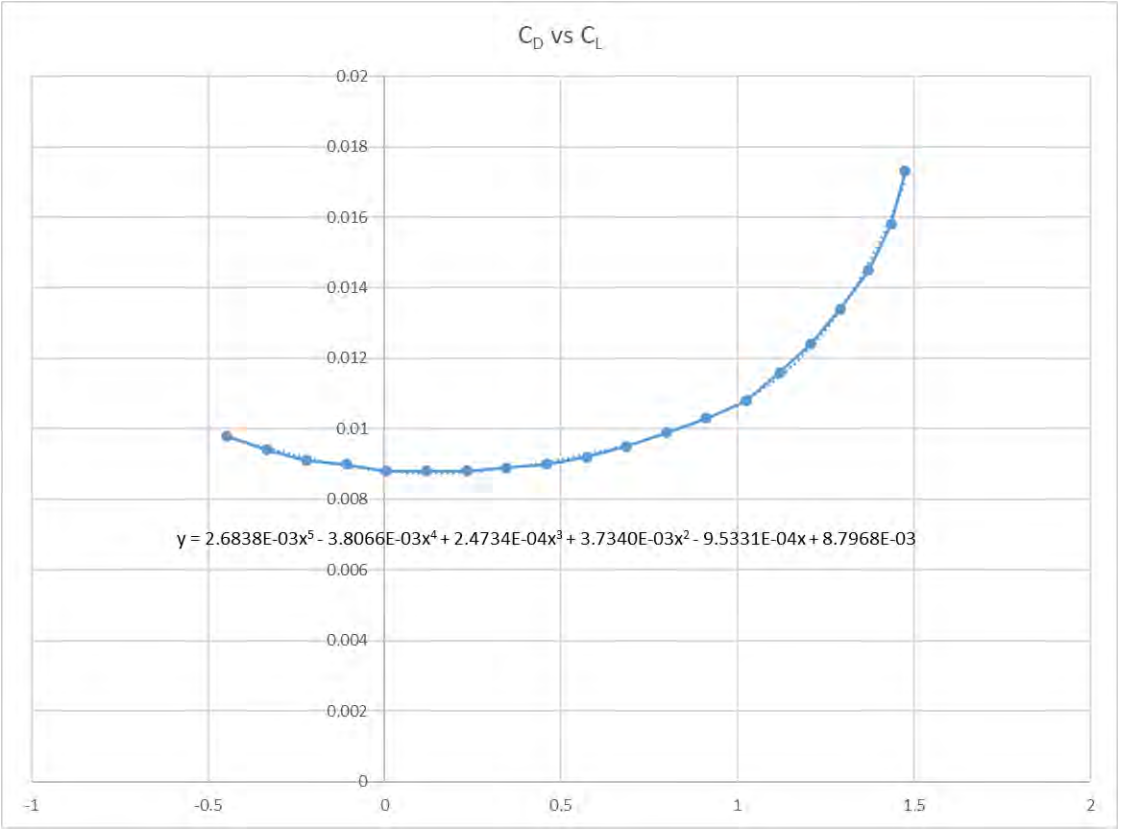

Figure 6-4 Drag Coefficient versus Lift Coefficient

6.39 'Rigid Wing' Row 25 multiplies the panel C_D by the panel area. Cell AN25 is double the sum of cells C25 to AL25, divided by the total wing area giving the overall wing drag co-efficient C_D.

6.40 **Induced Drag Distribution:** Induced drag was separated into induced drag at zero lift due to the wing washout and induced drag due to the wing planform (additional lift).

6.41 Induced drag due to washout was calculated using a vortex lattice program at Reference 1.8. This produced a spanwise induced drag distribution for the zero lift angle of attack of -1.31 degrees. A polynomial curve was fitted to the data on the 'USA35B Airfoil' worksheet as shown below in Figure 6-5.

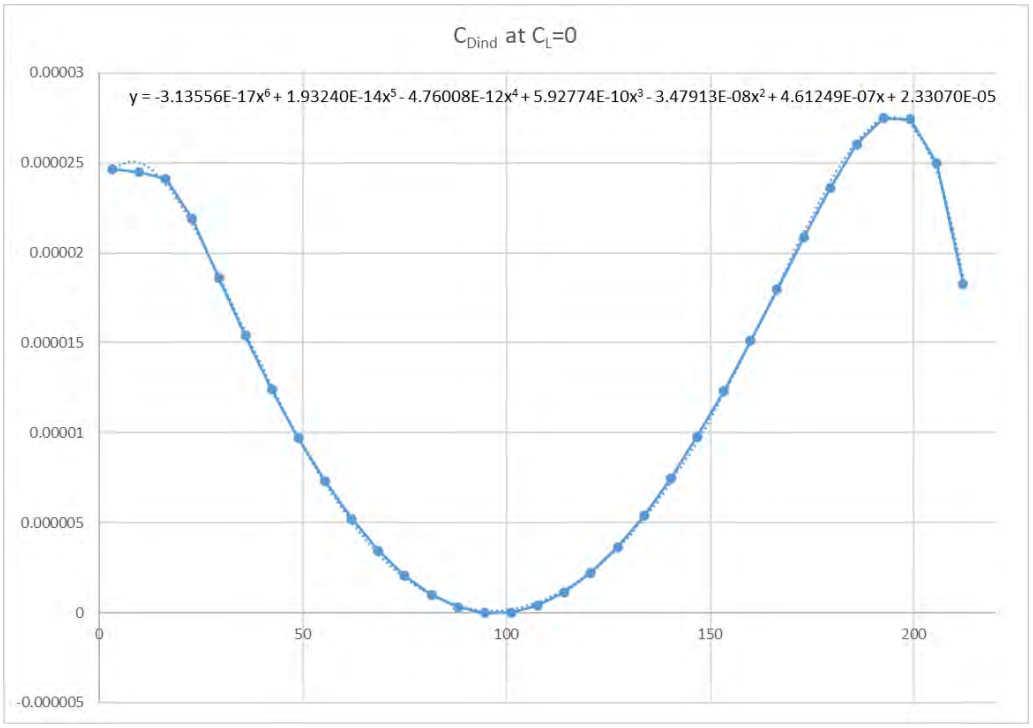

Figure 6-5 Induced Drag Co-efficient at Zero Lift

This induced drag distribution is by percentage span of the wing. At 'Rigid Wing' Row 26, the induced drag coefficient is calculated at the spanwise location and multiplied by the width of the panel divided by the wing semi span.

6.42 Induced drag due to planform (additional lift) was calculated using a vortex lattice program at Reference 1.8 for a wing without washout. The angle of attack was adjusted until the average lift coefficient was 1.0. A polynomial curve fit was used in order to calculate the local lift coefficient at the midspan of each panel as shown below at Figure 6-6.

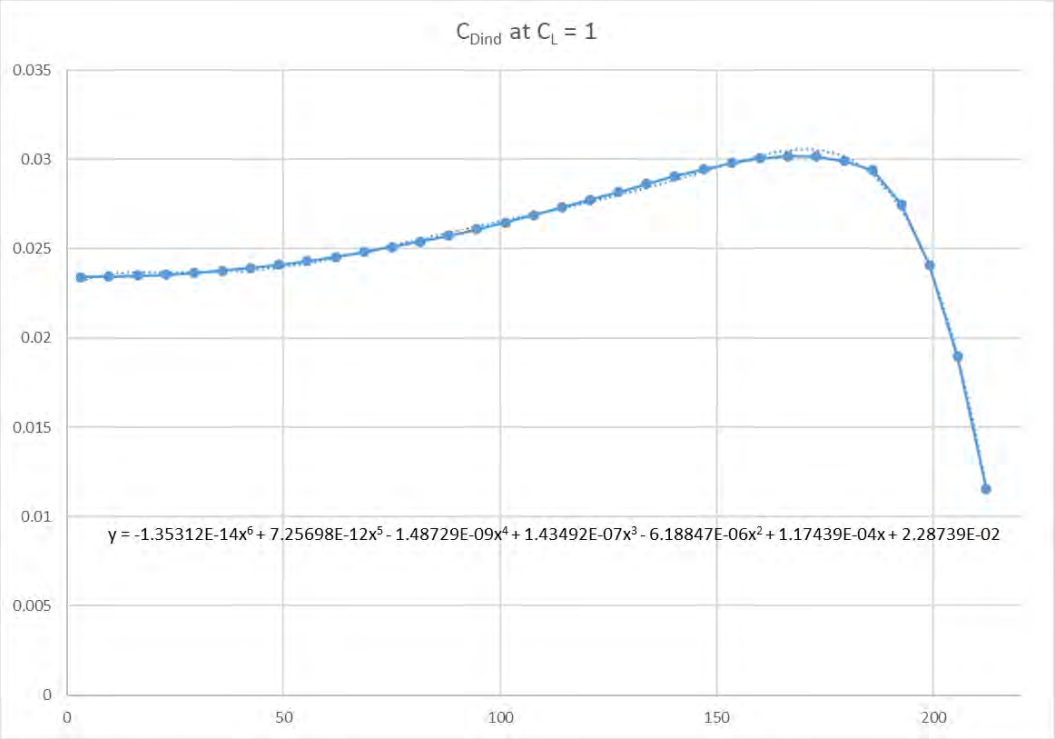

Figure 6-6 Induced Drag Due to Planform

6.43 This induced drag distribution is by percentage span of the wing. At Row 27, the induced drag coefficient is calculated at the spanwise location and multiplied by the square of the wing C_L and the width of the panel divided by the wing semi span. Cell AN27 is double the sum of cells C50 to AG50, giving the overall wing C_{Di}.

6.44 **Strut Drag:** The strut cross section is modelled as a NACA 0036-64 airfoil which has the same thickness to chord ratio of the strut section. Reference 1.5 was used to estimate a drag polar. A polynomial curve fit was applied on the 'Strut' worksheet. This curve fit was then used to estimate the drag coefficient of the strut at the aircraft estimated angle of attack. The strut drag is calculated at Cell B10 on the 'Strut' worksheet.

6.45 Half of the strut drag is assumed to be reacted at the strut connection on the wing and is applied at 'Rigid Wing' Cell X28 in the total drag calculation (below). The other half of the drag is assumed to be reacted at the fuselage connection.

6.46 **Total Drag:** The total drag for the panel is calculated at 'Rigid Wing' Row 28. This is then rotated into forces that are normal to the wing chord and parallel to the wing chord. The drag normal to the wing reference line is calculated at Row 29 by multiplying the panel drag by the Sine of the Angle of Attack. The drag parallel to the wing reference line is calculated at Row 30 by multiplying the panel drag by the Cosine of the Angle of Attack.

6.47 **Wing Weight**: The wing spars are a constant section from the root to almost the tip. The ribs are relatively evenly spaced. There is a small amount of additional structure at the strut attachment area consisting of a heavy cross brace between the two struts. For simplicity, the weight of each panel was estimated to be proportional to the area of the panel. This is done at 'Rigid Wing' Row 33. In comparison, Reference 1.2 assumes the wing weight is distributed across the span. Whilst similar, this method will make the wingtips slightly heavier and slightly reduce wing bending.

6.48 A number of wings without struts were weighed. Many of these wings were from wrecked aircraft. Whilst the wings were complete, the traceability was limited.

Wing	Weight	
Wing A	57.0	kg
Wing B	57.7	kg
Wing C	56.2	kg
Wing D	56.1	kg
Wing E	51.9	kg

Table 6-1 Wing Weight Samples

6.49 Aircraft E may have been from a Pawnee A with the lower maximum all up weight of 2,300 lb which may have lighter wing structure. This wing weight was ignored. For the purposes of the calculations, a wing weight of 123.48 lb (56 kg) was used. In comparison, Reference 1.2 used a weight of 39.2 kg (86.5 lb) per wing. This is conservative as the lighter wing weight yields a higher weight of non flying parts which results in a higher wing bending.

6.50 The wing weight is assumed to be distributed with 60% at the front spar and 40% at the rear spar. This is set at 'Rigid Wing' Cells E73 and E74. A large proportion of the wing weight is the spars. Using the cross section area of the spars:

$$Front\ Spar\ \% = \frac{0.7279}{0.7279 + 0.4950} = 59.5\%$$

Reference 1.2 uses a net wing bending moment where the wing weight is subtracted from the lift. Page II-34 of Reference 1.2 uses 79.5% of the net wing moment at the front spar. This effectively assumes 79.5 % of the weight is at the front spar. Given the weight of the flaps and ailerons and the relative weights of the front and rear spars, this is likely to be an inaccurate assumption which gives lower bending on the front spars.

6.51 **Strut Weight:** The struts on the B, C and D models are supported by two jury struts. These jury struts are attached to the front spar. The lift of the struts at the aircraft angle of attack is estimated at Cell B15 on the 'Strut' worksheet. The strut net weight at the g load is calculated at Cell B18.

6.52 The weight of each jury strut is estimated to be 2.0 lb (0.9 kg). This is identical to the assumed weight at Page II-9 of Reference 1.2 with the exception that the Pawnee B, C and D have 2 jury struts per wing whereas the Pawnee A had one jury strut per wing. The jury weight loads are at Row 23. The net weight of the strut per jury strut is estimated to be half of the weight of the length of strut to the next support point. The jury struts are attached to the strut at approximately one third intervals. The respective weight per jury strut are calculated at Row 24 on the 'Strut' worksheet.

6.53 The strut weight for the front and rear spars is at worksheet 'Rigid Wing' Row 40 and Row 43 respectively. These loads are then calculated into vectors that are normal and parallel to the chord respectively.

6.54 **Effect of Dihedral:** The wing lift and weight as calculated is vertical relative to the aircraft. To calculate the wing shear and bending relative to the wing reference plane, the loads must be rotated by the dihedral angle to give vectors normal to the chord and parallel to the chord. The lift normal to the dihedral is calculated by dividing the panel lift by the Cosine of the dihedral angle at 'Rigid Wing' Row 18.

6.55 The wing weight is also multiplied by the Cosine of the dihedral angle to give the vector normal to the wing reference plane. The wing weight multiplied by the Sine of the dihedral angle gives a small axial force which places the spars in compression under positive g. This is shown at Row 'Rigid Wing' 36.

6.56 **Effect of Angle of Attack:** As the aircraft angle of attack is increased, the lift and drag vectors rotate relative to the wing reference line. At high angles of attack, the rotation results in net wing lift applying a thrust on the wing parallel to the wing reference line. This thrust is reacted out as a moment couple which results in compression in the front spar and tension in the rear spar.

6.57 In a similar manner, the drag starts to apply a bending force normal to the wing reference line.

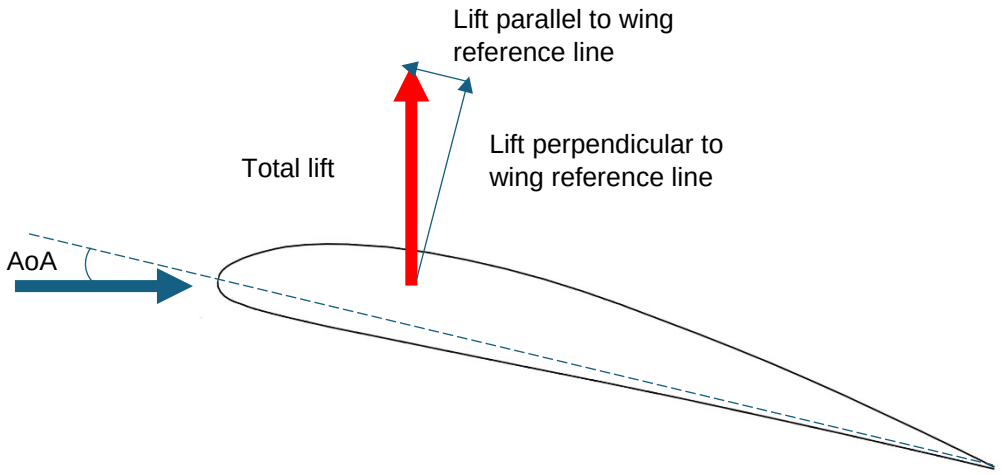

Figure 6-7 Lift Vectors at High Angles of Attack

6.58 **Lift and Drag Loads Normal to the Reference Line:** The front and rear spar lift and drag loads are proportioned according to the load distribution at Section 5 above. The pitching moment reaction for each panel is also added as a load normal to the wing reference plane at each spar at Rows 78 and 81 respectively.

6.59 **Spar Axial Loads Due to Loads Parallel to the Reference Line:** The Pawnee wing has internal diagonal bracing wires between the front and rear spars. The Pawnee D, with the fuel tank in the wing, has a bracing strut in lieu of the wires outboard of the strut connection. The bracing creates a wire braced truss where loads parallel to the reference line are reacted out as tension and compression axial loads in the front and rear spar.

6.60 The spar axial loads are calculated on the “Chordwise B+C” worksheet if Cell K2 on the ‘Input’ worksheet is “N”. If Cell K2 on the ‘Input’ worksheet is “Y”, the “Chordwise D” worksheet is used. Both the “Chordwise B+C” and “Chordwise D” worksheets take the wing air loads parallel to the chord, the wing weight parallel to the chord, and the strut weight parallel to the chord and show them on Rows 8 to 10. The kick loads from the front and rear struts are shown at Cells X11 and X12 respectively.

6.61 Row 14 adds the forces across the span and applies them at the compression rib. The forces at each rib are the sum of loads approximately half way to the next compression rib either side. Row 15 is the cumulative applied forces from tip to root. Rows 17 to 20 determine the angle of the bracing to the next inboard compression rib. Rows 21 and 22 determine the tension in the bracing wire and the horizontal component of that tension.

6.62 Rows 25 and 27 determine which of the bracing wires is in tension from the applied cumulative load and assigns the horizontal component of that tension to each corner of the truss. Rows 24 and 28 sum the horizontal components of the bracing tension to give a front and rear spar axial load respectively.

6.63 Worksheet ‘Chordwise D’ Cells Y27 and AE25 are different in that these represent the corners of a bracing tube. Where bracing wires can only carry tension, the tube can carry tension and compression. This alters the axial loads in the front and rear spar outboard of the strut attachment for the Pawnee D.

6.64 The front and rear spar axial loads resulting from loads parallel to the chord are used at Rows 65 and 69 on the ‘Rigid Wing’ worksheet.

6.65 **Strut Loads:** The wing is pinned at the root at Wing Station 19. A sum of moment around the wing root for air loads and wing mass is made at Row 57 for the front spar and Row 60 for the rear spar.

6.66 The strut attachment at the wing spar is offset above the neutral axis (see Section 9). The strut reaction load creates a moment at each spar that counters the wing bending from the air loads. The moments resulting from axial loads being applied at a vertical offset from the neutral axis are calculated at Rows 94 and 120 for the front and rear spar respectively. The reaction at the strut to balance the moments from axial loads is calculated at Cell V117 and V143 respectively.

6.67 The strut load normal to the wing reference plane is calculated at Cell W101 for the front spar and cells W127 for the rear spar by dividing the sum of the moments at cells AK79 and AK82 by the arm of the strut about the root and adding the axial load moment component from Cells X96 and X122. This is an iterative calculation as a large component of the axial load in the spar is from the strut.

6.68 The strut is at an estimated angle of 15 degrees to the wing reference plane. The strut horizontal load is found by multiplying the normal load by the Tangent of the angle. As the strut is typically in compression in flight, the reaction places the spar typically in tension.

6.69 Both struts sweep forward to a common point on the fuselage. This point is estimated to be 6 inches ahead of the forward spar. This corresponds to an angle of 3 dgrees for the front spar and 16.5 degrees for the rear spar. The reaction at the wing is a rearwards force on each spar. This ‘kick’ load is calculated at Cells X62 and X63 by multiplying the strut horizontal load by the tangent of the strut forward sweep angle.

7. LANDING

7.1 A modified version of Reference 1.6 was created at Reference 1.12. This calculates loads for the Landing condition.

7.2 **Descent Velocity:** The undercarriage is designed around the maximum take-off weight of 2900 lb. Using the descent velocity equation from Section 3.243 of Reference 1.7, the limit descent velocity for landing loads is:

$$V = 4.4 \times (\frac{W}{S})^{0.25} = 4.4 \times (\frac{2900}{183})^{0.25}$$

$$= 8.78\ ft/sec$$

7.3 The undercarriage leg is designed such that the centre of the main wheel is 23 inches outboard of the leg pivot. The undercarriage is sprung using bungees. These are attached to the undercarriage leg at 13 inches inboard of the pivot. The bungees consist of a loop that is 8 inches in length. Each bungee loop is folded such that the length of each rubber is 4 inches. The bungees conform to Type II described in Reference 1.10 and reach 100% load when they double their extension. The extension of the bungee at limit load is therefore:

$$Extension_{Limit} = \frac{4}{1.5} = 2.667\ inch$$

The travel of the main wheel at limit is therefore:

$$Travel_{Limit} = \frac{23}{13} \times 2.667 = 4.718\ inches$$

The peak acceleration experienced by the aircraft is given by:

$$a = \frac{V^2}{x} = \frac{8.78^2}{(\frac{4.718}{12})} = 196.07\ {}^{ft}/_{sec^2} = 6.094\ g$$

This is conservative as it does not consider tyre deflection.

The effective spring stiffness k is given by

$$k = \frac{mV^2}{x^2} = \frac{2900 \times 8.78^2}{(\frac{4.718}{12})^2}$$

$$= 1{,}446{,}218\ lb.s^{-2}$$

Therefore the undercarriage deflection for a given mass and descent velocity is:

$$x^2 = \frac{mV^2}{k}$$

$$x = V\sqrt{\frac{m}{k}}$$

Peak spring acceleration is given by:

$$ma = k.x$$

$$a = \frac{k}{m}.V\sqrt{\frac{m}{k}} = V\sqrt{\frac{k}{m}}$$

7.4 The Pawnee during agricultural operations is assumed to be landing without payload at 2005 lb.

Descent Velocity	Δn_z
0	0.000
1	0.835
2	1.669
3	2.504
4	3.339
5	4.173
6	5.008
7	5.842

Table 7-1 Descent Velocity Versus Peak Acceleration at 2005 lb

7.5 **Landing Flap:** Reference 1.5 is unable to provide results for a slotted flap. Reference1.11 is used instead to estimate the change in lift, drag and pitching moment for a slotted flap at 57 degrees deflection.

7.6 Figure 7 of Reference1.11 shows the lift, drag and pitching moment coefficients for the NACA 23012 airfoil with 0 flap deflection. The maximum lift of 1.55 at approximately 15.5 degrees angle of attack. Figure 17 of Reference1.11 shows the change in lift, coefficient for a slotted flap at various deflections. The maximum lift coefficient occurs at approximately 55 degrees and is increased from 1.55 for 0 flap deflection to 2.7 for 55 degrees flap deflection, an increase of 1.15. The stall angle is decreased from 15.5 degrees to 12.5 degrees.

7.7 A modified lift curve was created by adding 1.55 onto the CL and decreasing the angle of attack by 3 degrees.

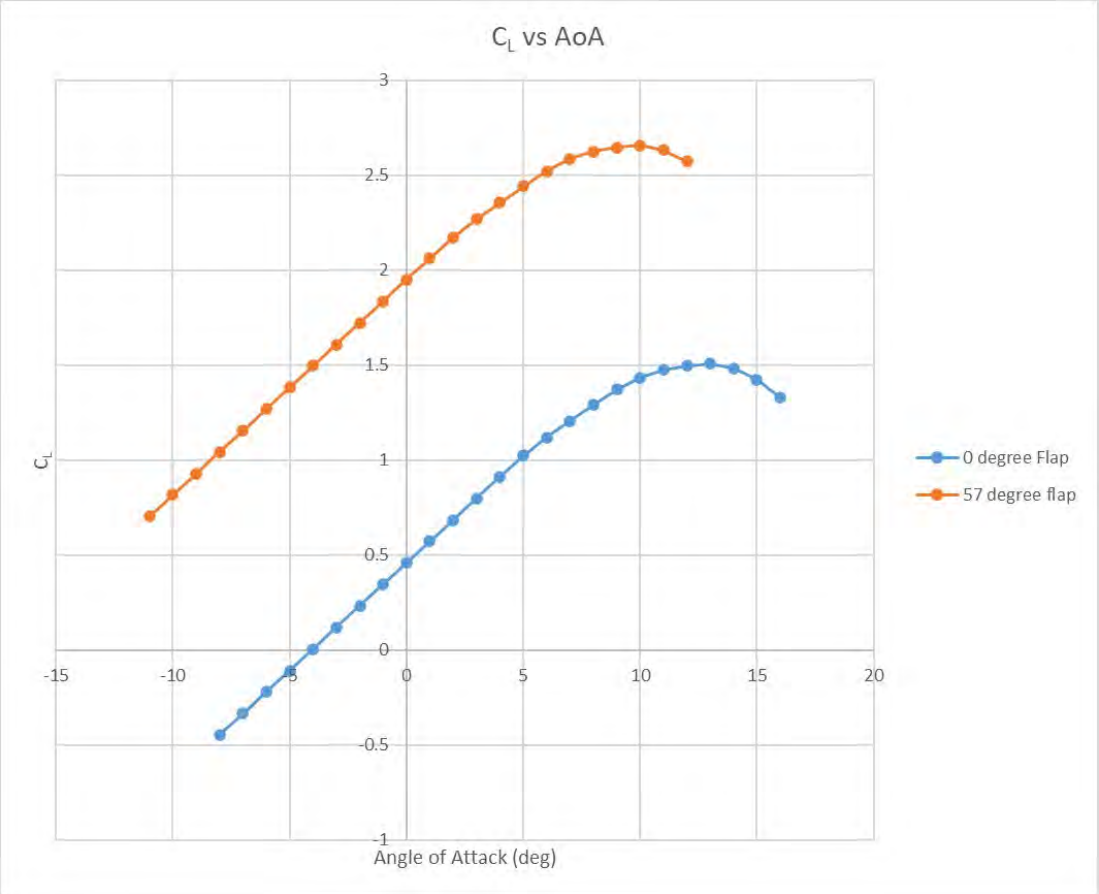

Figure 7-1 Lift Curve Modified for Landing Flap

7.8 A modified drag polar was created in a similar manner to the lift curve. At stall the drag coefficient with 0 flap deflection is 0.041 and at 0.185 at 57 degrees deflection at Figure 24 of Reference 1.11. The drag coefficient is increased by 0.144.

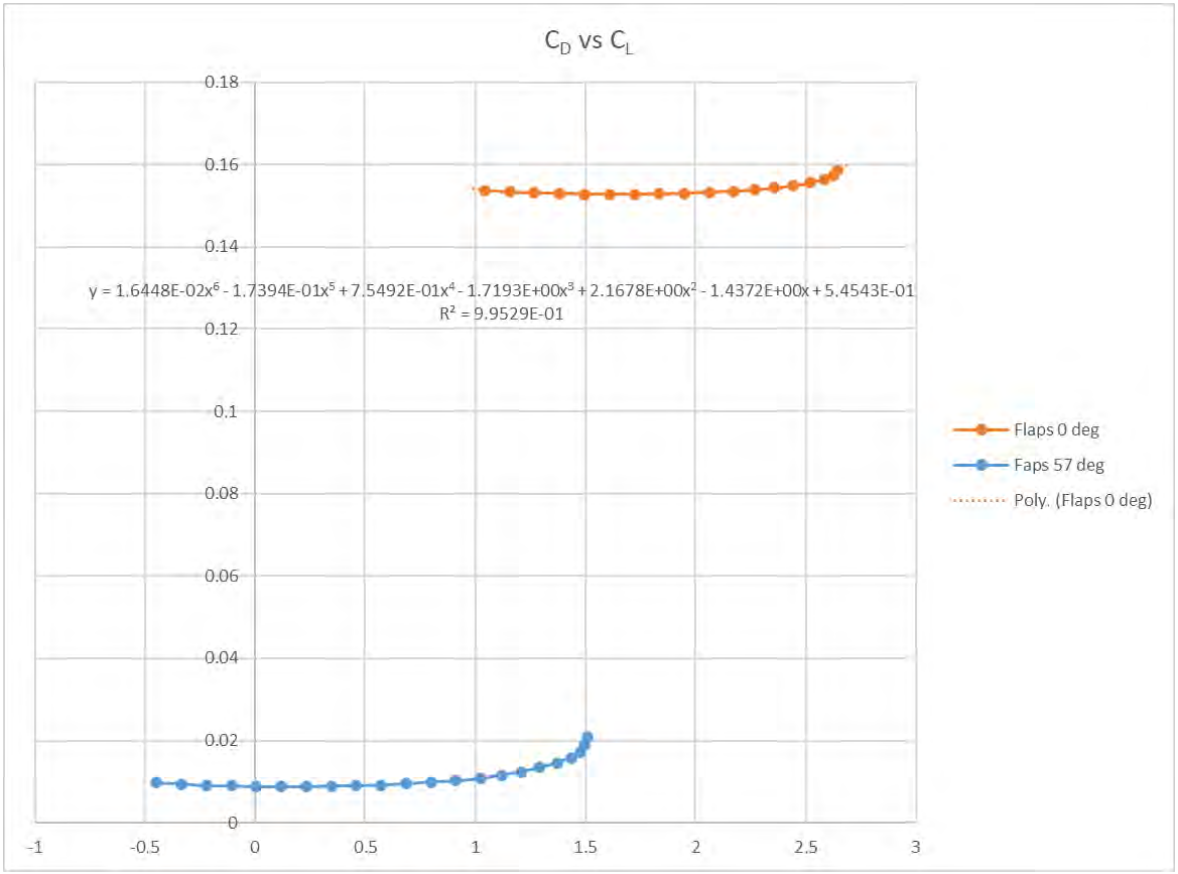

Figure 7-2 Drag Polar Modified for Landing Flap

7.9 A modified pitching moment coefficient was also created in a similar manner to the lift curve. The pitching moment coefficient with 0 flap deflection is -0.012 and approximately -0.300 at 57 degrees deflection at Figure 15 of Reference 1.11. The pitching moment coefficient is increased by -0.288. The curve fit used was adapted from the 0 flap curve fit.

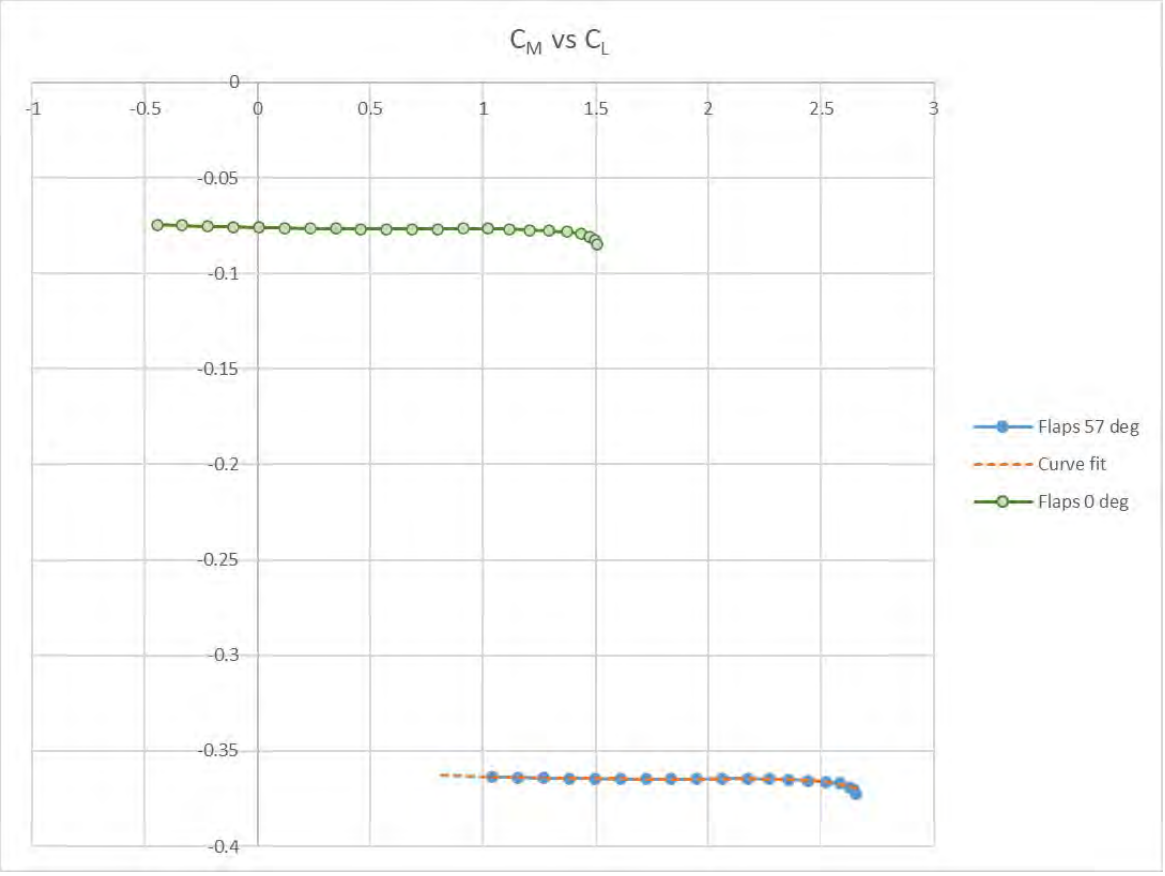

Figure 7-3 Pitching Moment Coefficient Modified for Landing Flap

7.10 **Landing Airspeed:** The landing flap load calculator spreadsheet is a modified version of the flight loads calculator spreadsheet with the exception that it is for a fixed condition. The airspeed is calculated for the maximum wing lift coefficient, the aircraft weight and the nominal g load.

7.11 **Aircraft Angle of Attack:** The aircraft is assumed to be in the 3 point landing attitude. Reference 1.1 shows the attitude to be 9 deg 42 sec (9.70 deg).

7.12 **Lift Coefficient:** The lift coefficient was calculated using the vortex lattice program at Reference 1.8 without washout applied. It applied 57 degrees of flap between wing station 39.3 and 85.675. The C_L distribution for the flap deflection was subtracted from the normal C_L distribution for a C_L of 1.81 to give a C_L distribution for just the flap deflected. This resulted in:

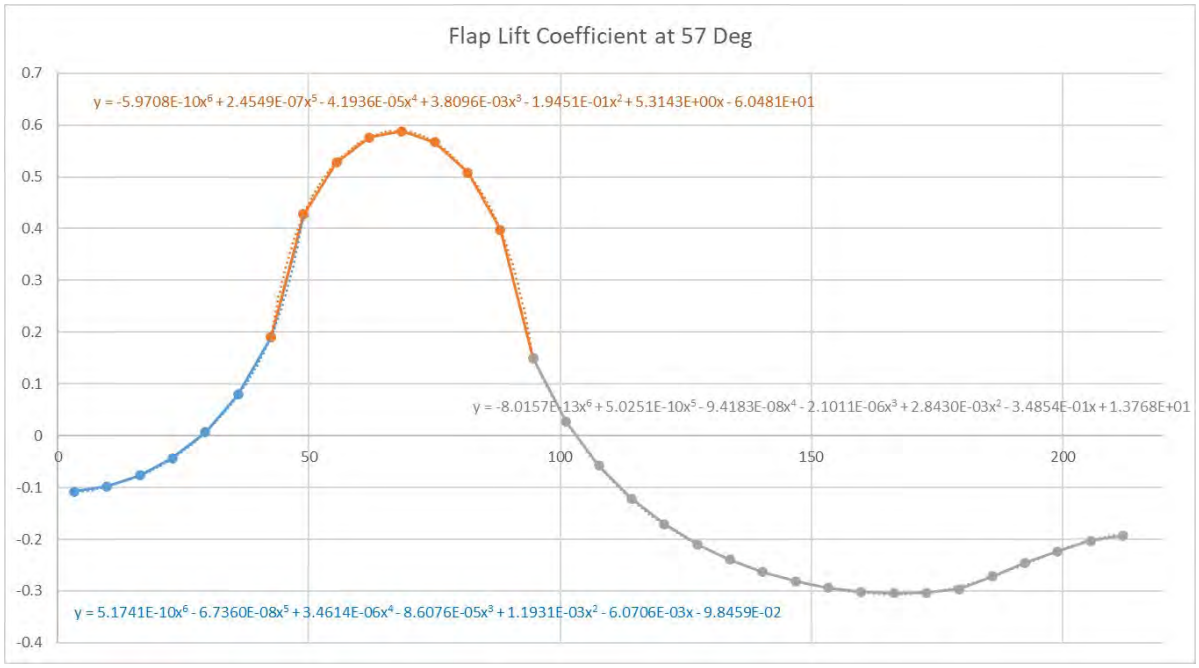

Figure 7-4 Lift Distribution For Landing Flap

7.13 Due to the complex nature of the distribution, it was broken into 3 segments to give an adequate curve fit.

7.14 The C_L distribution for just the flap deflected was added onto the Piper C_L distribution for C_L of 1.81 to give the net C_L distribution.

7.15 **Induced Drag:** The induced drag coefficient was calculated using the vortex lattice program at Reference 1.8 without washout applied. It applied 57 degrees of flap between wing station 39.3 and 85.675. The C_{DI} distribution is:

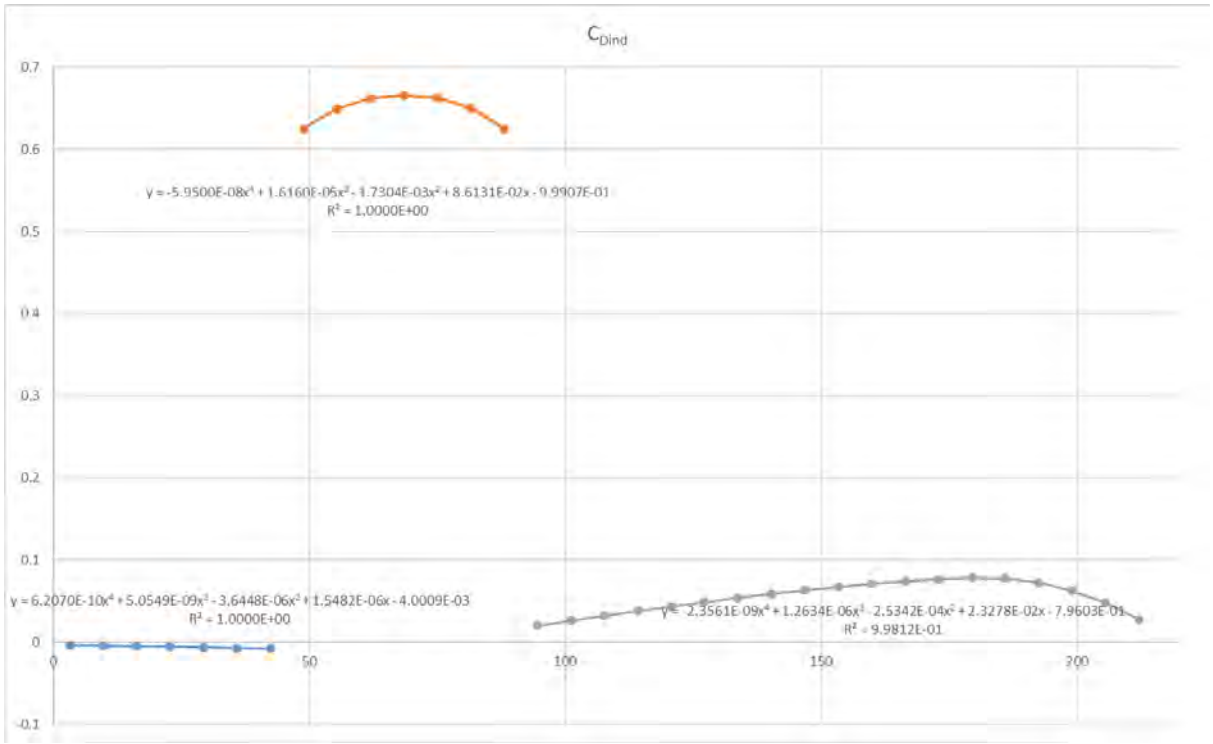

Figure 7-5 Induced Drag Distribution with Landing Flap

7.16 Due to the complex nature of the distribution, it was also broken into 3 segments to give an adequate curve fit.

7.17 Section 3.243 of Reference 1.7 allows the use of 0.67 of the lift loads to calculate design loads for landing. The intent of Reference 1.12 is to estimate fatigue stresses for the landing condition rather than loads for design purposes. As a result, the full lift load was used.

7.18 The landing condition is a dynamic case. Such cases in cantilever wing aircraft can have considerable stress amplification due to large masses and flexible structures. The PA-25 wing is very light weight and relatively stiff as it is supported by the strut. As a result, no stress amplification is used. However, a dynamic factor at Cell E23 is included in the spreadsheet. This is used to amplify the g resulting from the landing if considered necessary.

8. TAXI

8.1 A modified version of Reference 1.6 was created at Reference 1.13. This calculates loads for the Taxi condition.

8.2 The Taxi condition has the airspeed set to 0 and the air loads removed. The wing spar stresses are purely inertial from the weight of the wings and the weight of the struts. The aircraft is assumed to be in the 3 point landing attitude. Reference 1.1 shows the attitude to be 9 deg 42 sec (9.70 deg).

8.3 The taxi condition is a dynamic case. Such cases in cantilever wing aircraft can have considerable stress amplification due to large masses and flexible structures. The PA-25 wing is very light weight and relatively stiff as it is supported by the strut. As a result, no stress amplification is used. However, a dynamic factor at Cell E23 is included in the spreadsheet. This is used to amplify the g resulting from the taxiing if considered necessary.

9. SPAR CROSS SECTIONS

9.1 Both the front and rear spars consist of a single 6061-T6 extrusion. Both the upper and lower caps have flanges turned inwards with the free ends of the flanges having bulbs. The spar cross sections were measured on the wing of a damaged Pawnee.

9.2 **Front Spar:** The front spar was measured as:

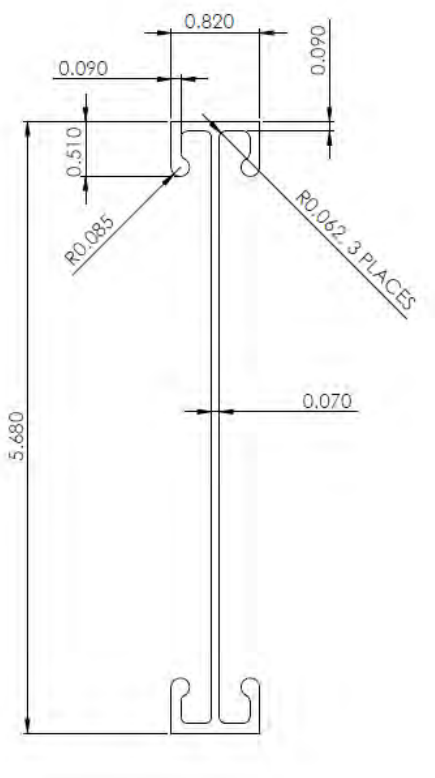

Figure 9-1 Front Spar Cross Section

The front spar section properties are calculated on the “Front Spar Section” worksheet with the following results:

Front Spar Area: 0.728 in^2 (compared to 0.748 in^2 at Page II-34 or Reference 1.2)

Front Spar Inertia: 3.373 in^4 (compared to 3.420 in^4 at Page II-34 or Reference 1.2)

Neutral Axis: 0.000 in from centreline

9.3 The front spar has a doubler fitted to the web at the wing root as shown in Figure 9-2. This doubler is estimated to be 0.063” thick. At wing station 29.15, the doubler consists of an upper and lower tang. The upper tang is estimated to be 1.00 in high and the lower tang 2.00 in high. This increased the spar properties to:

Front Spar + Doubler Area: 0.917 in^2

Front Spar Inertia: 3.923 in^4

Neutral Axis: -0.066 in from centreline

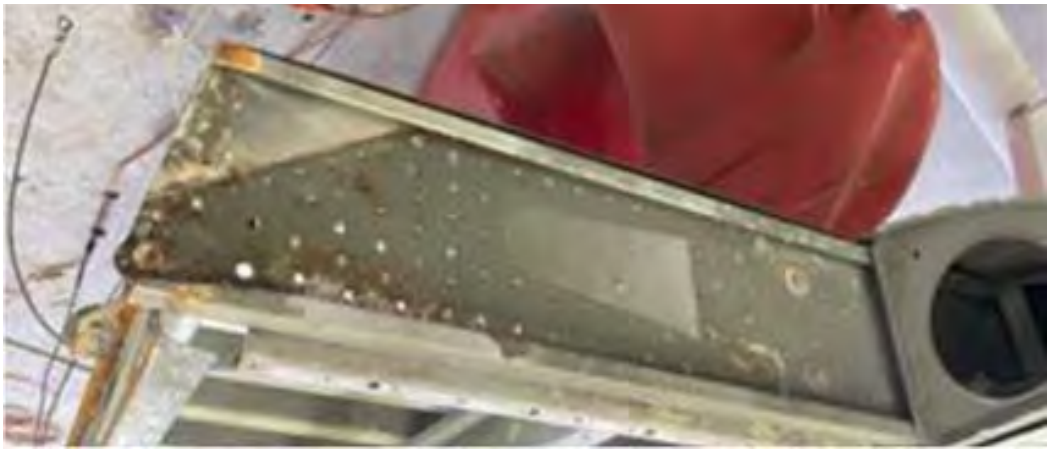

Figure 9-2 Front Spar Showing Outline of Doubler

9.4 At wing station 25 the doubler consists of a plate 5.00 in high. This increased the spar properties to:

Front Spar + Doubler Area: 1.043 in^2

Front Spar Inertia: 4.029 in^4

9.5 The front spar was found to have a 1.00" x 0.125" tension strap fitted to the aft face of the spar web above the lower cap. This extended across the rib bay immediately under the strut attachment and the next rib bay outboard. This increased the spar properties to:

Front Spar + Strap Area: 0.853 in^2

Front Spar Inertia: 3.746 in^4

Neutral Axis: -0.276 in from centreline

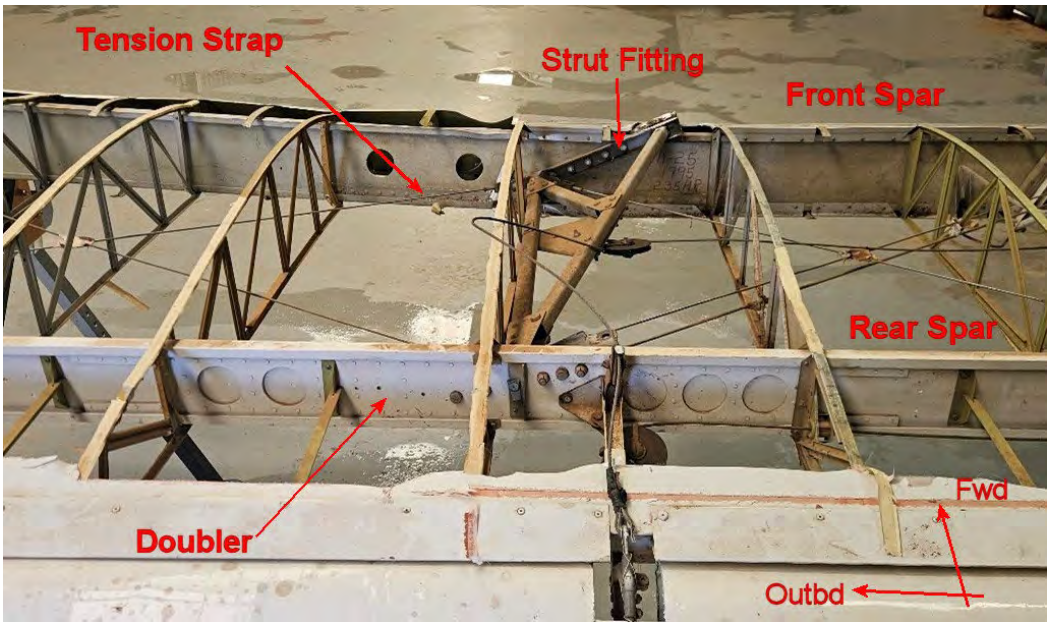

Figure 9-3 Spar Details at Strut Connection of Damaged Wing

9.6 The front spar area is shown at spanwise positions at Row 103 of the "Flexible Wing" and "Rigid Wing" worksheets. The front spar inertia is shown at spanwise positions at Row 104.

9.7 **Rear Spar:** The rear spar was measured as:

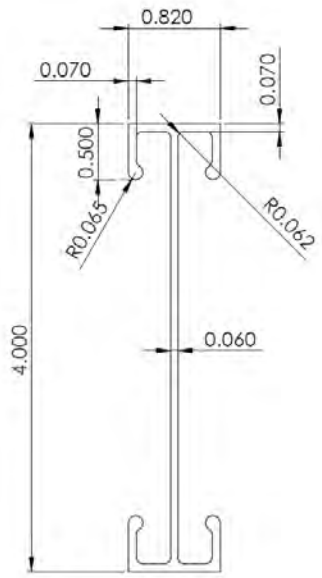

Figure 9-4 Rear Spar Cross Section

Rear Spar Area: 0.495 in^2 (compared to 0.504 in^2 at Page II-34 or Reference 1.2)

Rear Spar Inertia: 1.165 in^4 (compared to 1.220 in^4at Page II-34 or Reference 1.2)

Neutral Axis: 0.000 in from centreline

9.8 The rear spar was found to have a 1.00” x 0.080” doubler fitted to the aft face of the spar web at the strut attachment. This extended across the rib bay immediately under the strut attachment and the next rib bay outboard. This increased the spar properties to:

Rear Spar + Doubler: 1.043 in^2

Rear Spar Inertia: 1.773 in^4

Neutral Axis: 0.000 in from centreline

9.9 The rear spar area is shown at spanwise positions at Row 129 of the “Flexible Wing” and “Rigid Wing” worksheets. The rear spar inertia is shown at spanwise positions at Row 130.

10. SPAR FITTINGS OFFSETS

10.1 **Front Spar Wing Root Fitting:** The front spar wing root has a doubler plate and a pair of fittings which angle down to the wing root attachment bolt. The wing root attachment bolt was measured to be offset by 4.940 in from the top of the spar. The height of the wing root attachment bolt below the spar centreline is 4.940 - 2.840 = 2.100 in below the spar centreline. This is used at Cell E113.

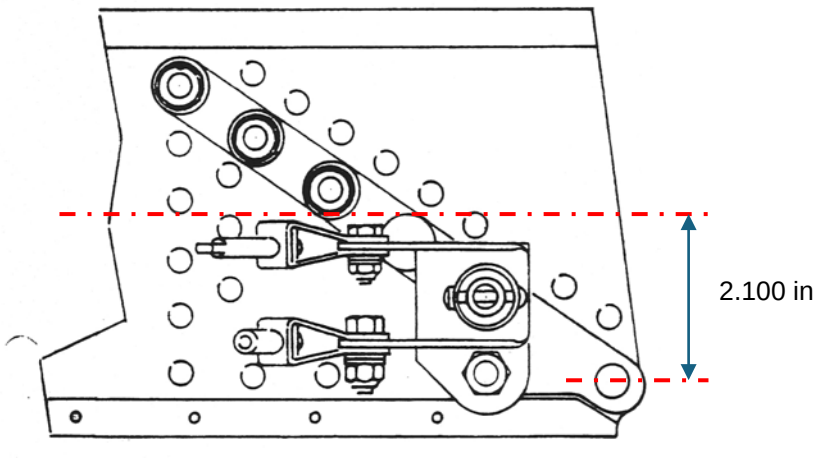

Figure 10-1 Front Spar Wing Root Fittings (Aft Face of Spar)

10.2 **Front Spar Strut Fitting:** The front strut spar fitting is secured by 6 fasteners. The centroid is judged to be at the midpoint of the fitting between fasteners 3 and 4. This point was measured to be 2.200 inch below the top of the spar. The height of the fitting centroid above the centreline is 2.840 – 2.200 = 0.640 in. This is used in Cell W113.

Figure 10-2 Centroid of Front Spar Strut Fitting

10.3 **Rear Spar Wing Root Fitting:** The rear spar has a pair of fittings which angle down to the wing root attachment bolt similar to the front spar. The wing root attachment bolt was measured to be offset by 3.050 in from the top of the spar. The height of the wing root attachment bolt below the spar centreline is 3.050 - 2.00 = 1.050 in below the spar centreline. This is used at Cell E139.

10.4 **Rear Spar Strut Fitting:** The rear strut spar fitting is secured by 6 fasteners. However, the fastener spacing is not even. The centroid is judged to be at the point shown in Figure 10-3 below. This point was measured to be 1.640 inch below the top of the spar. The height of the fitting centroid above the centreline is 1.640 – 2.000 = -0.360 in. This is used at Cell W139.

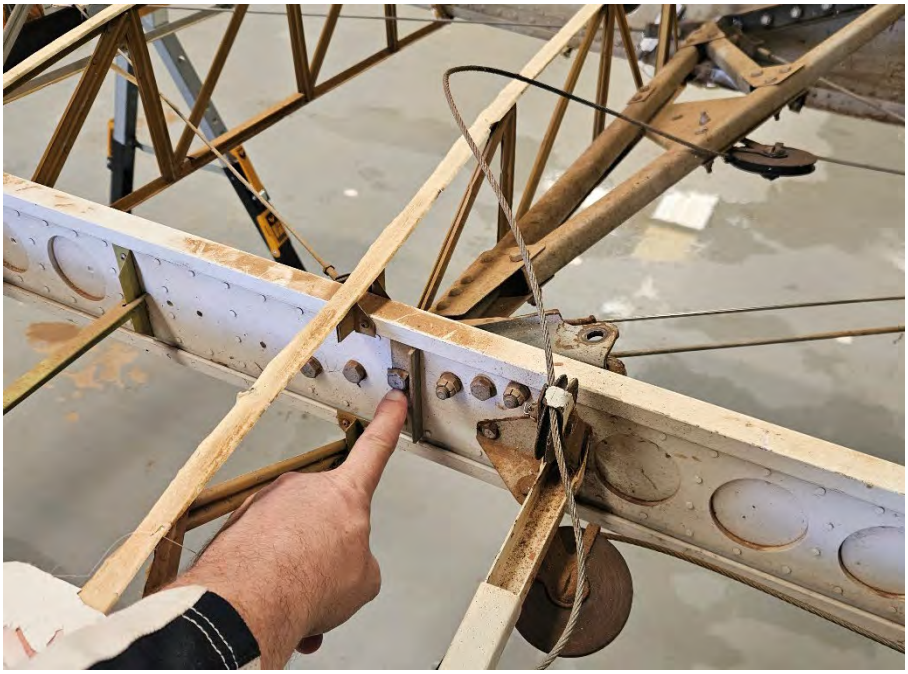

Figure 10-3 Centroid of Rear Spar Strut Fitting

11. WING SHEAR AND BENDING

11.1 **Front Spar Shear:** The net wing forces normal to the wing reference line at the front spar from each panel is calculated at Row 119. Cell E119 includes the wing root reaction normal to the wing reference line. Cell V119 includes the strut reaction normal to the wing reference line.

11.2 Row 120 is the cumulative sum of the front spar shear for each panel from the tip to the root. The result is used to produce a shear force diagram for the front spar.

11.3 **Rear Spar Shear:** The net wing forces normal to the wing reference line at the rear spar from each panel is calculated at Row 145. Cell E145includes the wing root reaction normal to the wing reference line. Cell V145 includes the strut reaction normal to the wing reference line.

11.4 Row 146 is the cumulative sum of the rear spar shear for each panel from the tip to the root. The result is used to produce a shear force diagram for the rear spar.

11.5 **Front and Rear Spar Bending:** Spar bending is calculated for the front and rear spars at Rows 122 and 148 respectively from the wing shear above.

12. SPAR AXIAL LOADS

12.1 Spar axial loads arise from three sources: weight, bracing wire reactions and the strut.

12.2 **Wing Weight:** The wing weight has a small axial component due to the wing dihedral. Rows 108 and 134 take the wing weight axial component from Row 58, multiply it by the weight factors at Cells E95 and E96 and progressively add them from the tip to the root for the front and rear spar respectively.

12.3 **Bracing Wires:** Rows 109 and 135 repeat the values from Rows 87 and Rows 91 respectively. These are the reactions from the bracing wires as described in Section 6.59.

12.4 **Strut:** The strut axial loads are calculated at Cells W102 and W128 for the front and rear spar respectively. The spanwise distribution s shown at rows 110 and 136.

12.5 **Total Axial Loads:** Rows 111 and 137 sum rows 108 to 110 and 134 to 136 to give a total axial load for the front and rear spars respectively. Cells E111 and E137 also include the reaction from the wing root.

13. SPAR CAP STRESSES

13.1 The spar cap stresses have two components, the axial stress and the bending stress. The axial stress is found by dividing the spar axial load by the section area. The bending stress is calculated by:

$$\sigma = \frac{My}{I}$$

13.2 At the wing roots, the axial load remaining in the spar extrusion was estimated to be 7% based on the thickness of the web relative to the doubler and wing root fittings. The remainder of the axial load is carried by the doubler and spar wing root fittings.

13.3 Similarly, the bending moment at the root is transferred into the spar root fitting. It is estimated that 7%, based on the thickness of the web relative to the doubler and wing root fittings, remains in the spar extrusion. The remainder of the bending moment is carried by the doubler and spar wing root fittings.

13.4 As a result, peak stress near the wing root occurs at wing station 25. The transition to wing station 19 will not be linear, but will step down as the fasteners in the wing root fittings, remove the load from the spar section.

13.5 Similarly, the peak in stress at the wing strut attachment point will step up / down over a short span as load is transferred into the spar section by individual fasteners. An example of this is shown below at Figure 13-1where a finite element model at Reference 1.14 was used to validate the spreadsheet calculation of the bending moments.

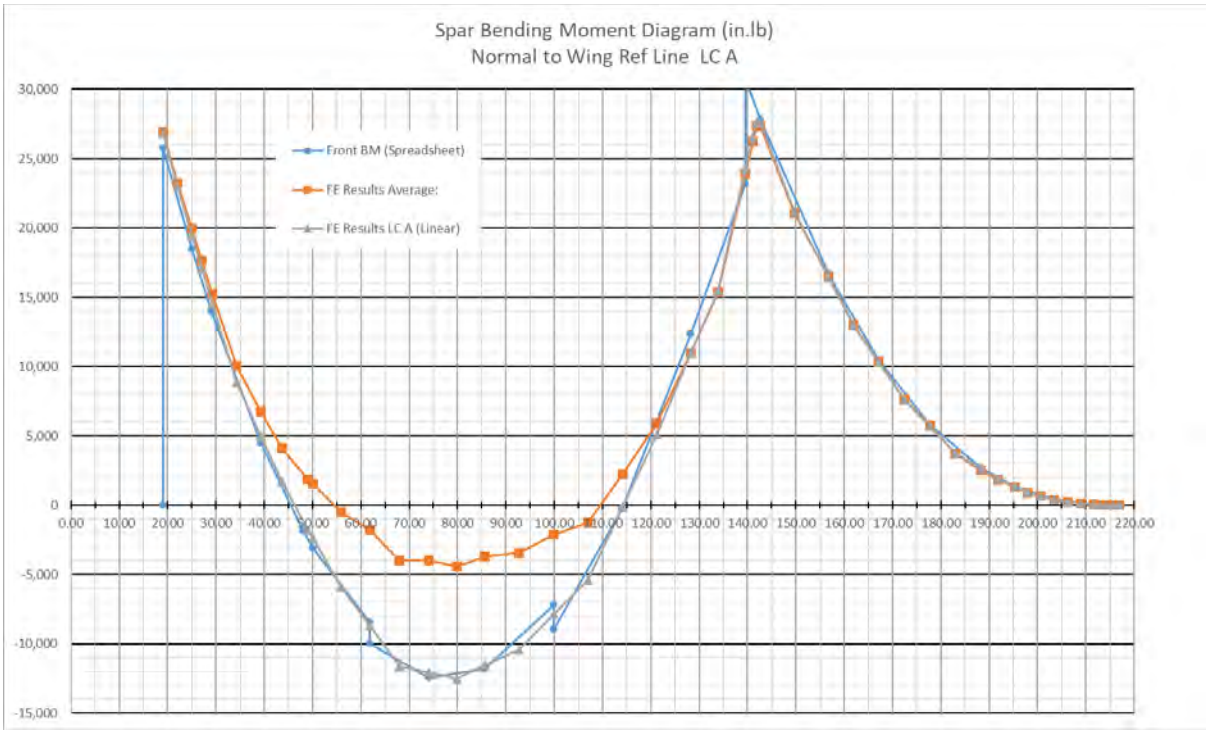

Figure 13-1 Bending Moment Diagram from Finite Element Model showing Reduction in Bending at Wing Strut Attachment Compared to Rigid Wing Bending

14. LOAD CASES

14.1 There are two cases to consider, the weight for agricultural operations and the weight for aerotow operations. Wing bending is a function of the weight of the non-lifting parts. To make direct comparisons between the two cases, the fuel and pilot weights were kept constant and the payload in the hopper varied ie the weight of non-lifting parts is varied.

14.2 The Pawnee D has fuel tanks in each wing outboard of the wing strut attachment which feed to a header tank in the fuselage. Several earlier model Pawnees operating in Australia were modified in New Zealand and fitted with wing tanks as well. In these cases, the fuel load is removed from the weight of non-lifting parts and added to each wing.

14.3 There are 8 two seat Pawnees identified with gliding operations in Australia. These have a higher empty weight due to the wider fuselage, dual controls, and ballast in the forward fuselage.

14.4 **Agricultural Operations:** Agricultural operations are limited by the maximum take-off weight. However, CASA was historically authorising Agricultural operations above the maximum take-off weight. The weight cases for Agricultural operations are: Overweight, maximum take-off weight, and landing weight.

14.5 Overweight**:** The design of the Pawnee allows up to 1200 lb payload in the hopper. However, a full payload, full fuel, and a heavy pilot results in the following:

Item	Weight	
Empty Weight	1531.0	lb
Fuel (38.5 gal)	231.4	lb
Pilot (110 kg)	242.6	lb
Payload in hopper (max)	1200.0	lb
Total	**3205.0**	**lb**

Table 14-1 Maximum Weights Resulting in Overload

14.6 This represents a significant overload of the aircraft with the excess weight concentrated in the fuselage. This would result in high wing bending stresses and is suspected of being a contributing factor in recent accidents overseas. The flight envelope at 3205 lb is at Figure 14-1 below:

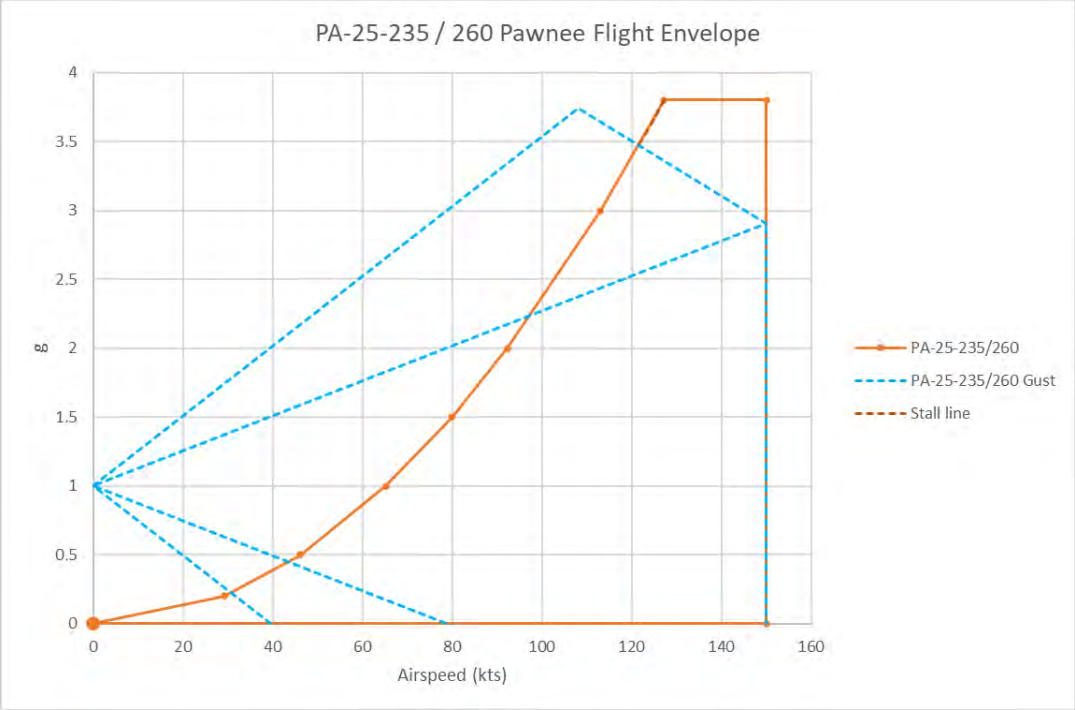

Figure 14-1 Overweight Flight Envelope

14.7 The gust cases are either outside the stall curve or are exceeded by the manoeuvre load cases. There are two corners of the envelope to consider:

127 kts at 3.8 g, and

150 kts at 3.8 g.

14.8 Maximum Take-Off Weight: Reducing the payload in the hopper to be at maximum take-off weight results in the following:

Item	Weight	
Empty Weight	1531.0	lb
Fuel (38.5 gal)	231.4	lb
Pilot (110 kg)	242.6	lb
Payload in hopper	895.0	lb
Total	**2900.0**	**lb**

Table 14-2 Weights for Maximum Take-Off Weight

14.9 The flight envelope at 2900 lb is at Figure 4-1. Similar to the overweight case, the gust cases are either outside the stall curve or are exceeded by the manoeuvre load cases. There are three corners of the envelope to consider:

121 kts at 3.8 g, and

150 kts at 3.8 g.

14.10 Landing Weight: The weight of the fuel and pilot is the same as agricultural operations and the payload in the hopper is removed. This results in:

Item	Weight	
Empty Weight	1531.0	lb
Fuel (38.5 gal)	231.4	lb
Pilot (110 kg)	242.6	lb
Payload in hopper	0.0	lb
Total	**2005.0**	**lb**

Table 14-3 Weights for Landing Weight

14.11 The flight envelope at 2005 lb is at Figure 14-2 below:

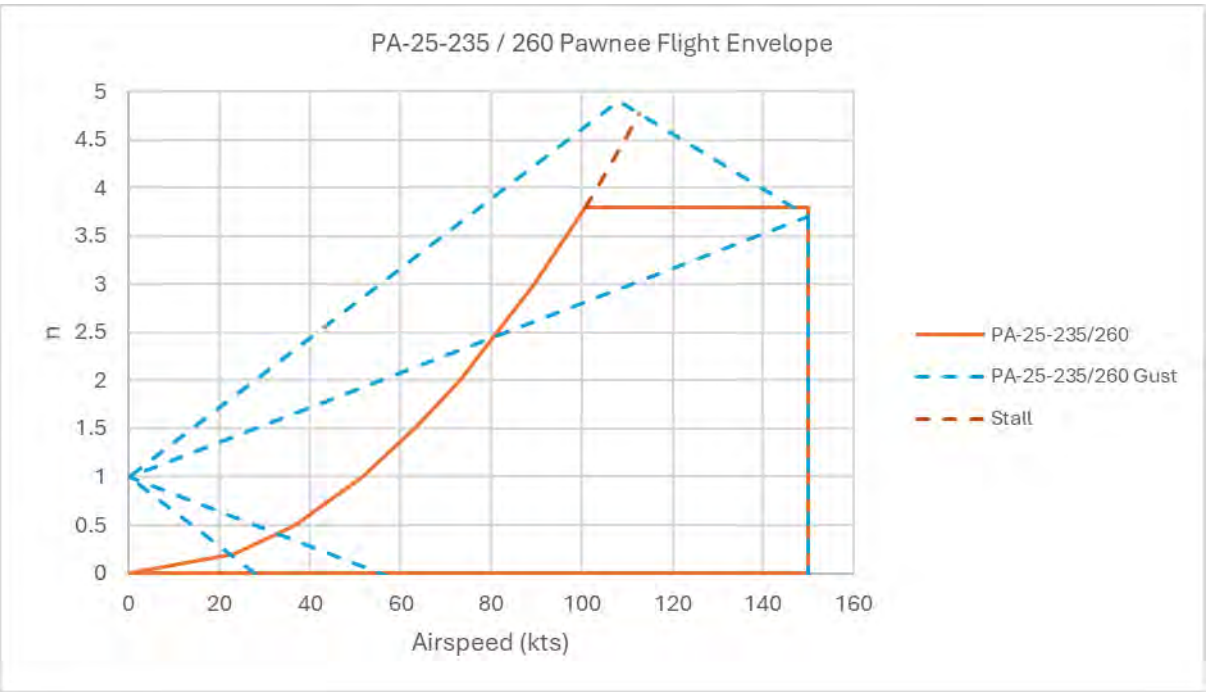

Figure 14-2 Flight Envelope for PA-25-235 and PA-25-260 at 2005 lb

14.12 The 30 ft/sec gust response at 108 kts is outside the envelope as the Pawnee will stall prior to achieving 4.895 g at that speed. The intercept of the stall line and the gust envelope occurs at 113 kts with a gust of 27.75 ft/sec giving a g response of 4.770 g. There are four corners of the envelope to consider:

101 kts at 3.8 g,

113 kts at 27.75 ft/sec gust, and

150 kts at 3.8 g.

14.13 **Aerotow Operations:** There are two weight cases to consider: operations of single seat Pawnees and with dual pilots operations.

14.14 Single seat operations: In Europe and the UK, Pawnees used in glider towing operations are operating under a 1,000 kg (2,205 lb) MTOW limit. Under ideal circumstances, a Pawnee could carry out glider towing operations at the weight of 2005 lb (909 kg). However, with repairs, fitment of other engines and options like retractable towing cable systems, the empty weight would increase. For consistency with international operations the empty weight is increased from 1531 lb (694 kg) to 1731 lb (785 kg) giving:

Item	Weight	
Empty Weight	1731.0	lb
Fuel (38.5 gal)	231.4	lb
Pilots (110 kg)	242.6	lb
Payload in hopper	0.0	lb
Total	**2205.0**	**lb**

Table 14-4 Weights for Single Pilot Towing Operations

14.15 The flight envelope at 2460 lb is at Figure 14-3 below:

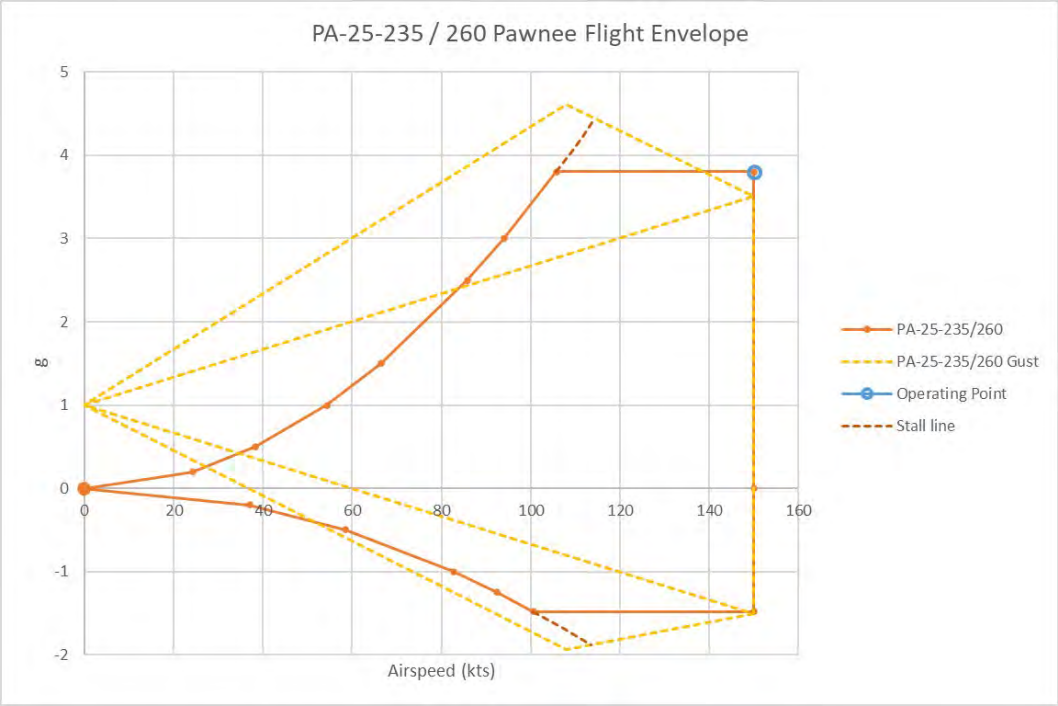

Figure 14-3 Flight Envelope for PA-25-235 and PA-25-260 at 2205 lb

14.16 The 30 ft/sec gust response at 108 kts is outside the envelope as the Pawnee will stall prior to achieving 4.610 g at that speed. The intercept of the stall line and the gust envelope occurs at 114 kts with a gust of 27.1 ft/sec giving a g response of 4.443 g.

14.17 There are four corners of the envelope to consider at 2205 lb:

106 kts at 3.8 g,

114 kts at 27.1 ft/sec gust, and

150 kts at 3.8 g.

14.18 Dual pilot operations: Several Pawnees have been rebuilt in Australia with a wider cockpit, a bench seat and dual controls. These are used for pilot conversion and currency training. The cockpit weight is limited by the aft CG limit. They are frequently fitted with ballast at the firewall to bring the CG forward which further increases the empty weight.

Item	Weight	
Empty Weight	1831.7	lb
Fuel (38.5 gal)	231.4	lb
Pilots (180 kg)	396.9	lb
Payload in hopper	0.0	lb
Total	**2460.0**	**lb**

Table 14-5 Weights for Dual Pilot Towing Operations

14.19 The flight envelope at 2460 lb is at Figure 14-2 below:

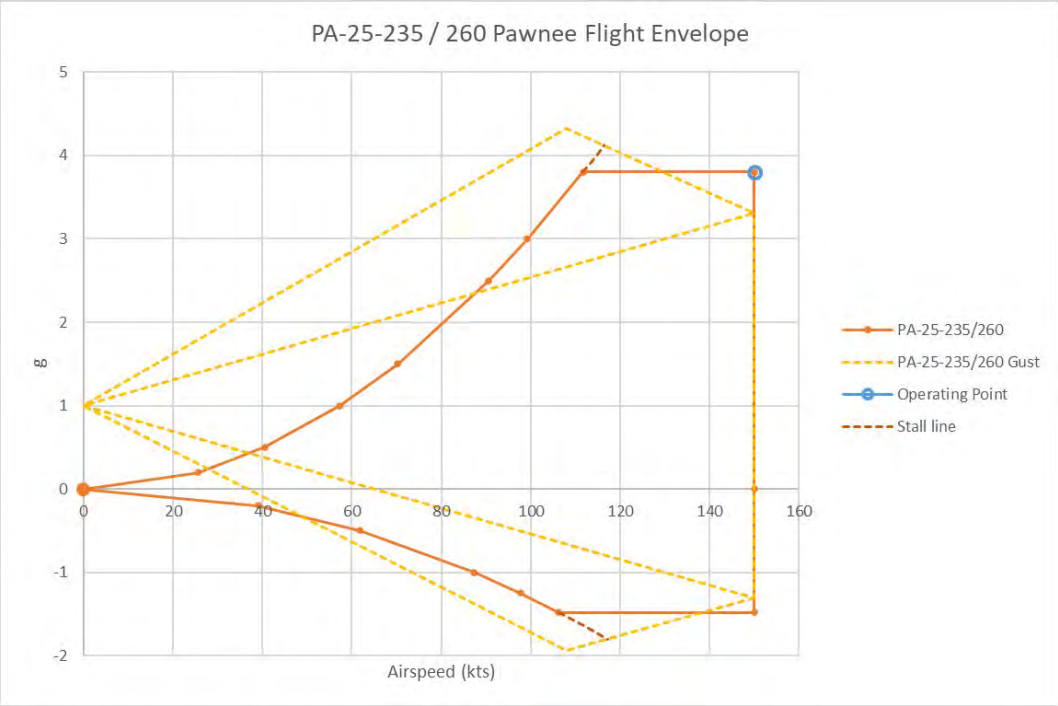

Figure 14-4 Flight Envelope for PA-25-235 and PA-25-260 at 2460 lb

14.20 The 30 ft/sec gust response at 108 kts is outside the envelope as the Pawnee will stall prior to achieving 4.326 g at that speed. The intercept of the stall line and the gust envelope occurs at 116 kts with a gust of 26.2 ft/sec giving a g response of 4.123 g.

14.21 There are four corners of the envelope to consider at 2460 lb:

112 kts at 3.8 g,

116 kts at 26.2 ft/sec gust, and

150 kts at 3.8 g.

15. PAWNEE B AND C RESULTS - AGRICULTURAL

15.1 **Load Case: 3205 lb at 127 kts and 3.8 g.** In comparison to the max take off weight (2900 lb) high angle of attack results, the wing root stress in the lower cap is increased from 24,211 psi to 27,050 psi (112%). The stress in the lower cap at the strut attachment is increased from 22,772 psi to 25,331 psi (111%). This agrees well to the increase in weight (111%).

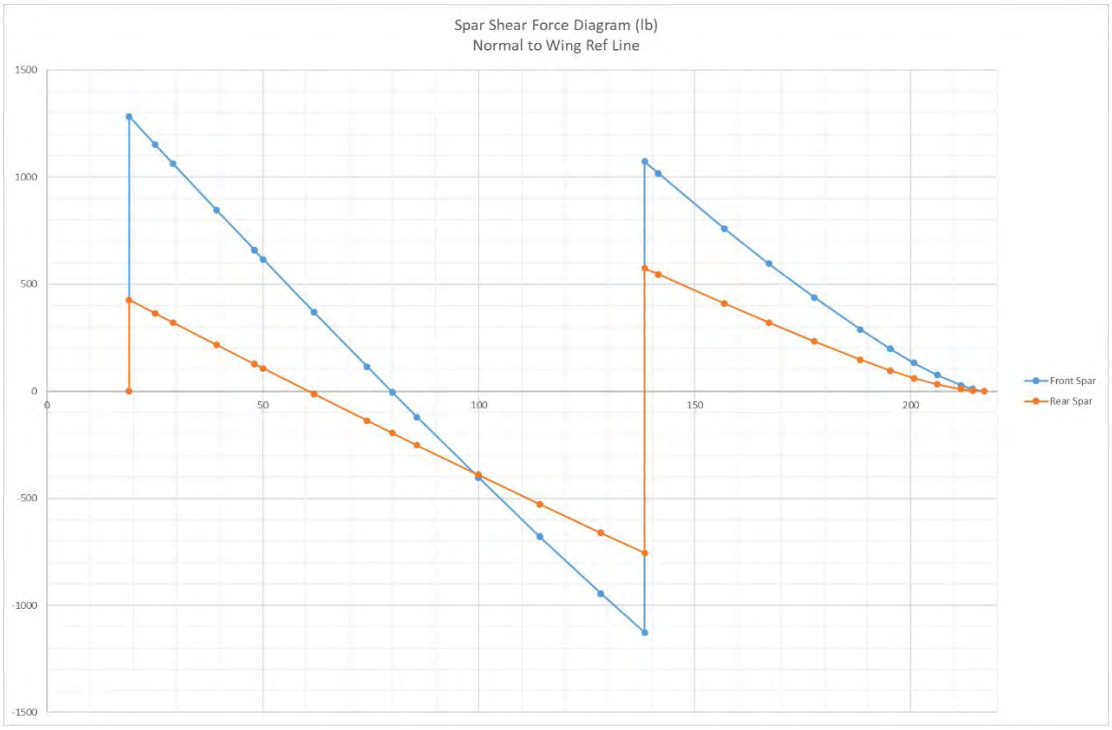

Figure 15-1 Spar Shear Force for 3205 lb at 127 Knots and 3.8 g

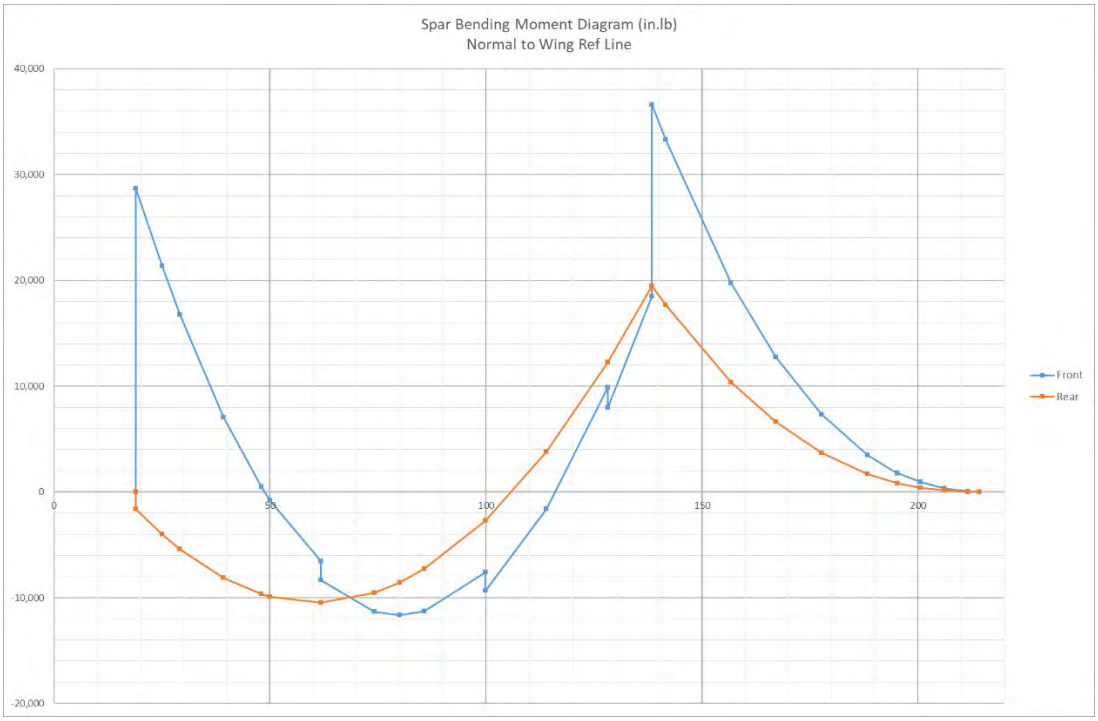

Figure 15-2 Spar Bending Moments for 3205 lb at 127 Knots and 3.8 g

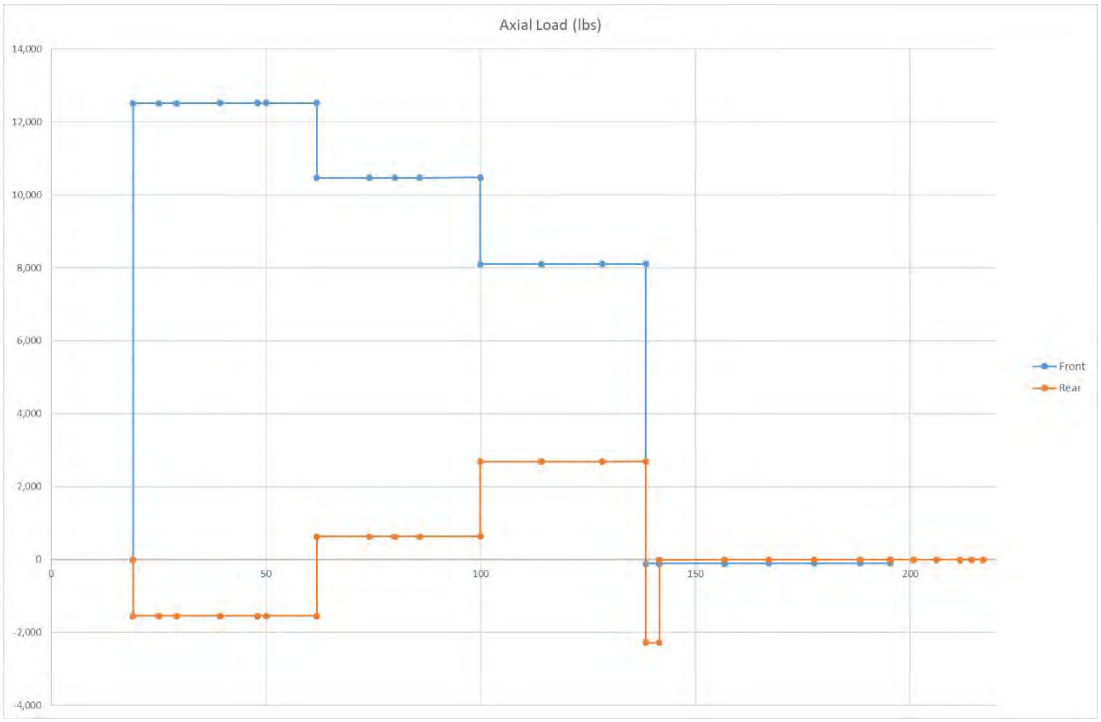

Figure 15-3 Spar Axial Loads for 3205 lb at 127 Knots and 3.8 g

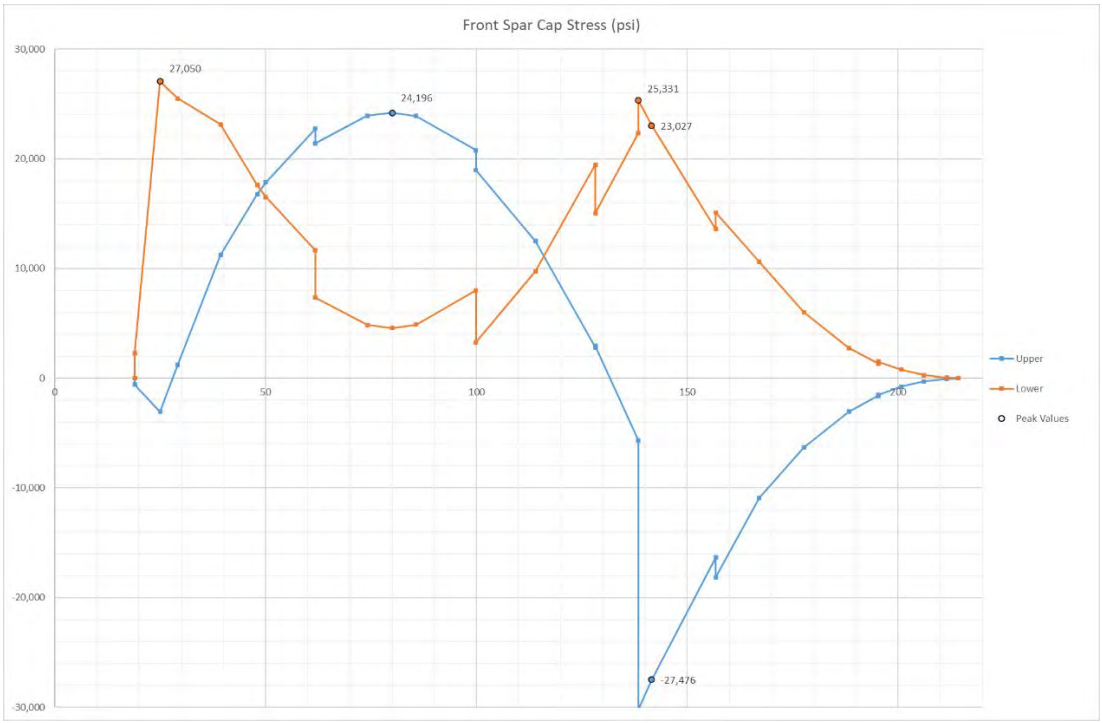

Figure 15-4 Front Spar Cap Stresses for 3205 lb at 127 Knots and 3.8 g

15.2 **Load Case: 3205 lb at 150 knots and 3.8 g**. In comparison to the max take off weight (2900 lb) low angle of attack results, the wing root stress in the lower cap is increased from 25,966 psi to 28,617 psi (110%). The stress in the lower cap at the strut attachment is increased from 19,939 psi to 23,062 psi (116%). The non-proportional increase in the stress at the strut attachment is due to the change in C_L between the load cases increasing the lift at the outer wing.

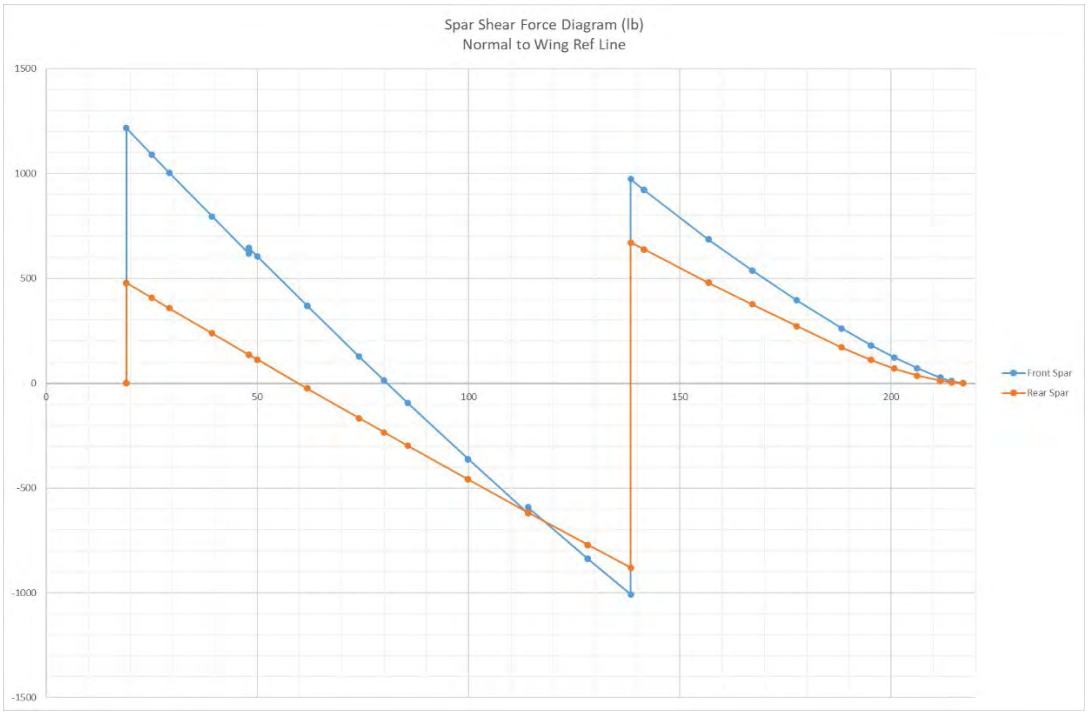

Figure 15-5 Spar Shear Force for 3205 lb at 150 Knots and 3.8 g

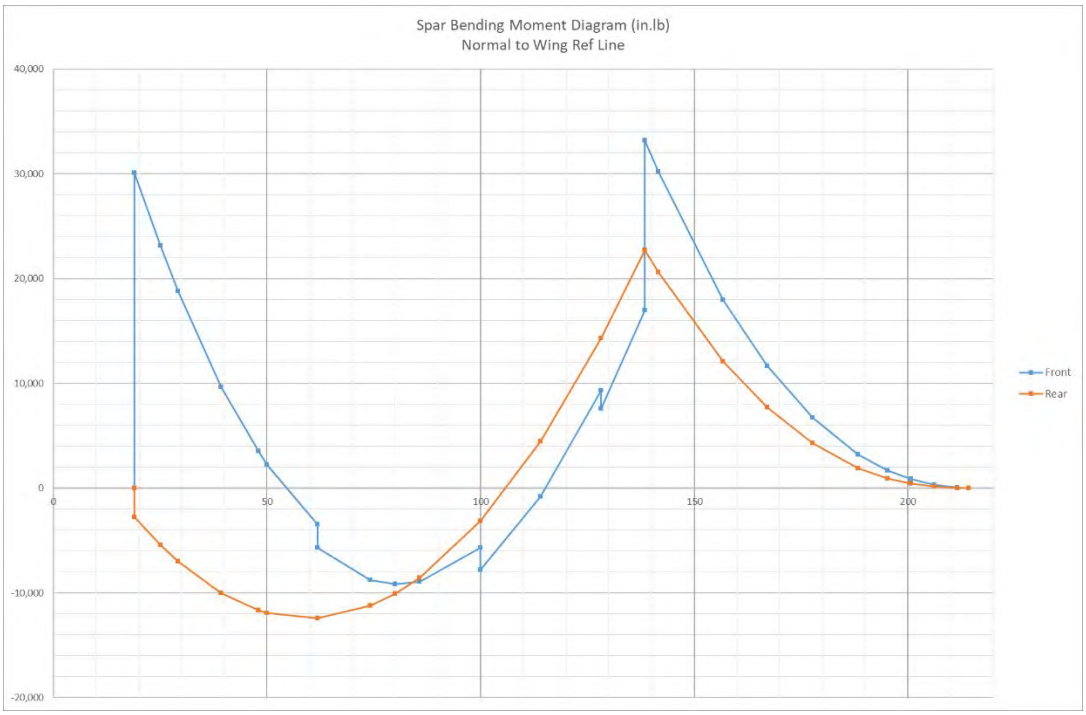

Figure 15-6 Spar Bending Moments for 3205 lb at 150 Knots and 3.8 g

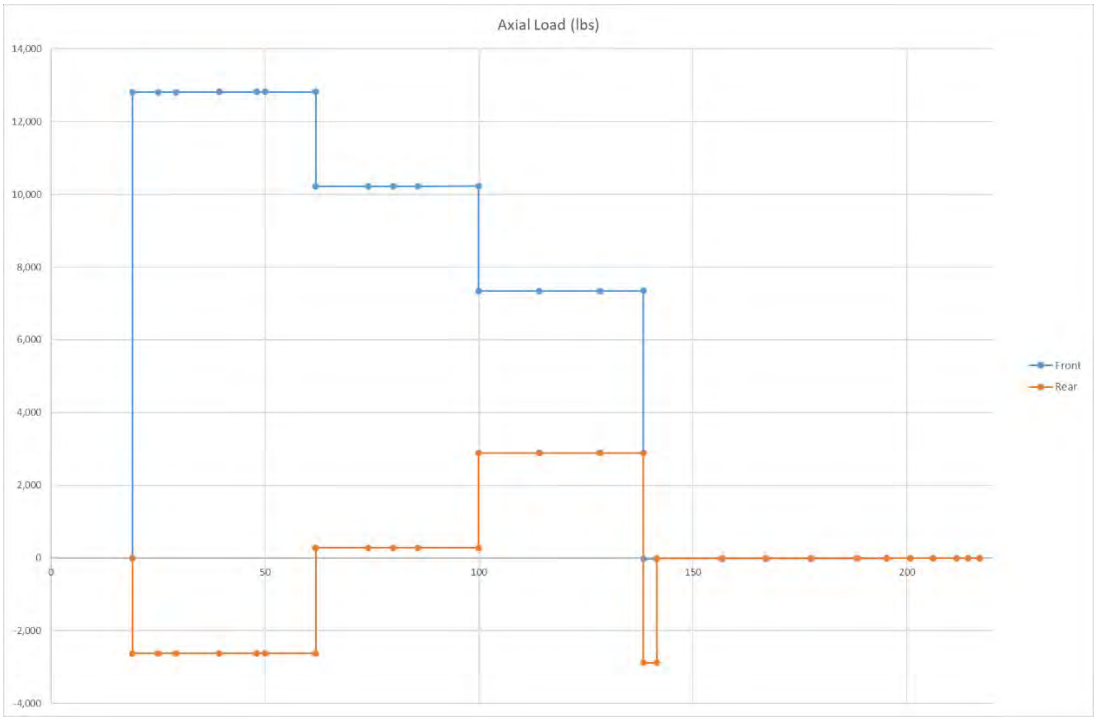

Figure 15-7 Spar Axial Loads for 3205 lb at 150 Knots and 3.8 g

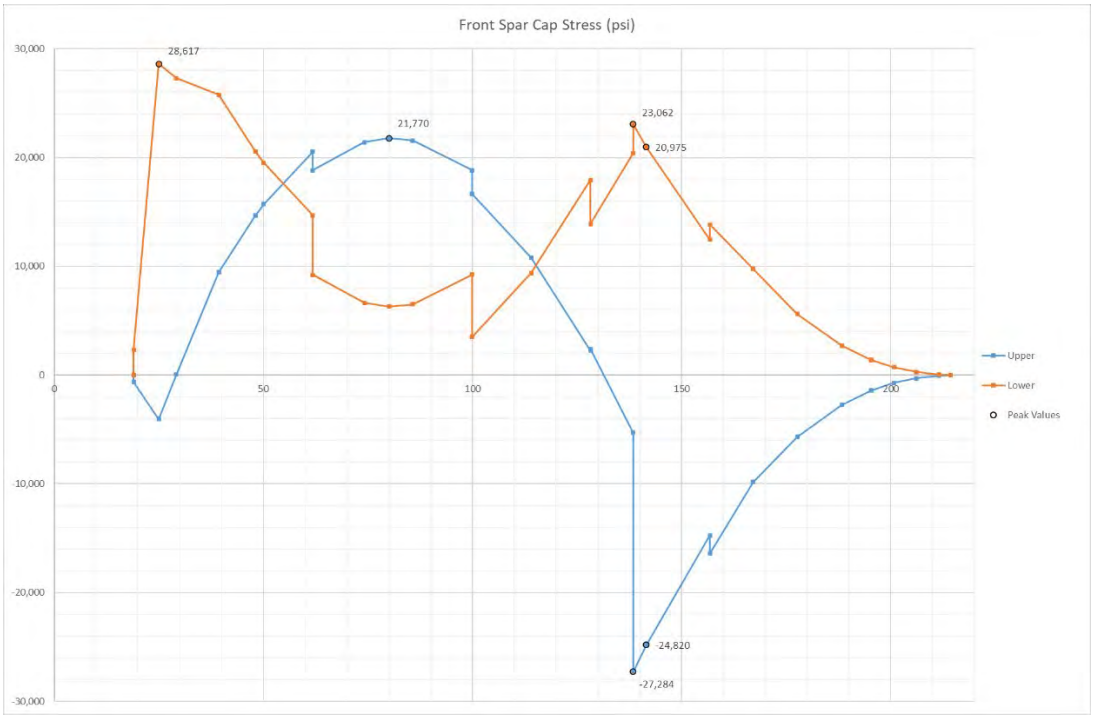

Figure 15-8 Front Spar Cap Stresses for 3205 lb at 150 Knots and 3.8 g

15.3 **Load Case: 2900 lb at 121 knots and 3.8 g**. This load case produced the highest spar cap tension stress 24,211 psi at the lower cap at the wing root. The peak compression stress is -27,156 psi in the upper cap at the strut attachment within the normal flight envelope. This is due to the high angle of attack reducing the effect of washout and creating higher loads at the outer wing. The stress asymmetry at the strut attachment is due to the reinforcing strap moving the neutral axis lower on the spar.

15.4 These stresses at the strut attachment will be over estimated slightly as the strut attachment is treated as a point load. In reality, the strut loads are stepped in over 6 fasteners which steps in the axial load (tension) from the strut. This would diminish the peak to be between -24,709 psi and -27,156 psi. Allowable limit stress is -25,333 psi.

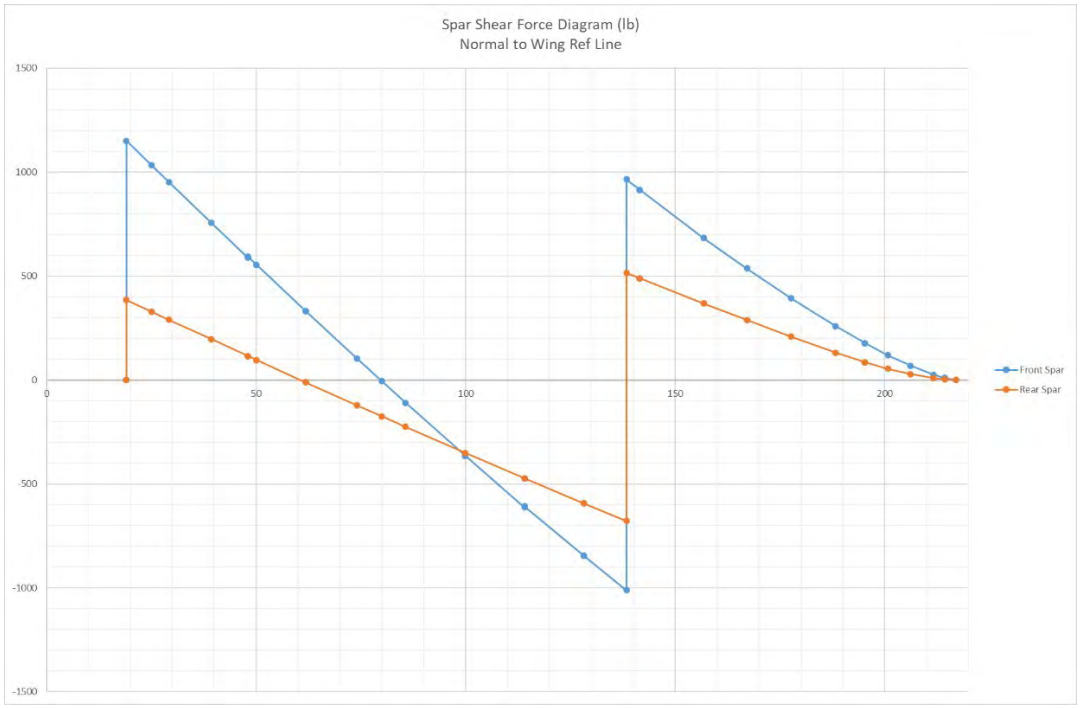

Figure 15-9 Spar Shear Force for 2900 lb at 121 Knots and 3.8 g

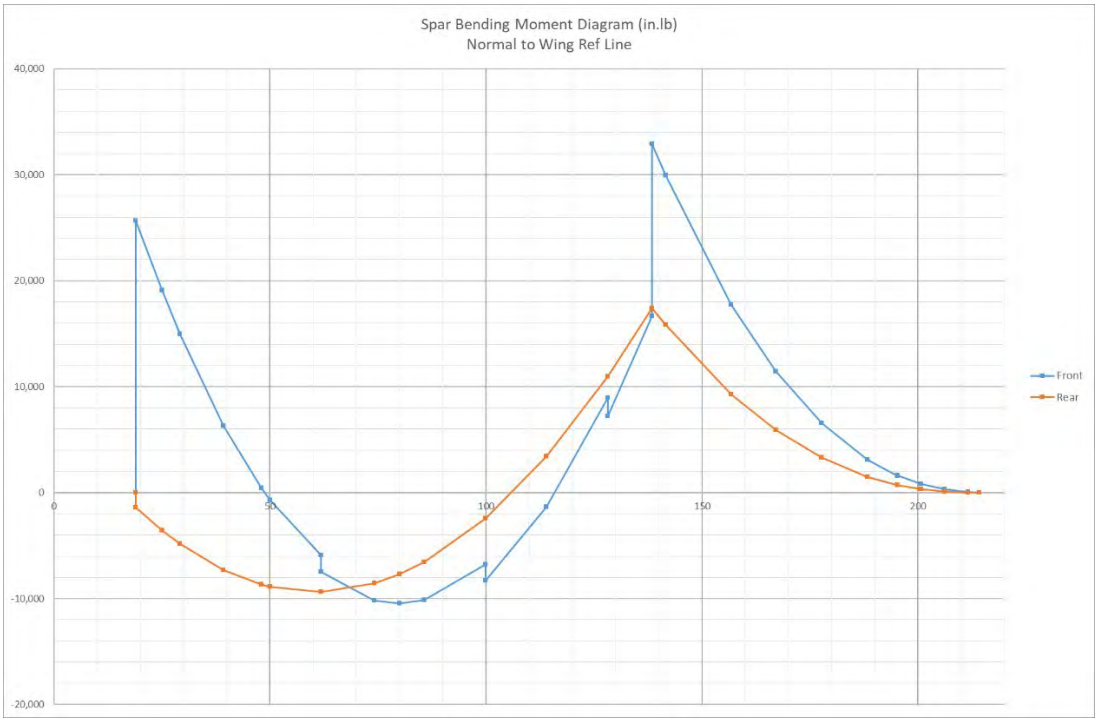

Figure 15-10 Spar Bending Moments for 2900 lb at 121 Knots and 3.8 g

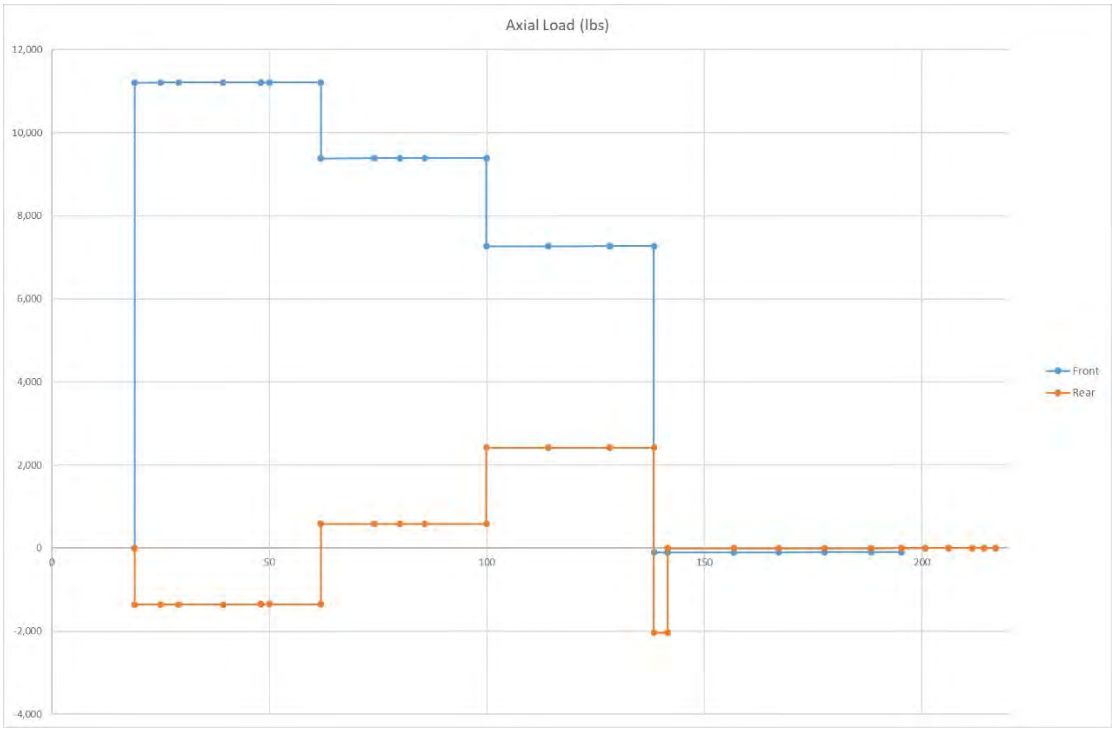

Figure 15-11 Spar Axial Loads for 2900 lb at 121 Knots and 3.8 g

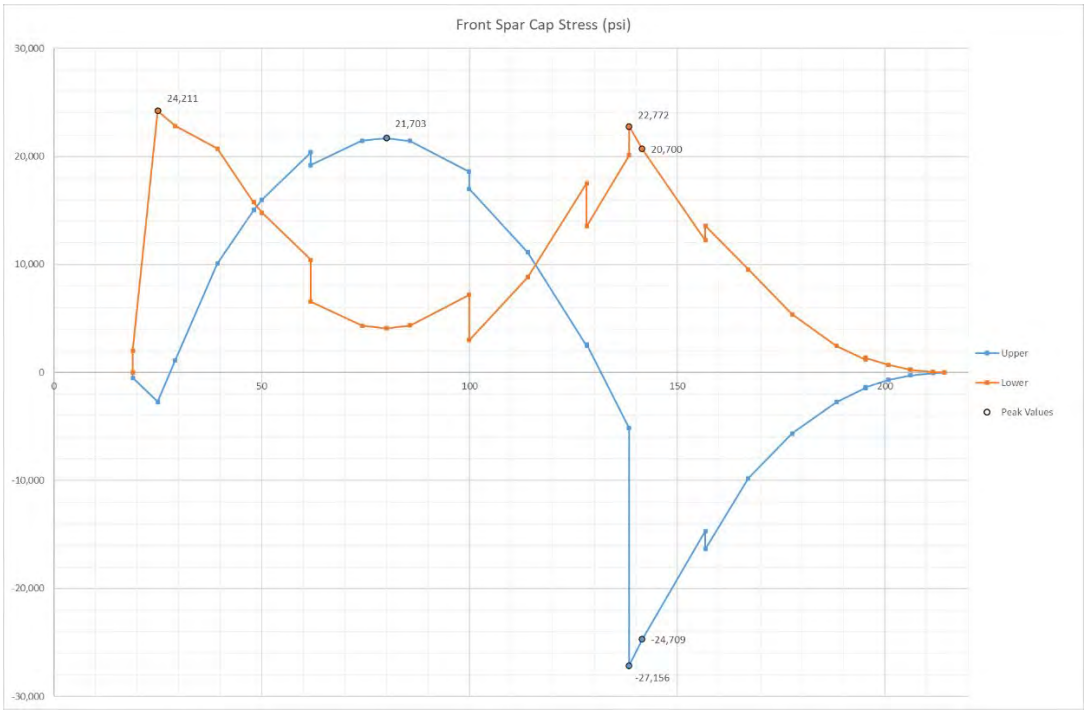

Figure 15-12 Front Spar Cap Stresses for 2900 lb at 121 Knots and 3.8 g

15.5 **Load Case: 2900 lb at 150 knots and 3.8 g**. This load case produced the highest spar cap stresses (within the normal flight envelope) 25,966 psi for the wing root at wing station 25. This is due to the lower angle of attack increasing the effect of washout and creating slightly higher loads at the inner wing. The high speed produces very high drag load which produces higher tension in the front spar. The maximum limit stress is 25,333 psi. The spreadsheet is overestimating the stresses by 2.5% compared to the assumed Piper maximum stress, possibly from the inclusion of the tail down load at the forward centre of gravity limit.

15.6 Inboard of wing station 25, the axial tension and bending is drawn into the wing root fittings. This results in a decrease in cap stresses.

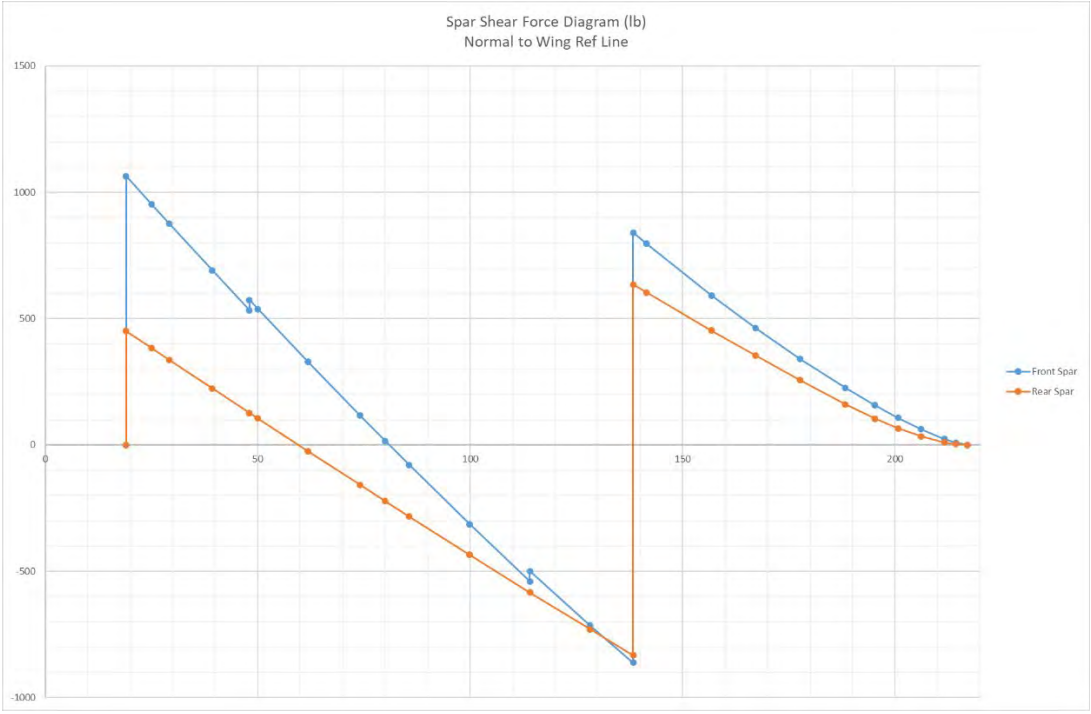

Figure 15-13 Spar Shear Force for 2900 lb at 150 Knots and 3.8 g

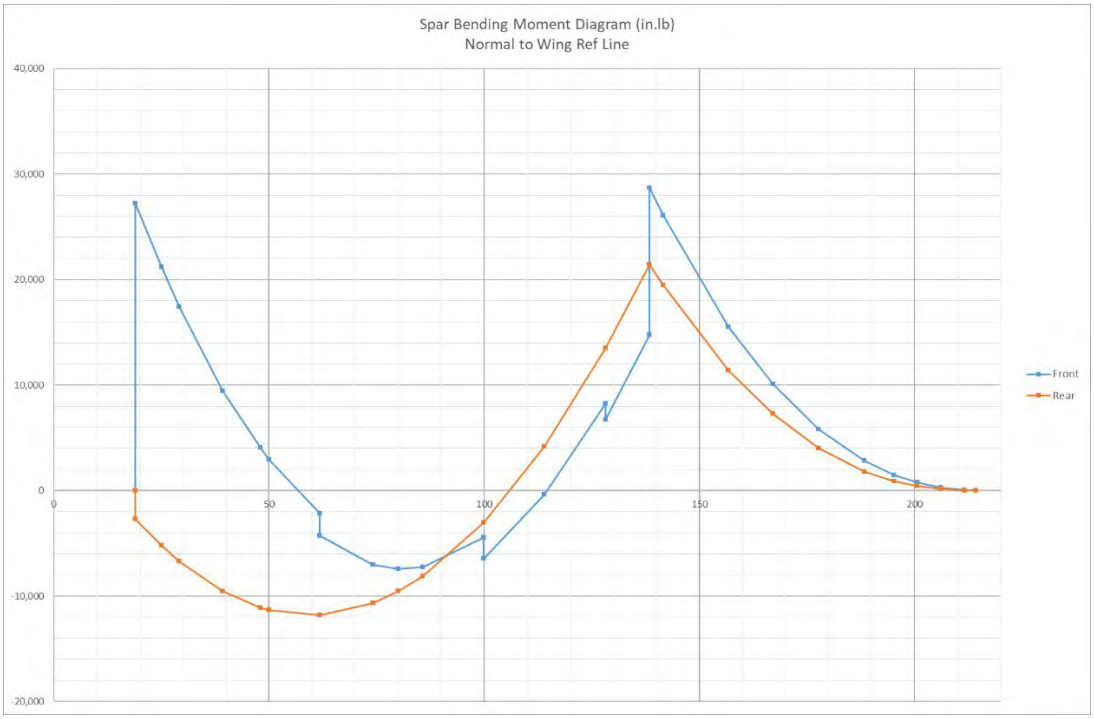

Figure 15-14 Spar Bending Moment for 2900 lb at 150 Knots and 3.8 g

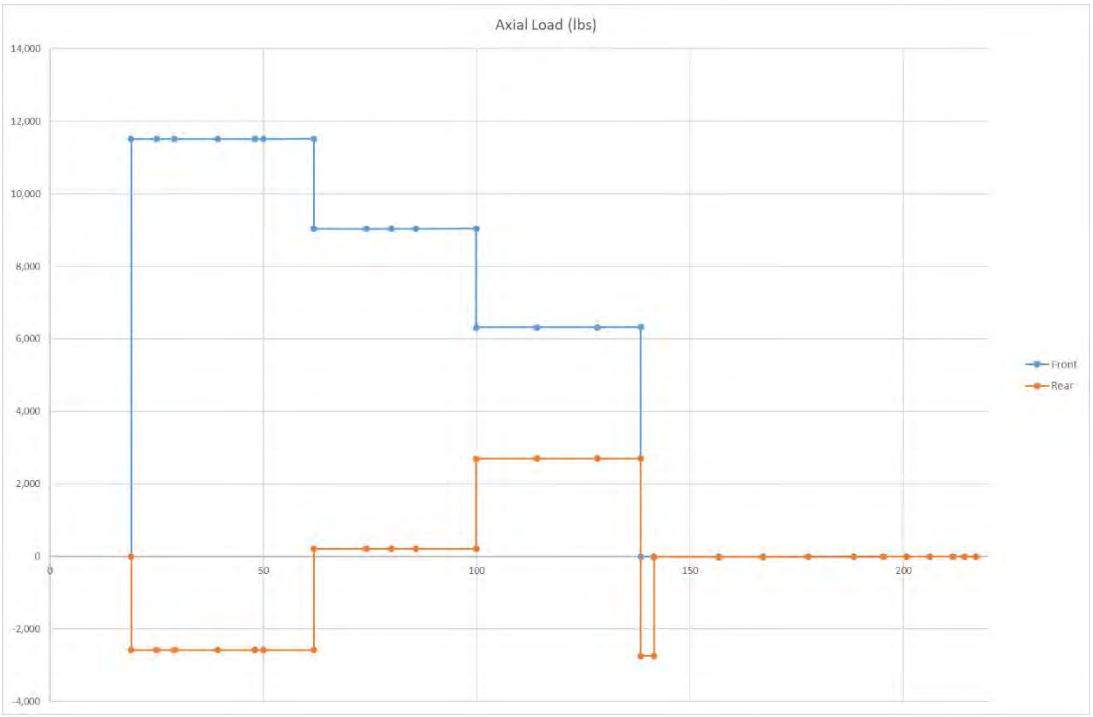

Figure 15-15 Spar Axial Loads for 2900 lb at 150 Knots and 3.8 g

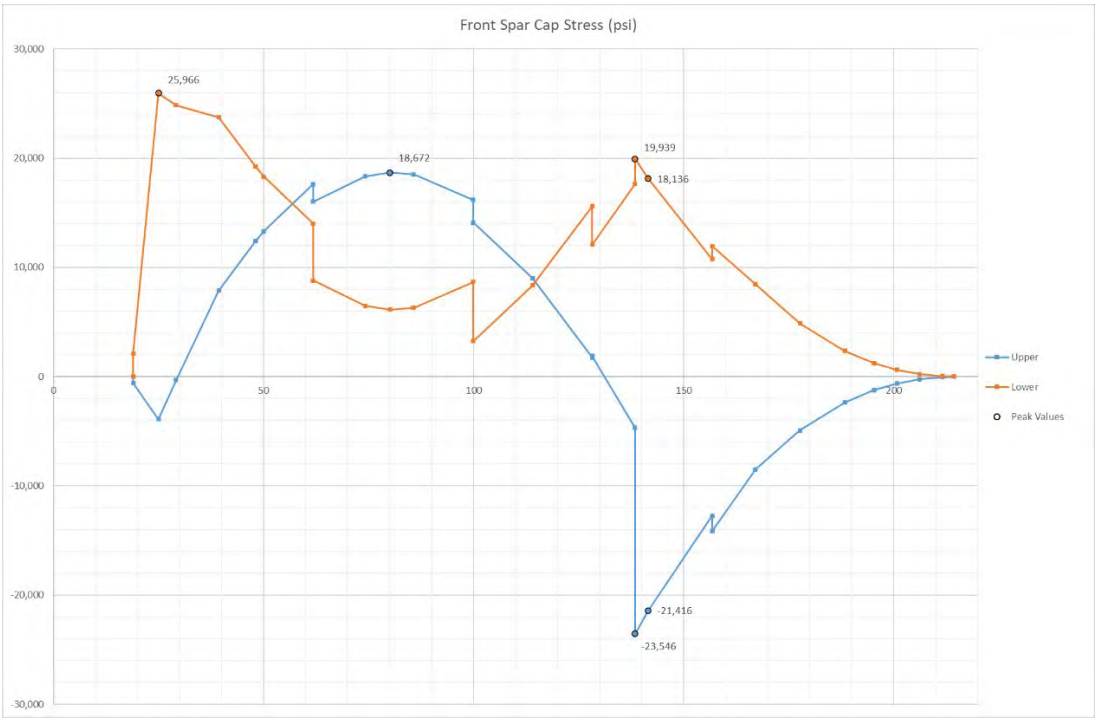

Figure 15-16 Front Spar Cap Stresses for 2900 lb at 150 Knots and 3.8 g

15.7 **Load Case: 2005 lb at 101 knots and 3.8 g**. This is the single seat aerotow comparative case to the agricultural 2900 lb at 121 kts and 3.8 g. Stresses are reduced by ~35% consistent with the reduction in weight of non flying parts.

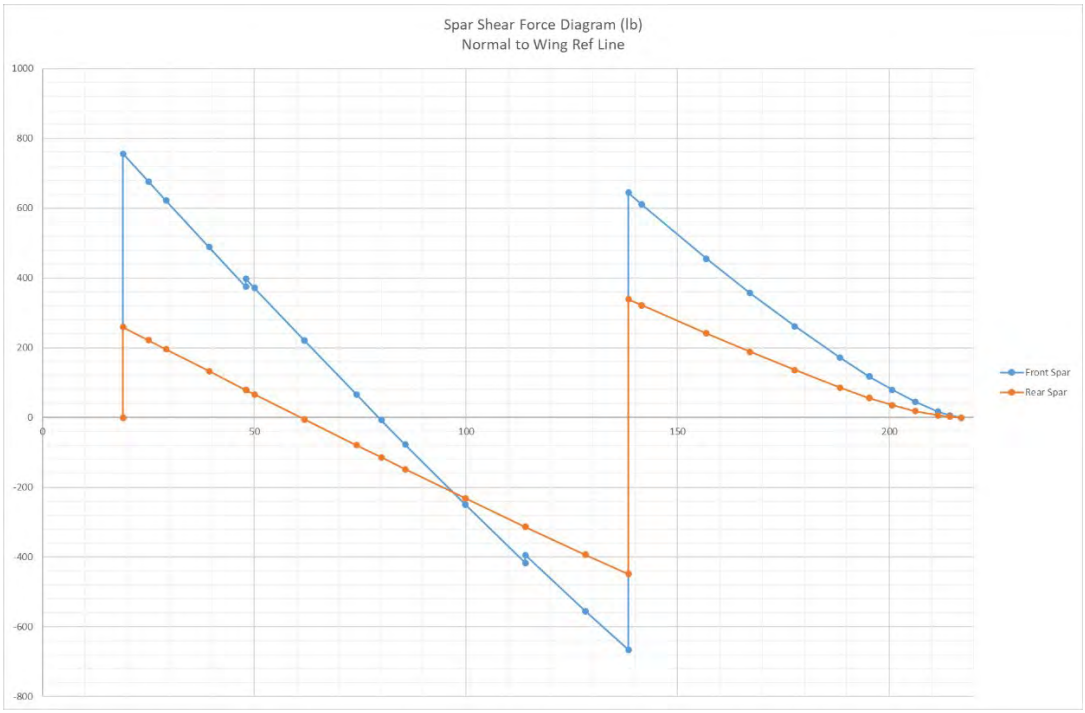

Figure 15-17 Spar Shear Force for 2005 lb at 101 Knots and 3.8 g

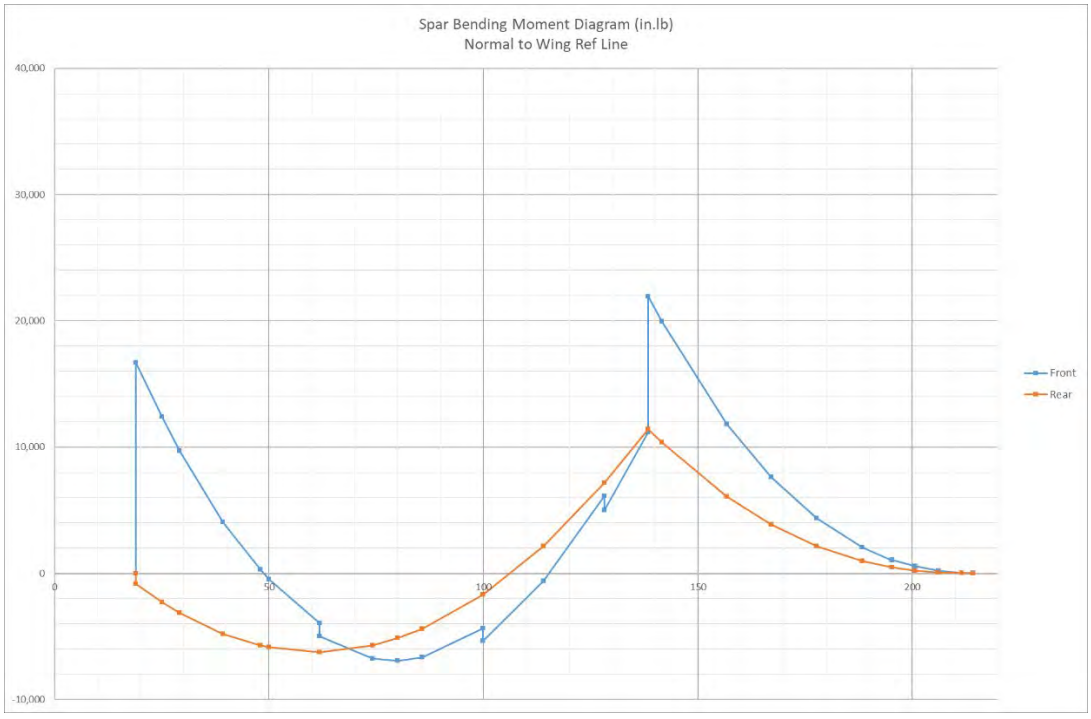

Figure 15-18 Spar Bending Moment for 2005 lb at 101 Knots and 3.8 g

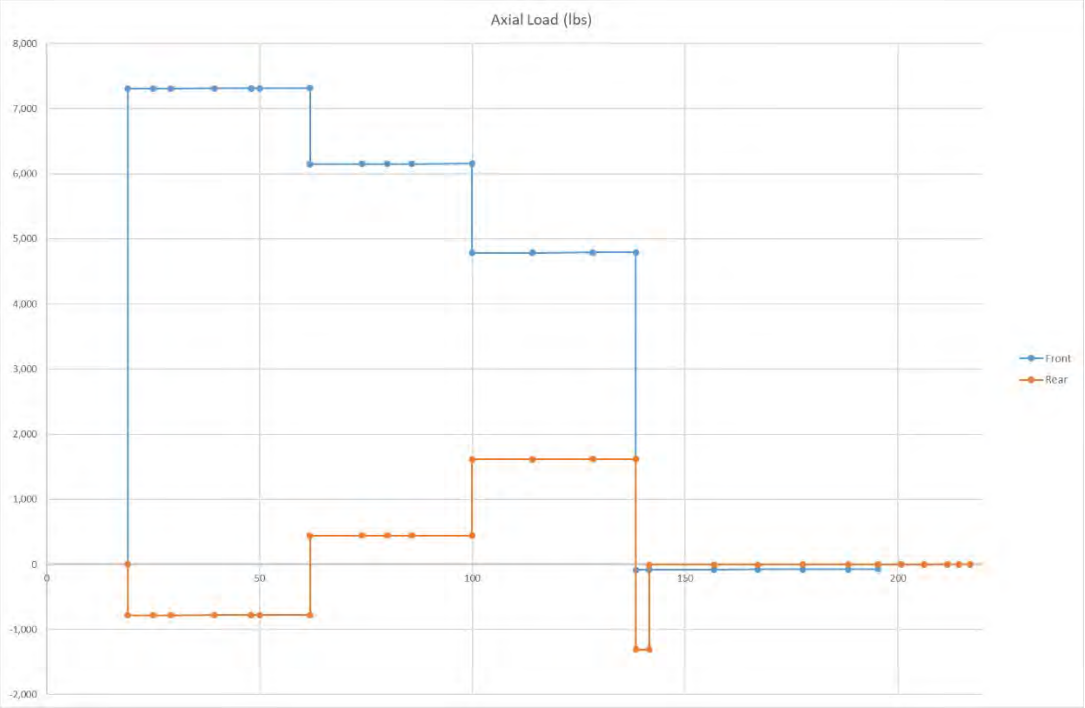

Figure 15-19 Spar Axial Loads for 2005 lb at 101 Knots and 3.8 g

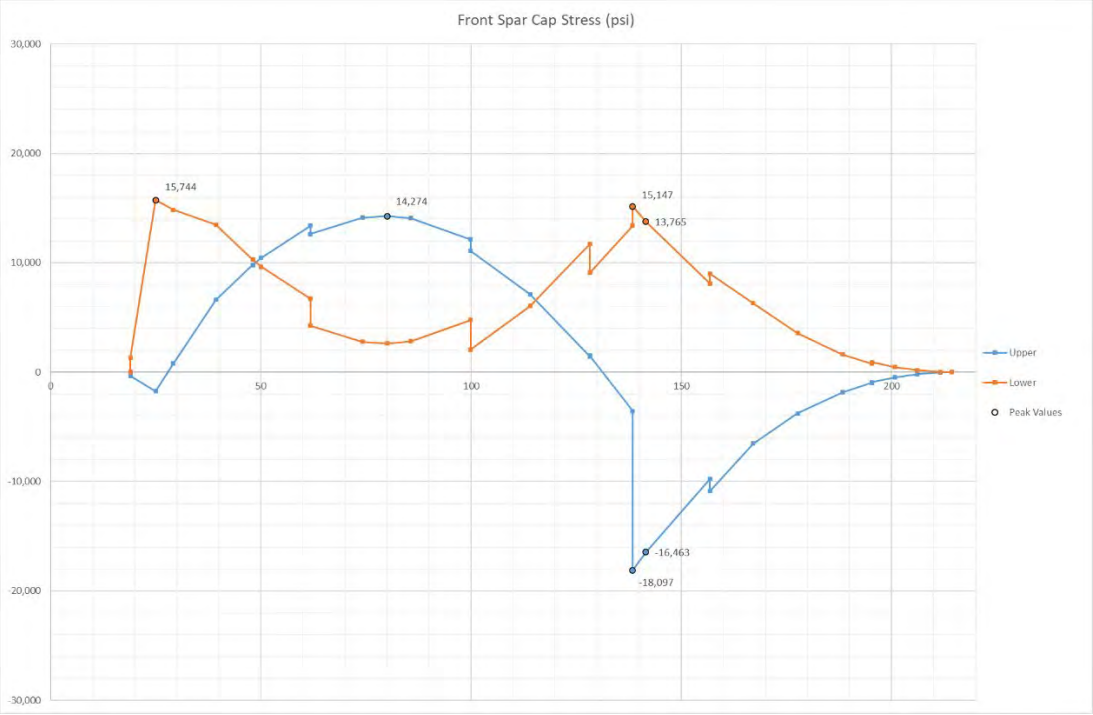

Figure 15-20 Front Spar Cap Stress for 2005 lb at 101 Knots and 3.8 g

15.8 **Load Case: 2005 lb at 113 knots and 27.7 ft/sec gust**. The lower wing loading produces a large g response to a gust of the same velocity. This increased g response reduces the reduction in stresses due to operating a lower weight.

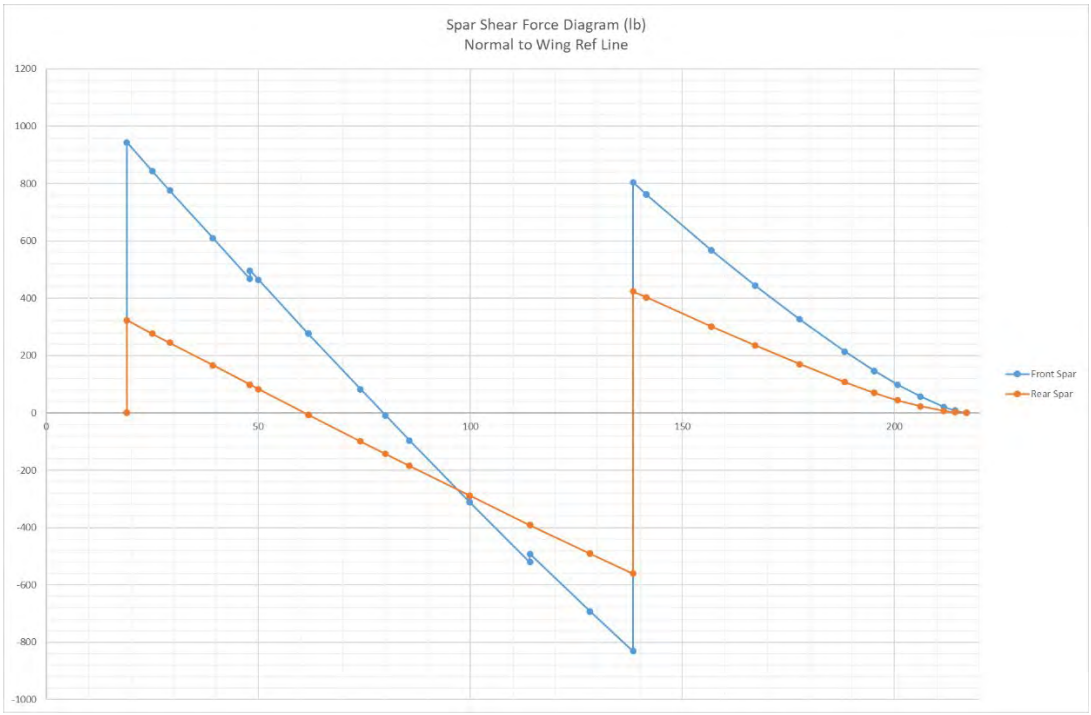

Figure 15-21 Spar Shear Force for 2005 lb at 113 Knots and 27.7 ft/sec gust

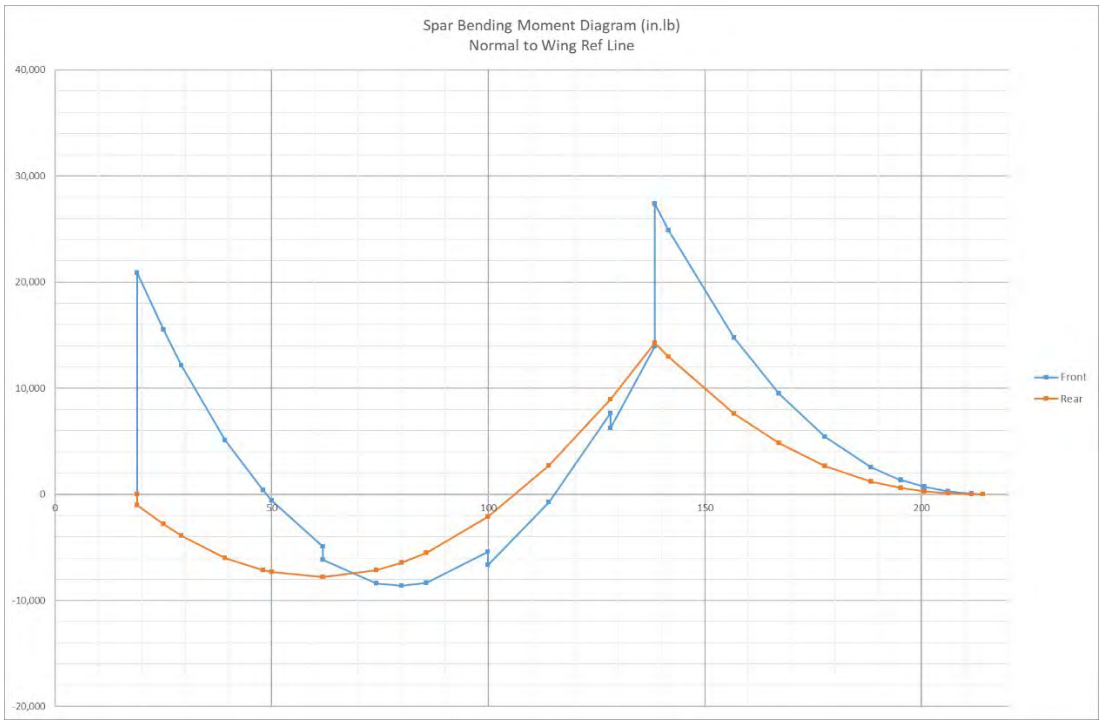

Figure 15-22 Spar Bending Moment for 2005 lb at 113 Knots and 27.75 ft/sec gust

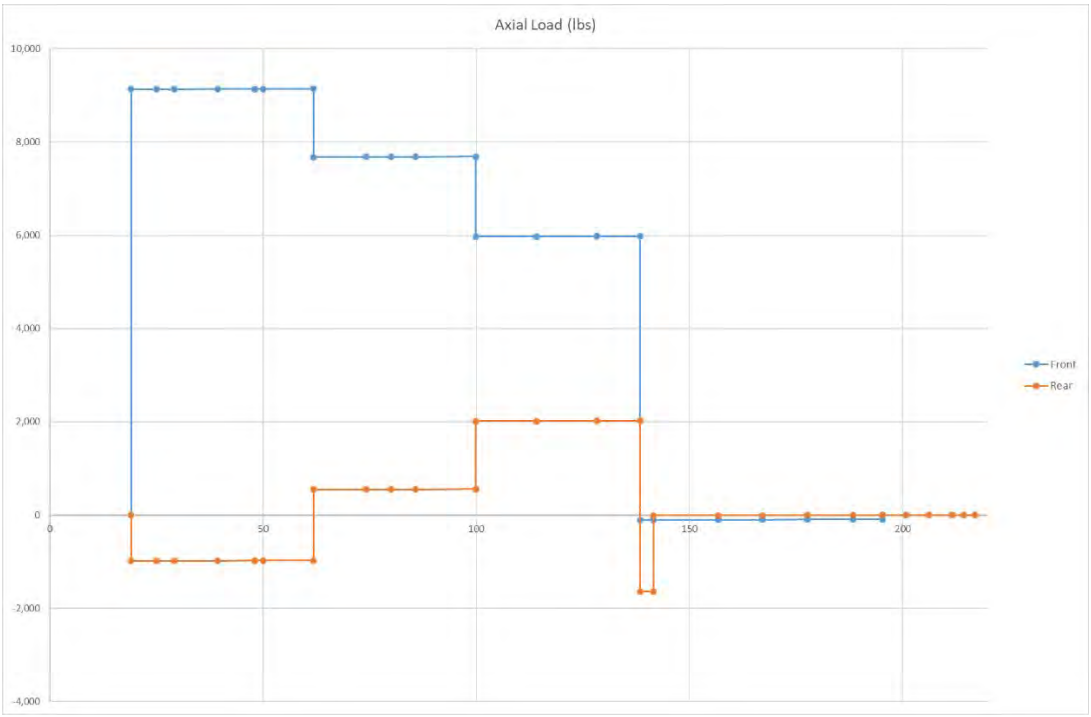

Figure 15-23 Spar Axial Loads for 2005 lb at 113 Knots and 27.7 ft/sec gust

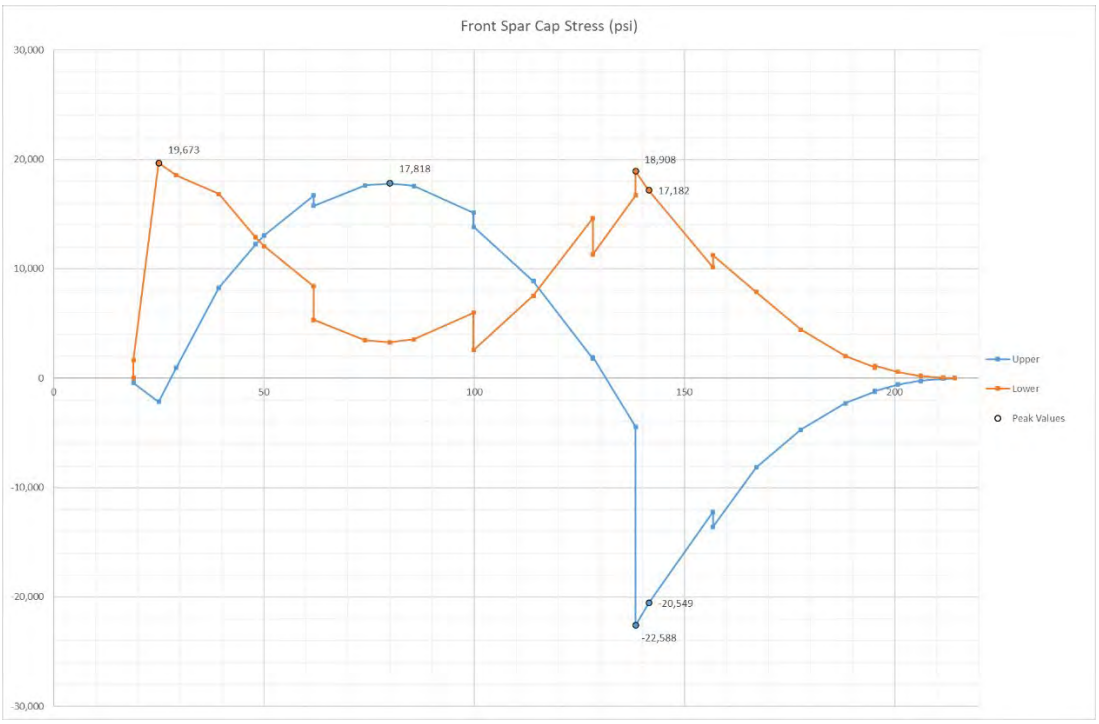

Figure 15-24 Front Spar Cap Stress for 2005 lb at 113 Knots and 27.7 ft/sec gust

15.9 **Load Case: 2005 lb at 150 knots and 3.8 g**.

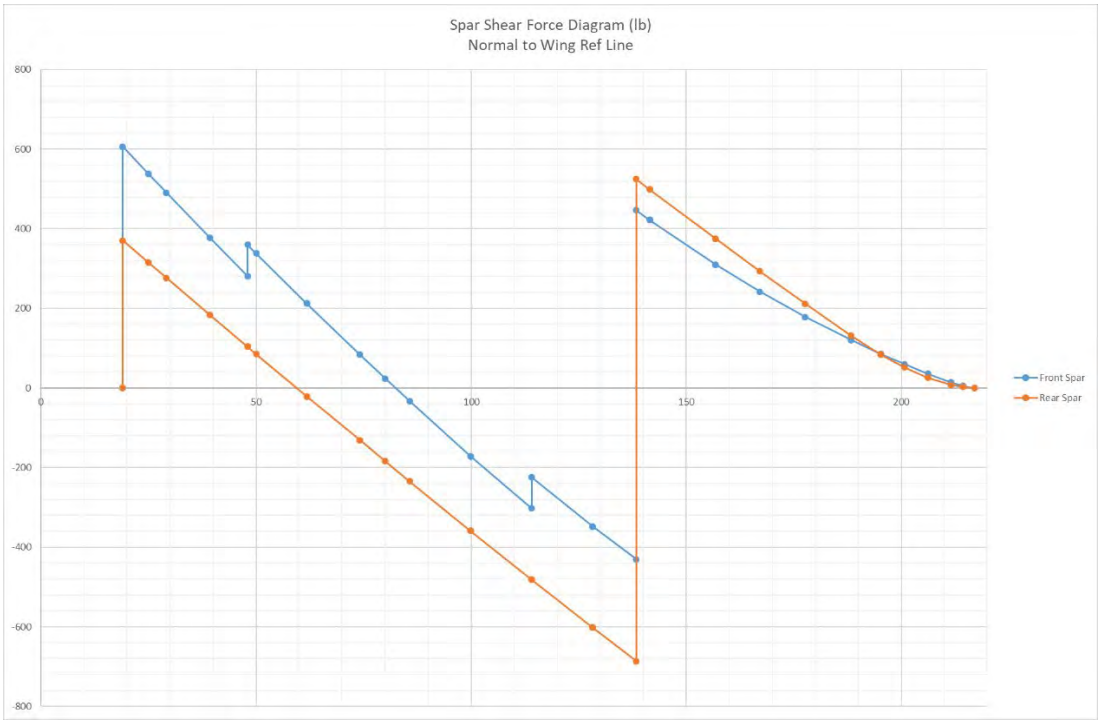

Figure 15-25 Spar Shear Force for 2005 lb at 150 Knots and 3.8 g

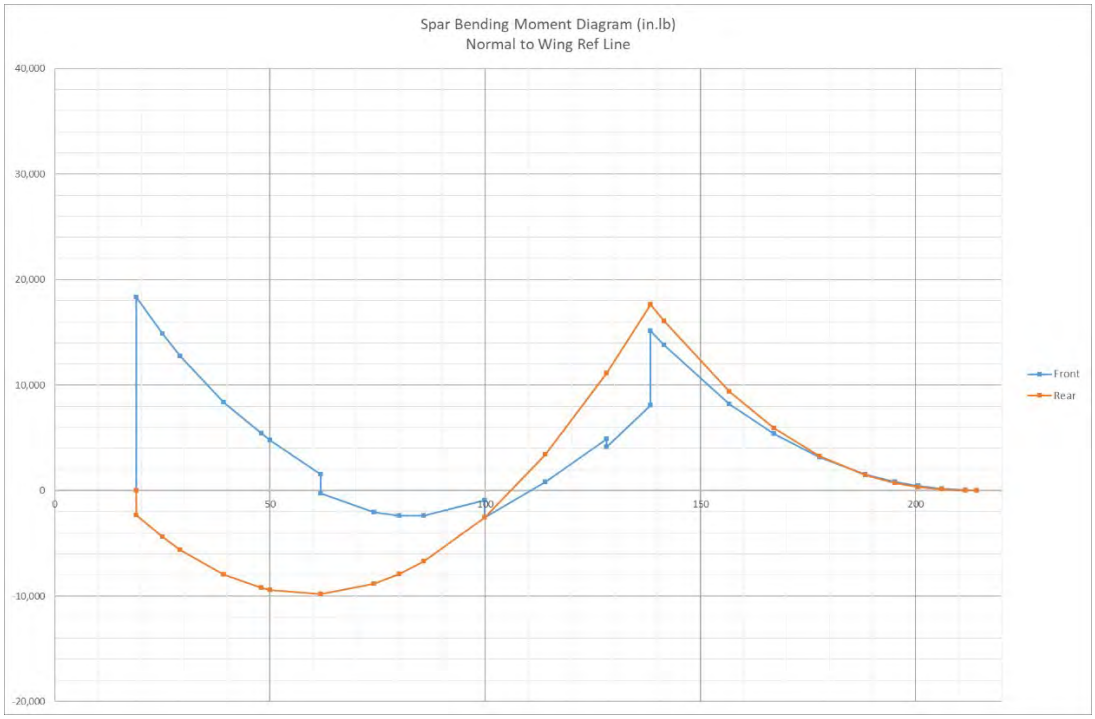

Figure 15-26 Spar Bending Moment for 2005 lb at 150 Knots and 3.8 g

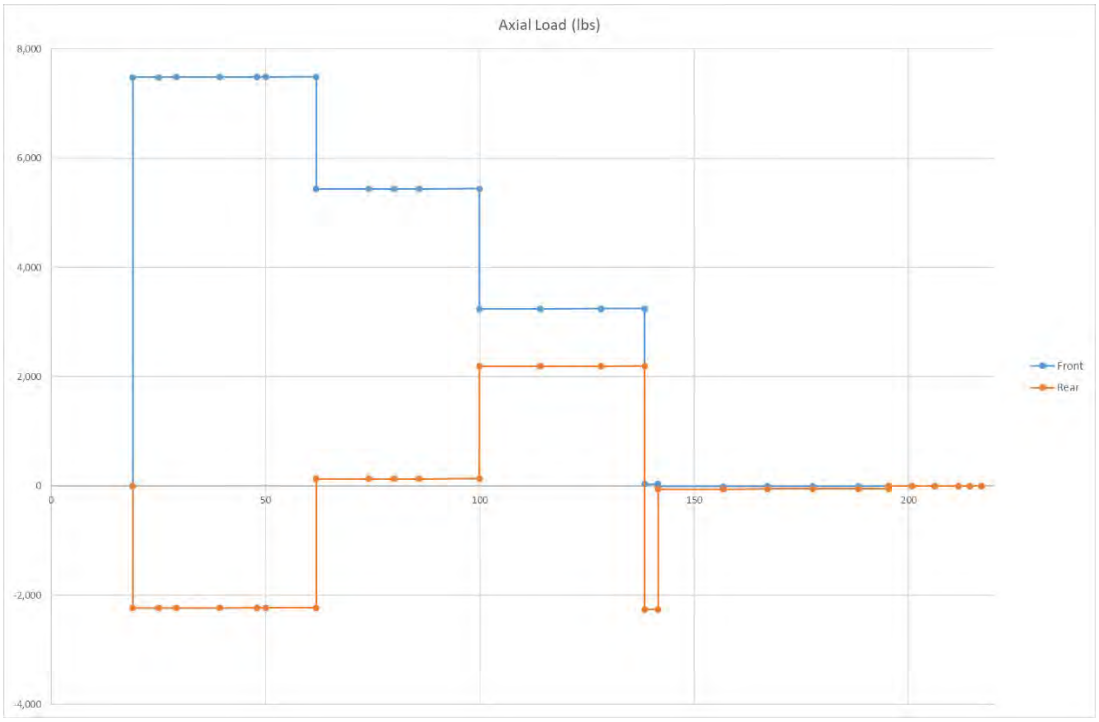

Figure 15-27 Spar Axial Loads for 2005 lb at 150 Knots and 3.8 g

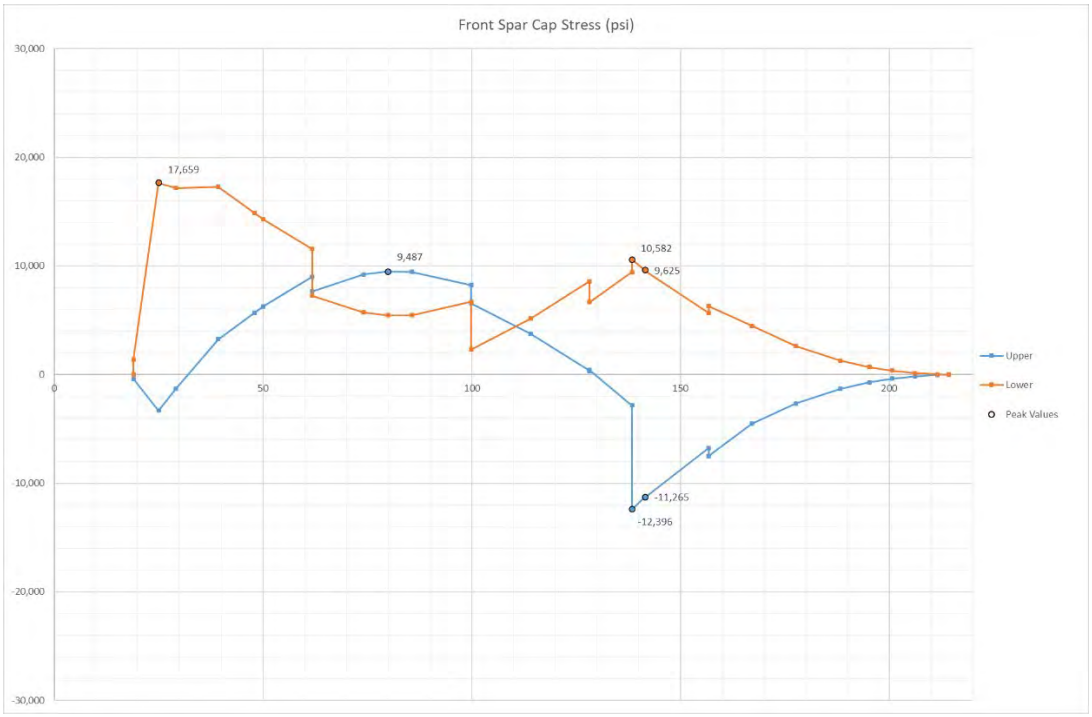

Figure 15-28 Front Spar Cap Stress for 2005 lb at 150 Knots and 3.8 g

16. PAWNEE B AND C RESULTS – GLIDER TOWING

16.1 **Load Case: 2205 lb at 106 knots and 3.8g**. This is the single seat glider towing at 2205 lb (1000 kg) comparative case to the agricultural 2900 lb at 121 kts and 3.8 g. Stresses are reduced by ~27% with 17,666 psi at wing station 25 and 16,856 psi / -20,125 psi at the strut connection.

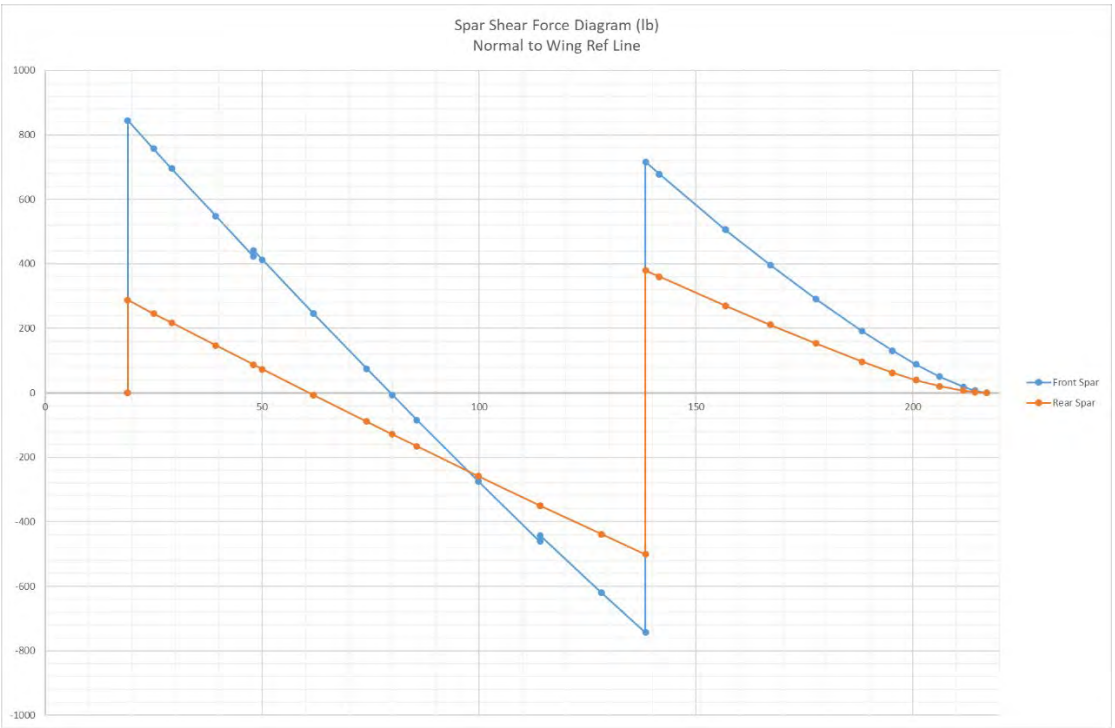

Figure 16-1 Spar Shear Force for 2205 lb at 106 Knots and 3.8 g

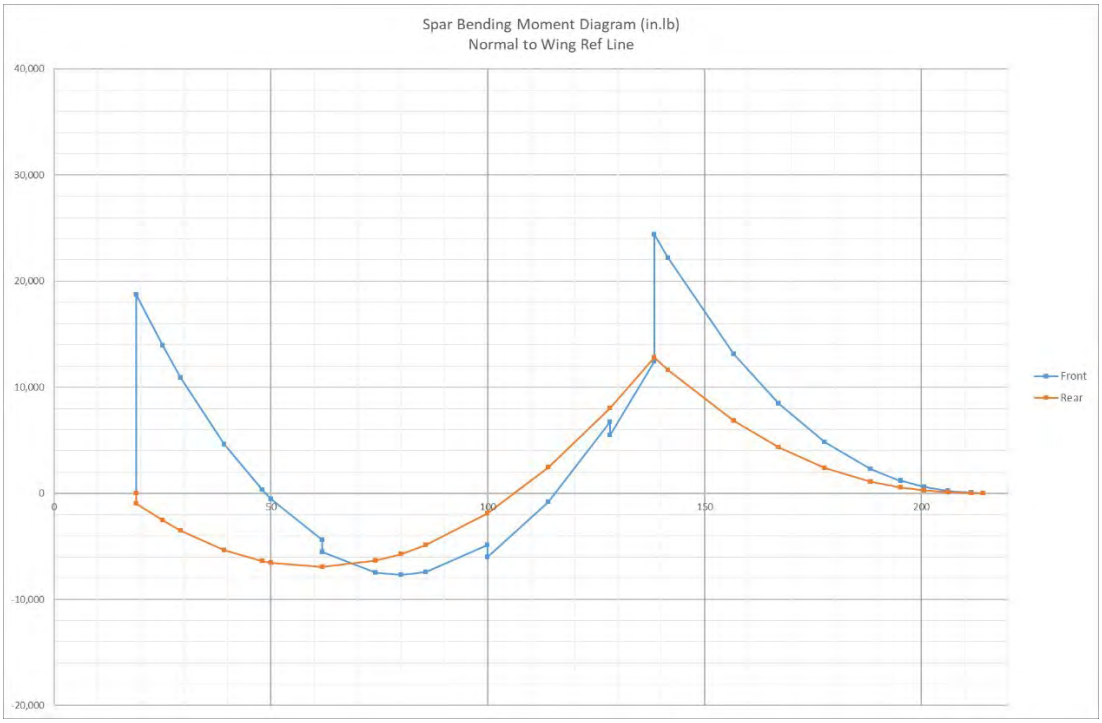

Figure 16-2 Spar Bending for 2205 lb at 106 Knots and 3.8 g

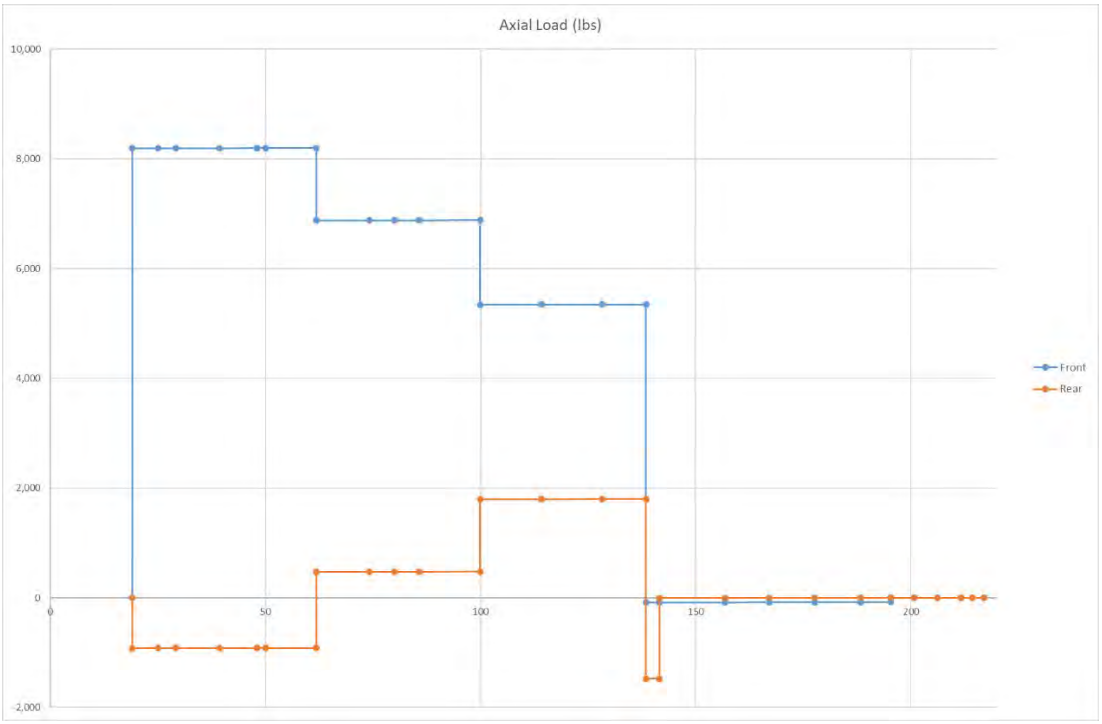

Figure 16-3 Spar Axial Loads for 2206 lb at 106 Knots and 3.8 g

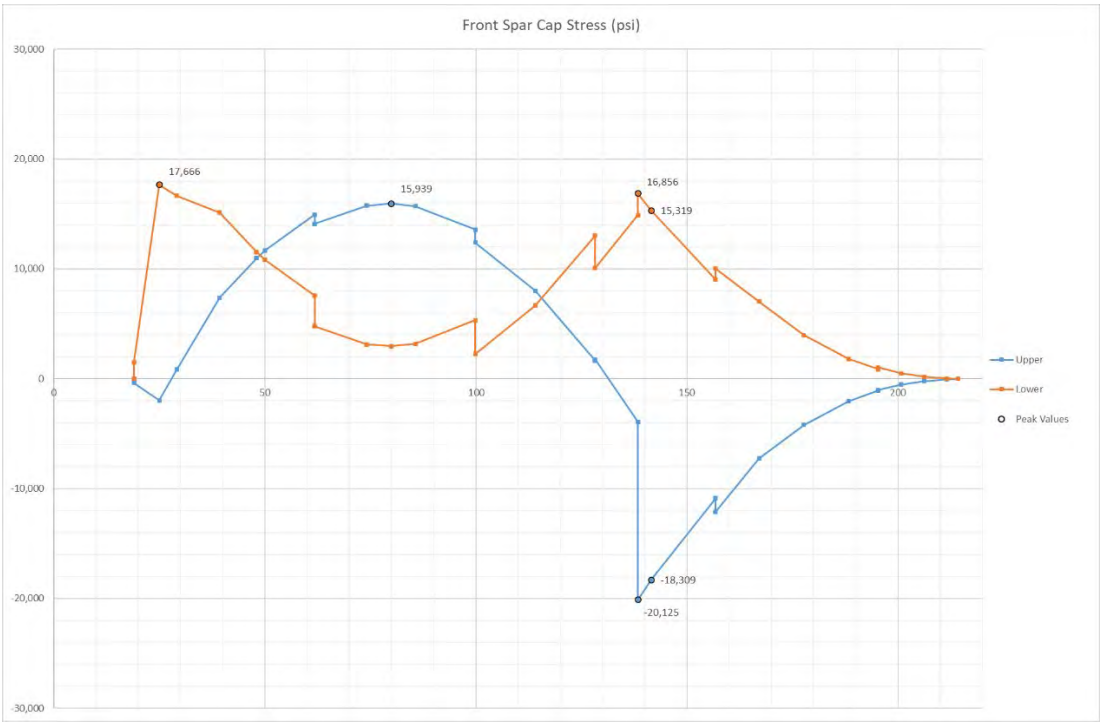

Figure 16-4 Front Spar Cap Stress for 2205 lb at 106 Knots and 3.8 g

16.2 **Load Case: 2205 lb at 114 knots and 27.1 ft/sec gust**. This is the single seat glider towing comparative gust case.

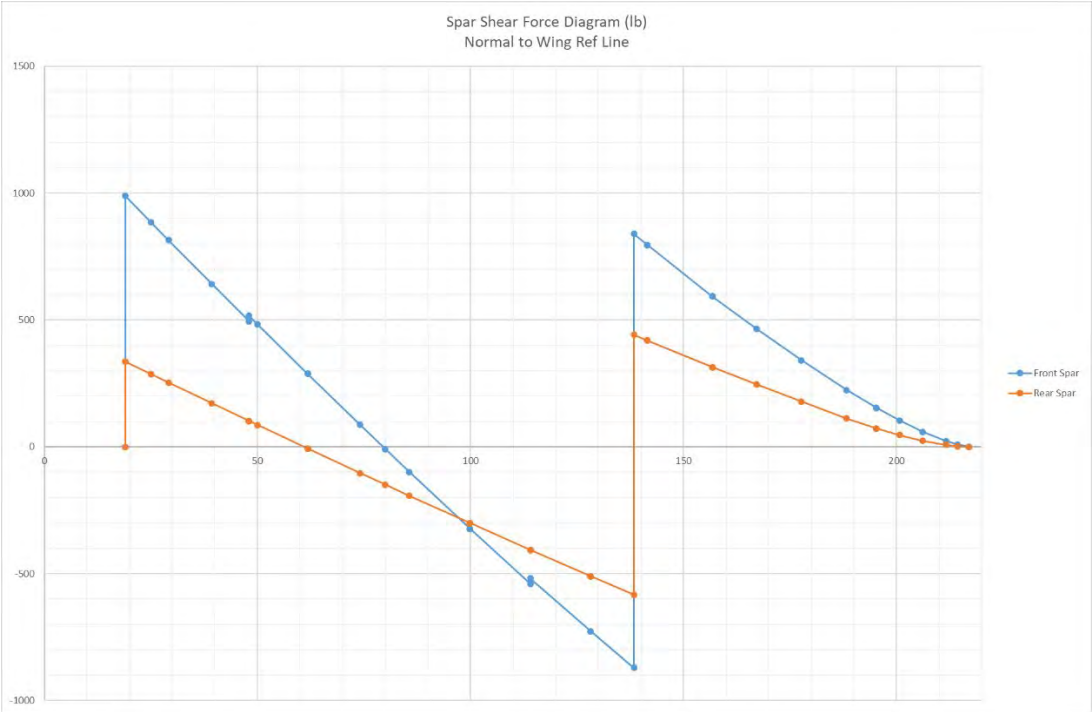

Figure 16-5 Spar Shear Force for 2205 lb at 114 knots and 27.1 ft/sec gust

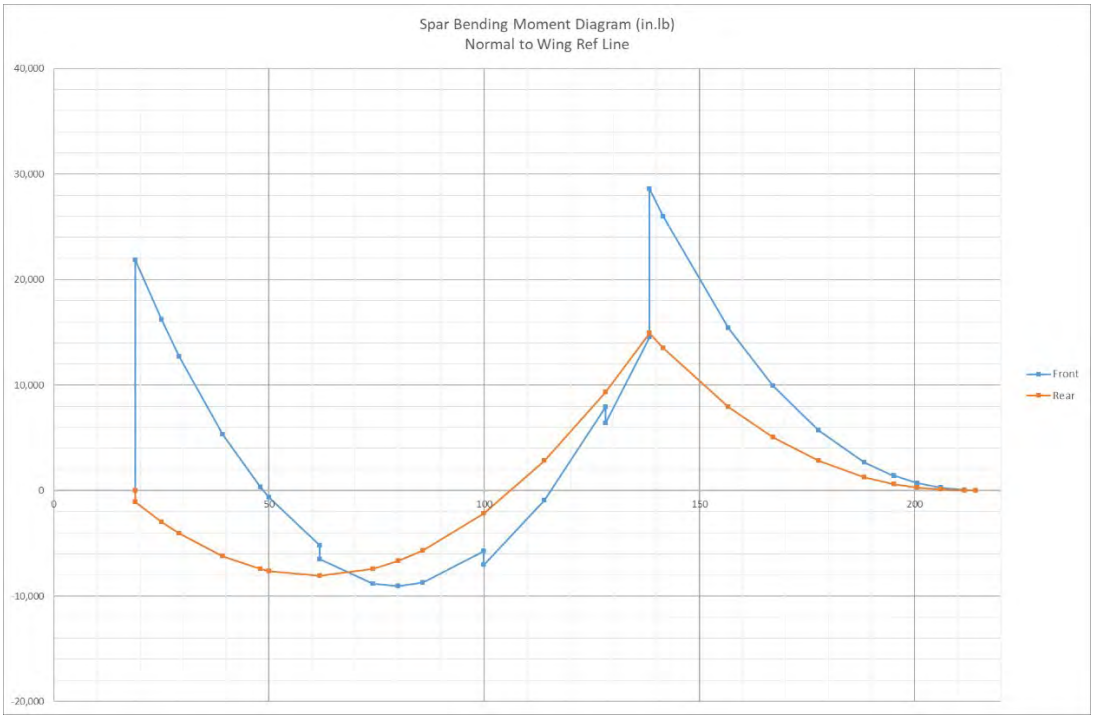

Figure 16-6 Spar Bending for 2205 lb at 114 knots and 27.1 ft/sec gust

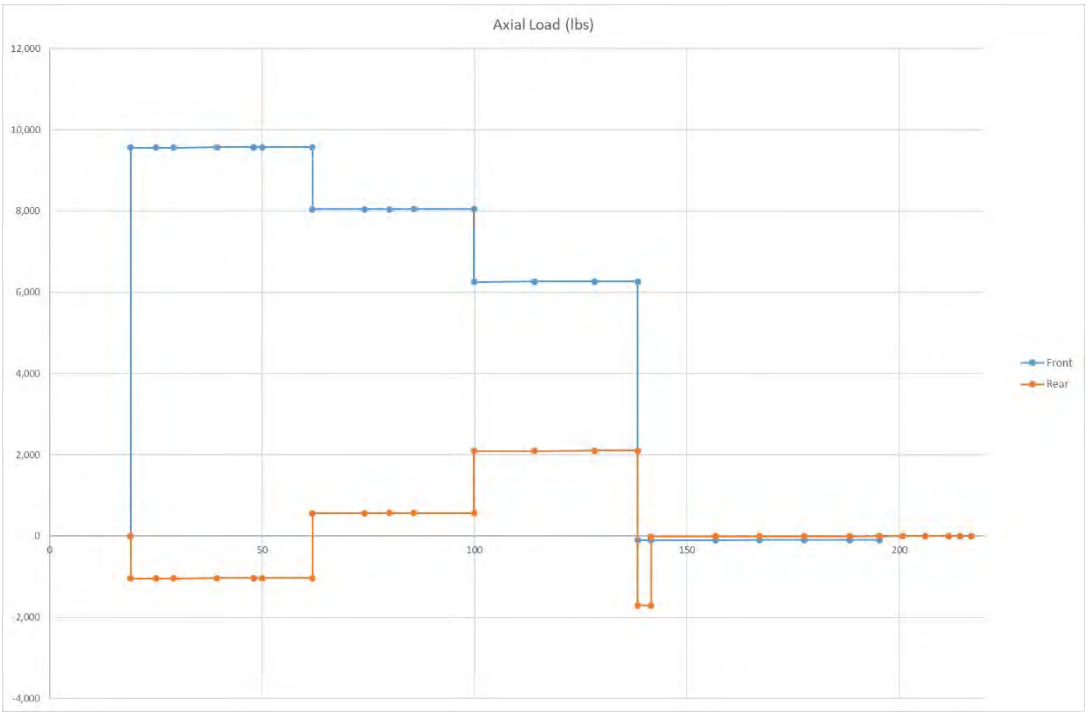

Figure 16-7 Spar Axial Loads for 2205 lb at 114 knots and 27.1 ft/sec gust g

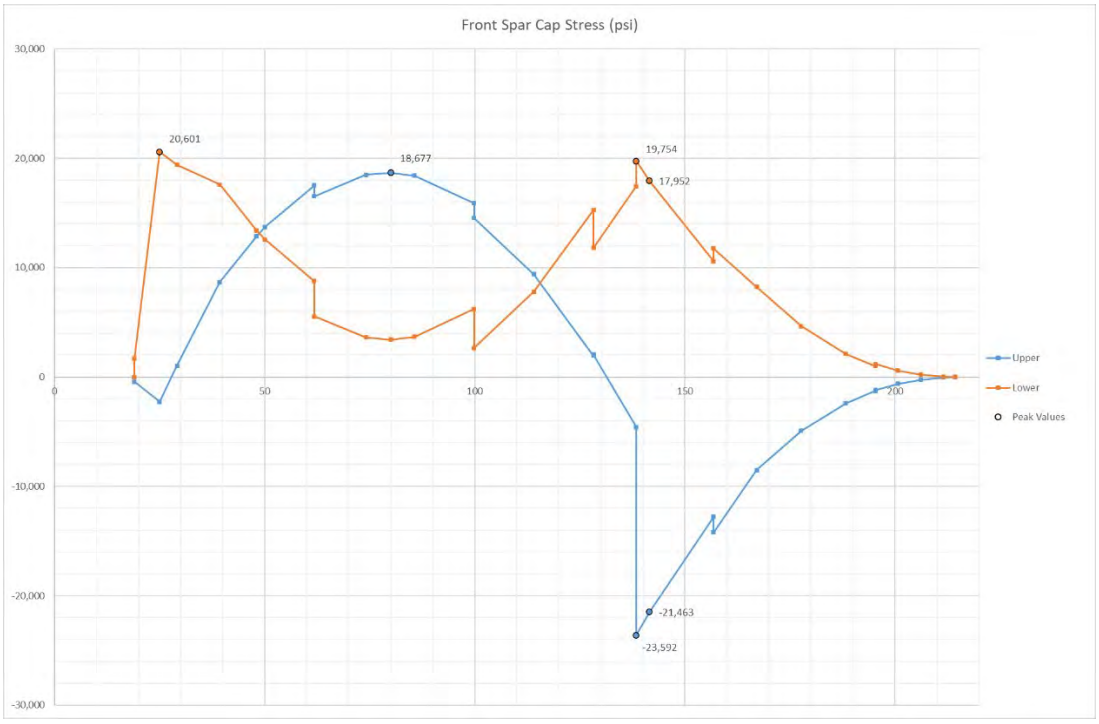

Figure 16-8 Front Spar Cap Stress for 2205 lb at 114 knots and 27.1 ft/sec gust

16.3 **Load Case: 2205 lb at 150 knots and 3.8 g**. This is the single seat glider towing comparative case to the agricultural 2900 lb at 150 kts and 3.8 g. Stresses are reduced by ~25% with 19,585 psi at wing station 25 and ~37% with 12,696 psi / -14,909 psi at the strut connection. The non-proportional increase in the stress at the strut attachment is due to the change in angle of attack.

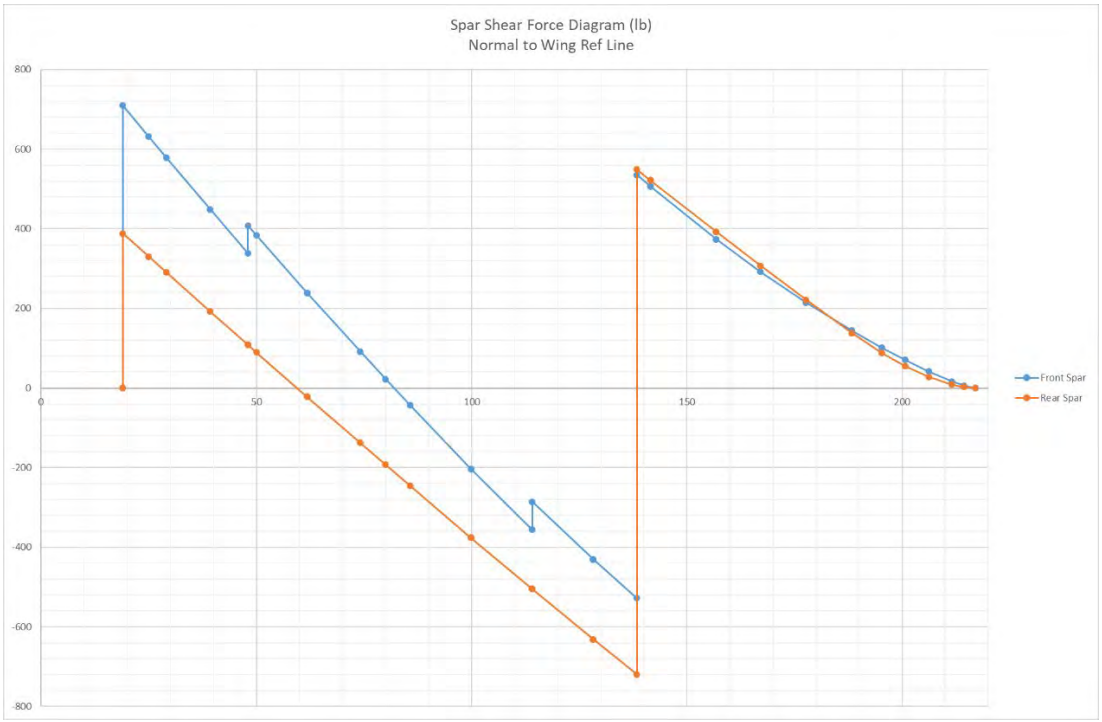

Figure 16-9 Spar Shear Force for 2205 lb at 150 Knots and 3.8 g

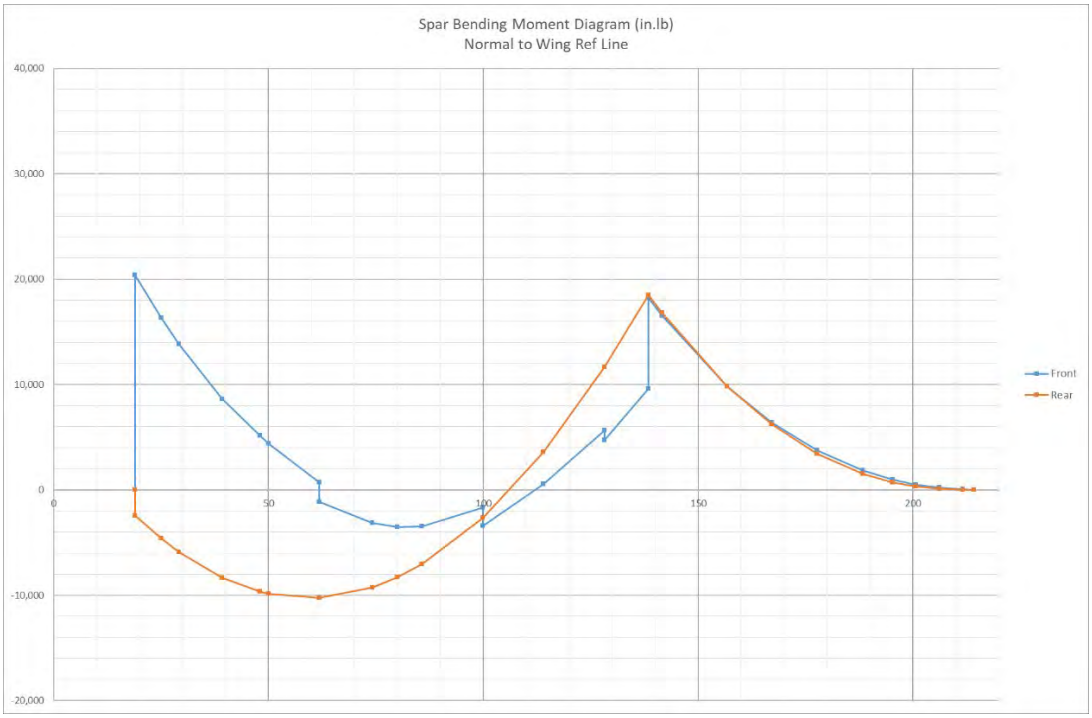

Figure 16-10 Spar Bending for 2205 lb at 150 Knots and 3.8 g

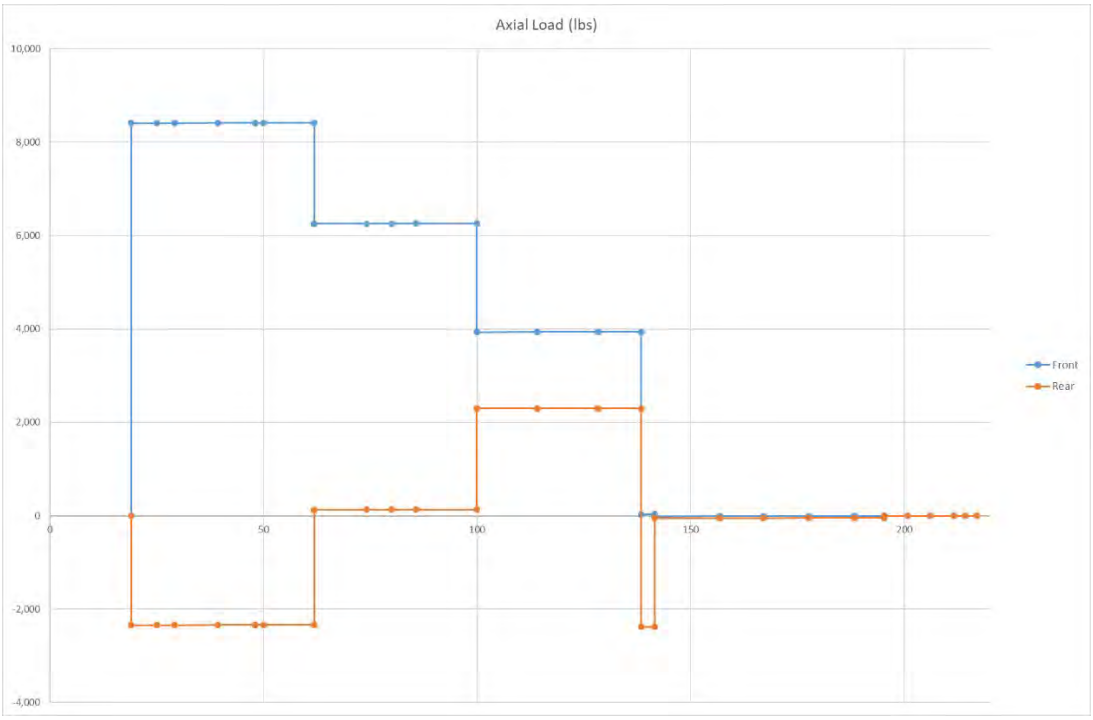

Figure 16-11 Spar Axial Loads for 2205 lb at 150 Knots and 3.8 g

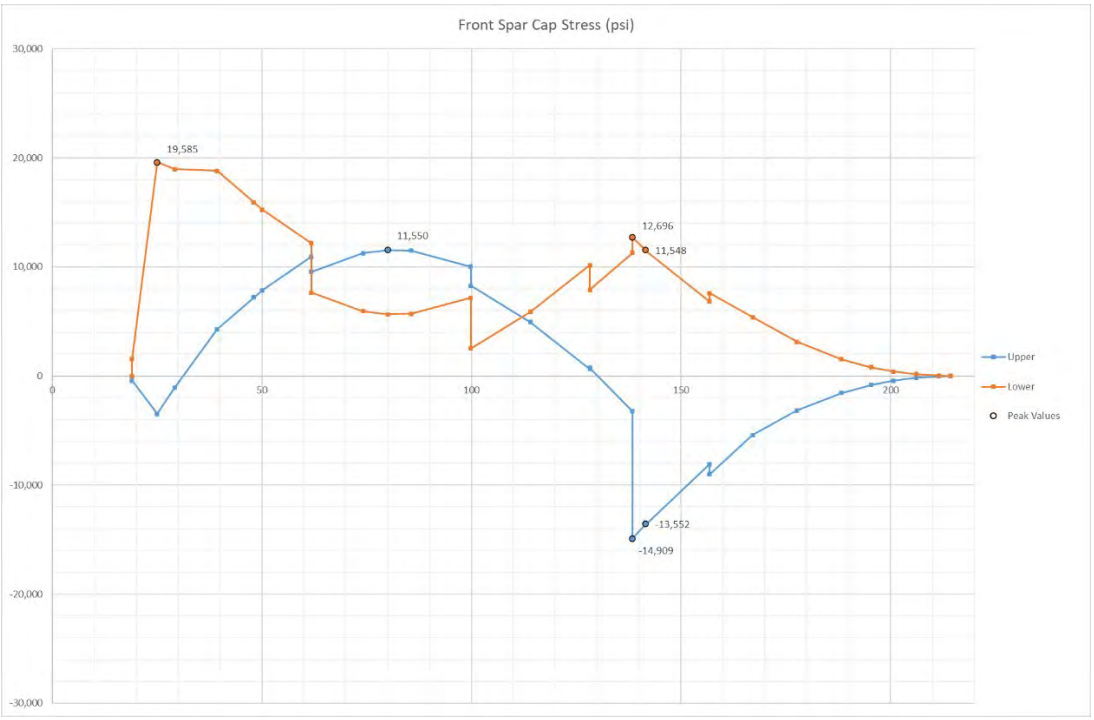

Figure 16-12 Front Spar Cap Stress for 2205 lb at 150 Knots and 3.8 g

16.4 **Load Case: 2460 lb at 112 knots and 3.8 g**. This is the dual seat aerotow comparative case to the agricultural 2900 lb at 121 kts and 3.8 g.

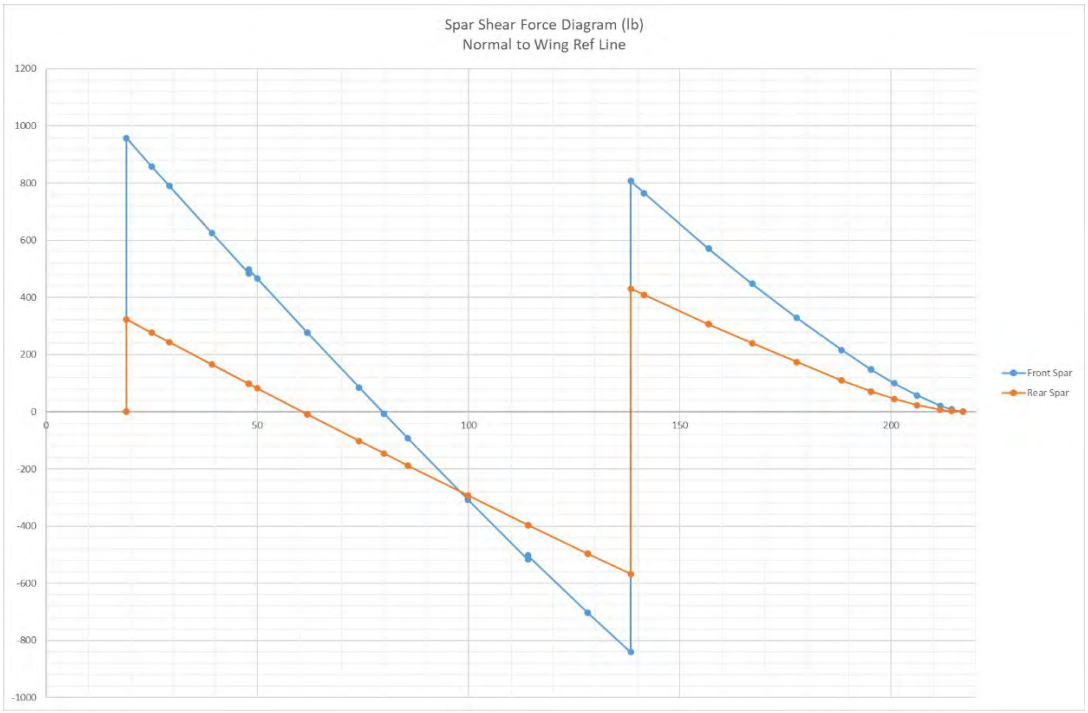

Figure 16-13 Spar Shear Force for 2460 lb at 112 Knots and 3.8 g

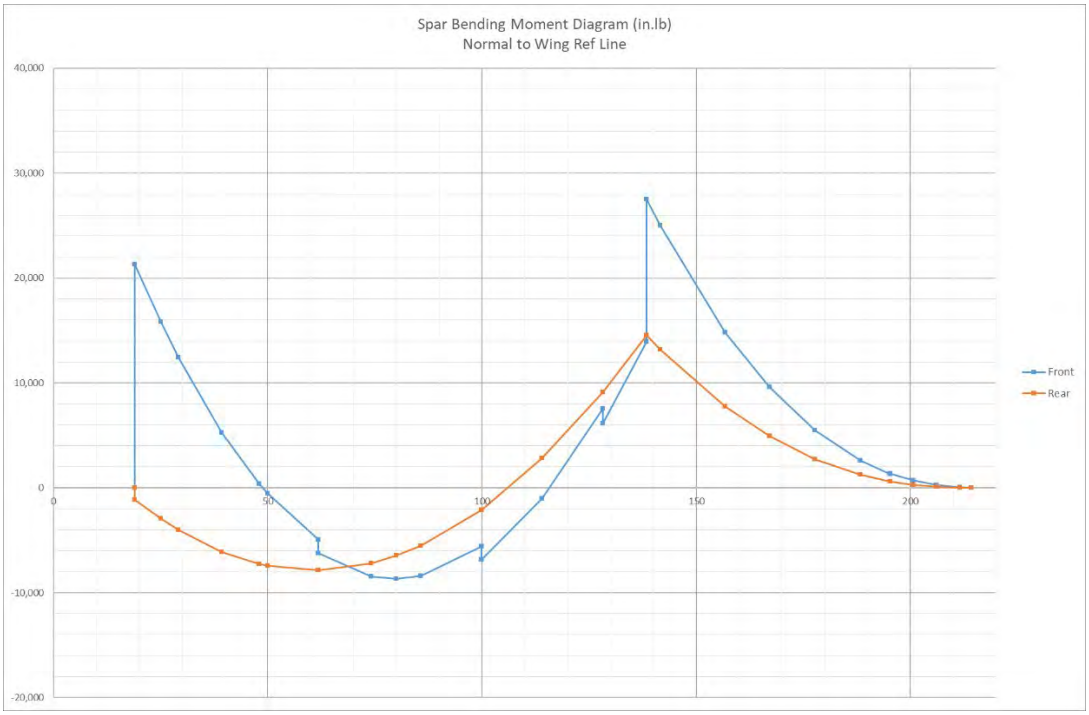

Figure 16-14 Spar Bending for 2460 lb at 112 Knots and 3.8 g

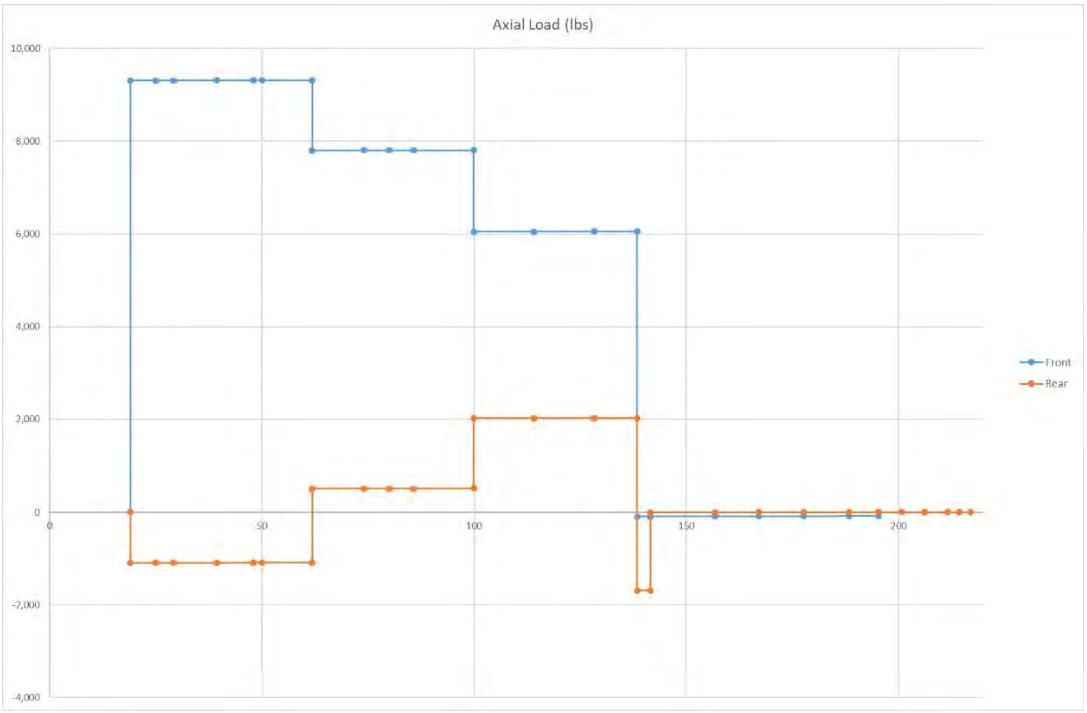

Figure 16-15 Spar Axial Loads for 2460 lb at 112 Knots and 3.8 g

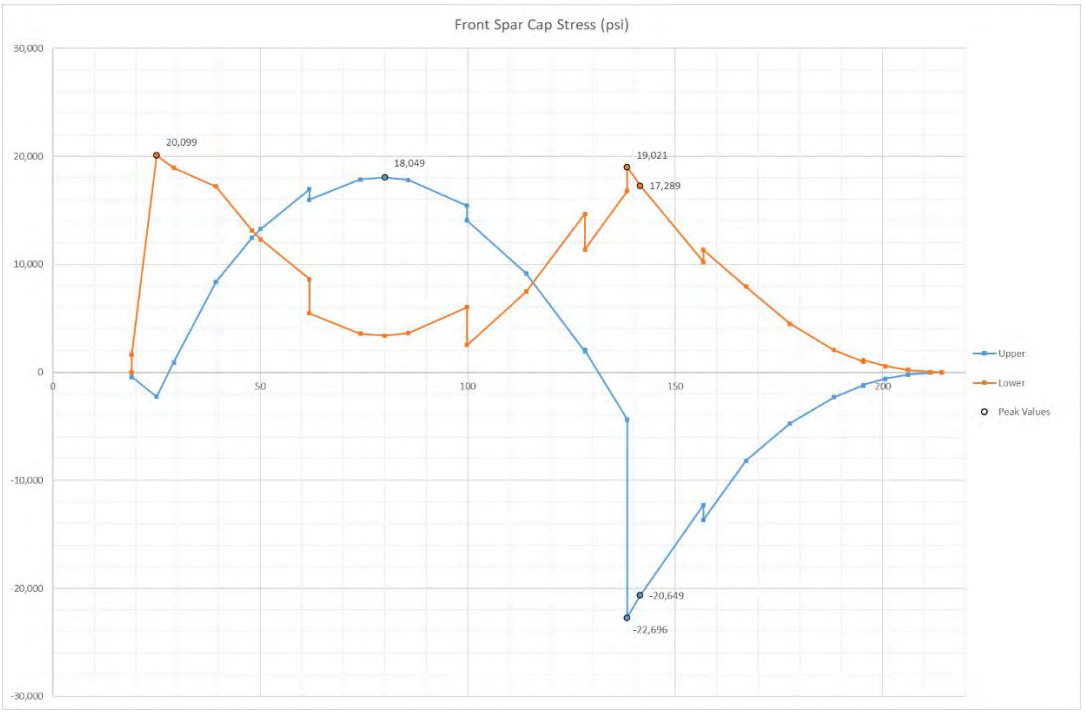

Figure 16-16 Front Spar Cap Stress for 2460 lb at 112 Knots and 3.8 g

16.5 **Load Case: 2460 lb at 116 knots and 26.2 ft/sec gust**. This is the dual seat aerotow comparative gust case.

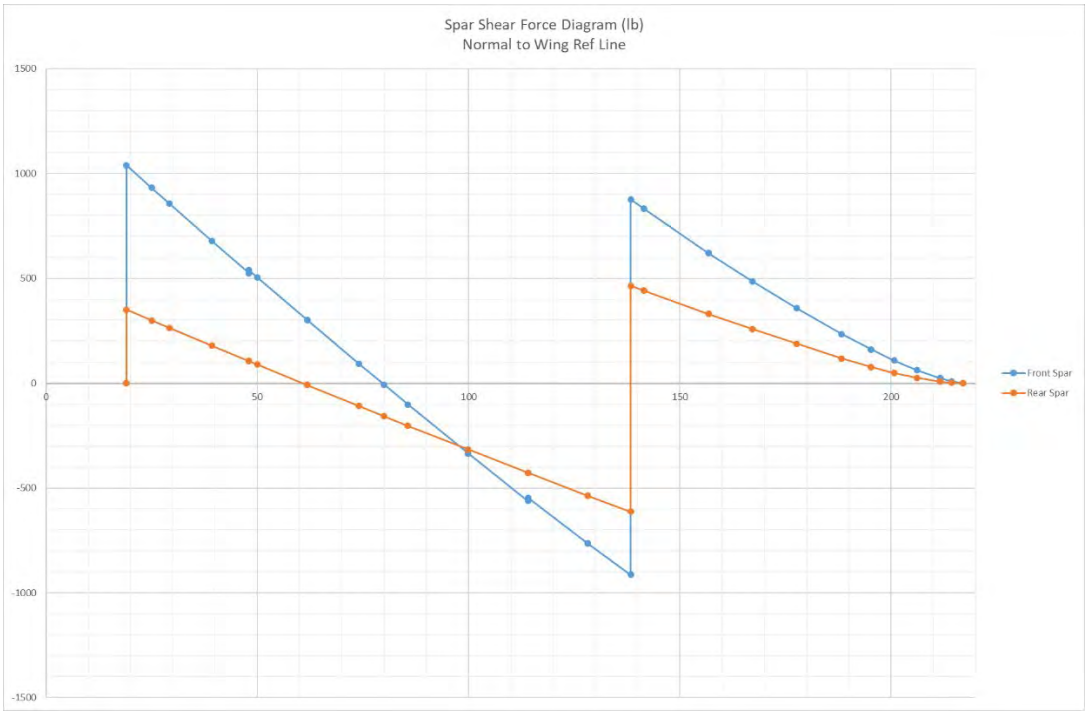

Figure 16-17 Spar Shear Force for 2460 lb at 116 Knots and 26.2 ft/sec gust

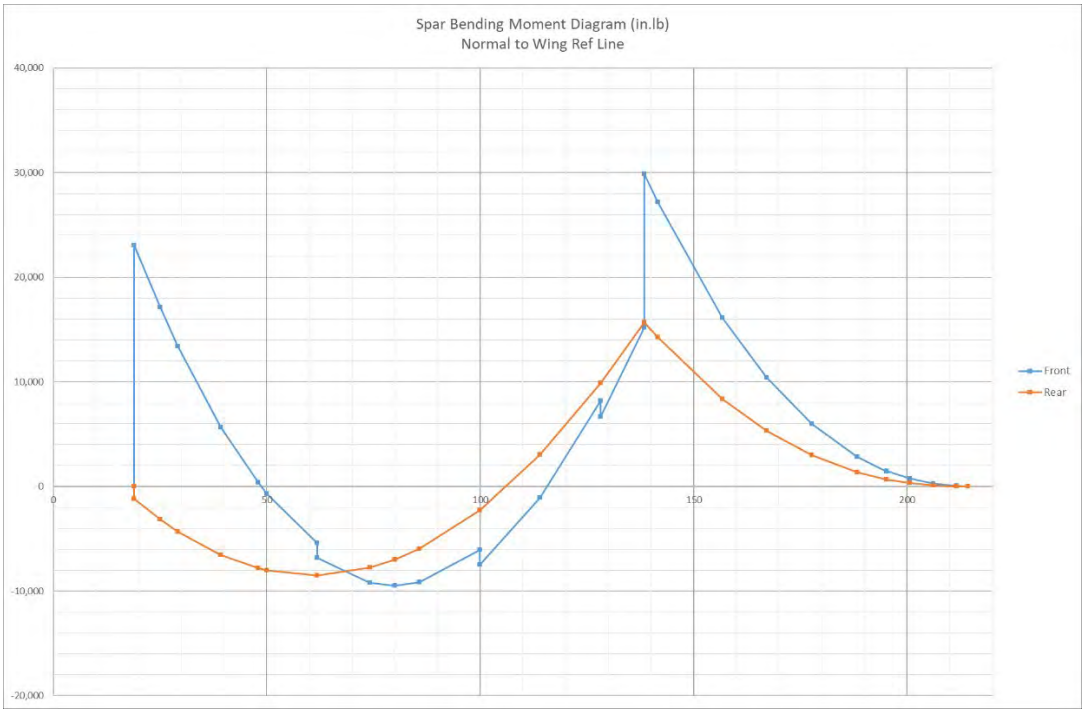

Figure 16-18 Spar Bending Moment for 2460 lb at 116 Knots and 26.2 ft/sec gust

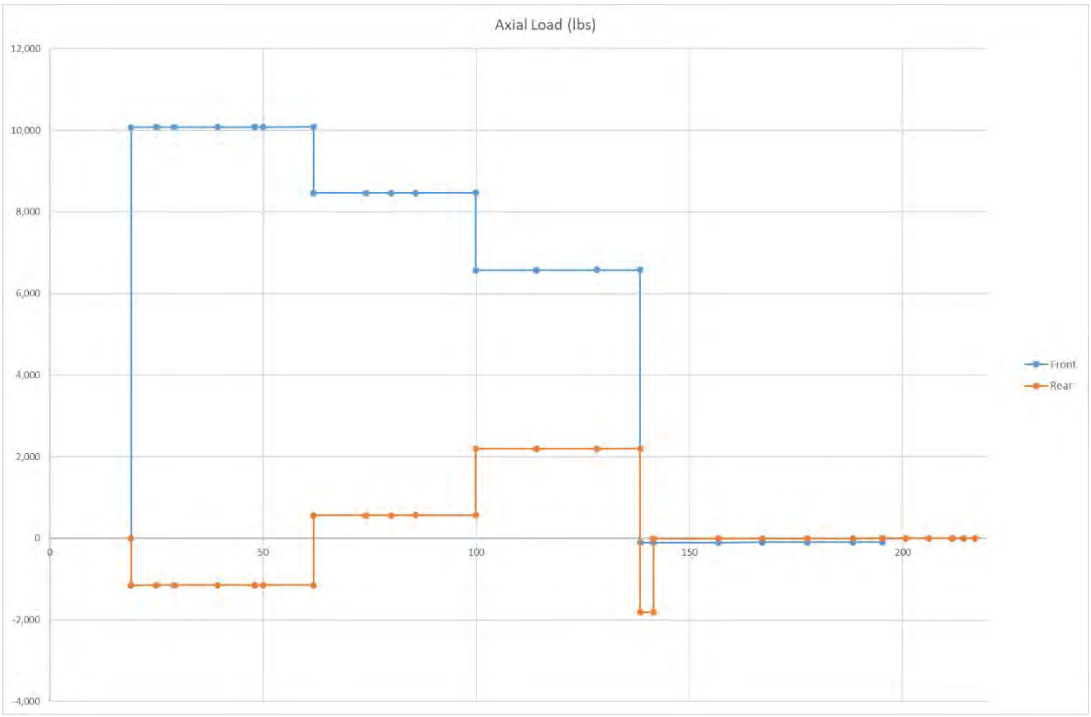

Figure 16-19 Spar Axial Loads for 2460 lb at 116 Knots and 26.2 ft/sec gust

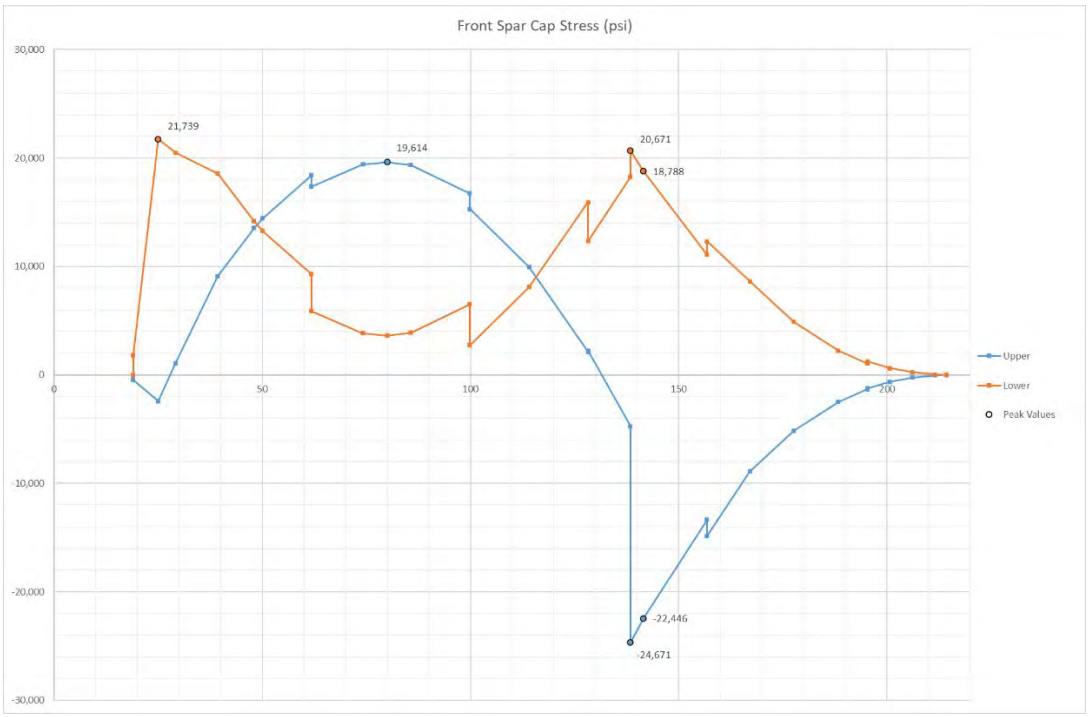

Figure 16-20 Front Spar Cap Stress for 2260 lb at 115 Knots and 26.8 ft/sec gust

16.6 **Load Case: 2460 lb at 150 knots and 3.8 g**. This is the dual seat aerotow comparative case to the agricultural 2900 lb at 121 kts and 3.8 g.

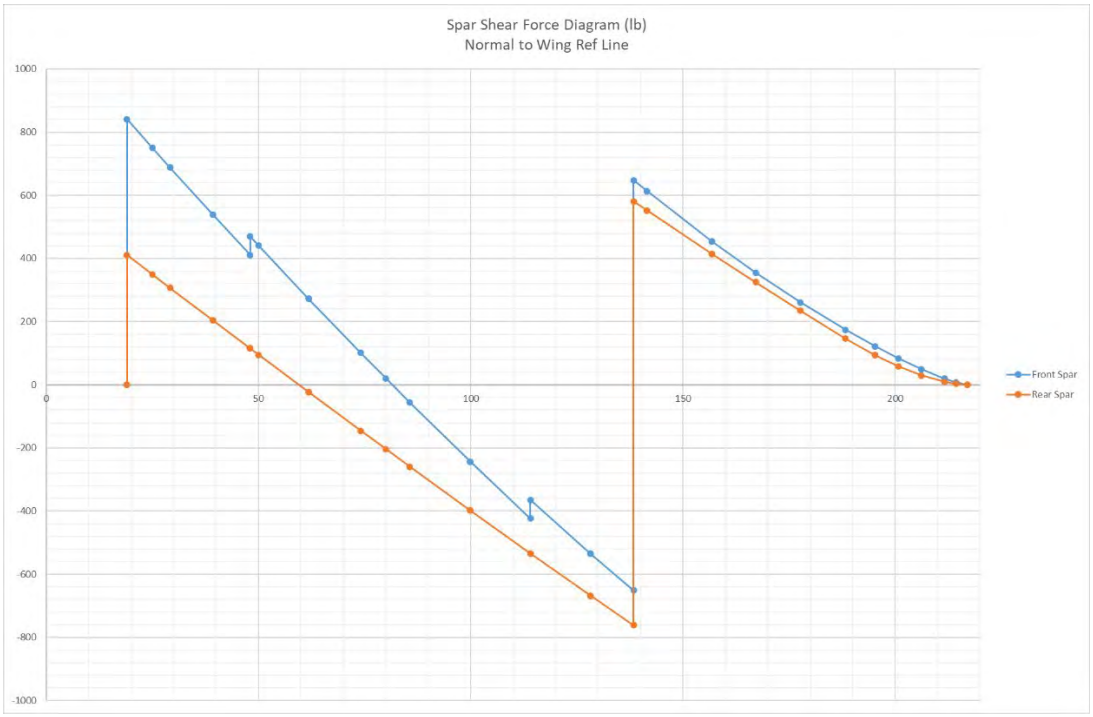

Figure 16-21 Spar Shear Force for 2460 lb at 150 Knots and 3.8 g

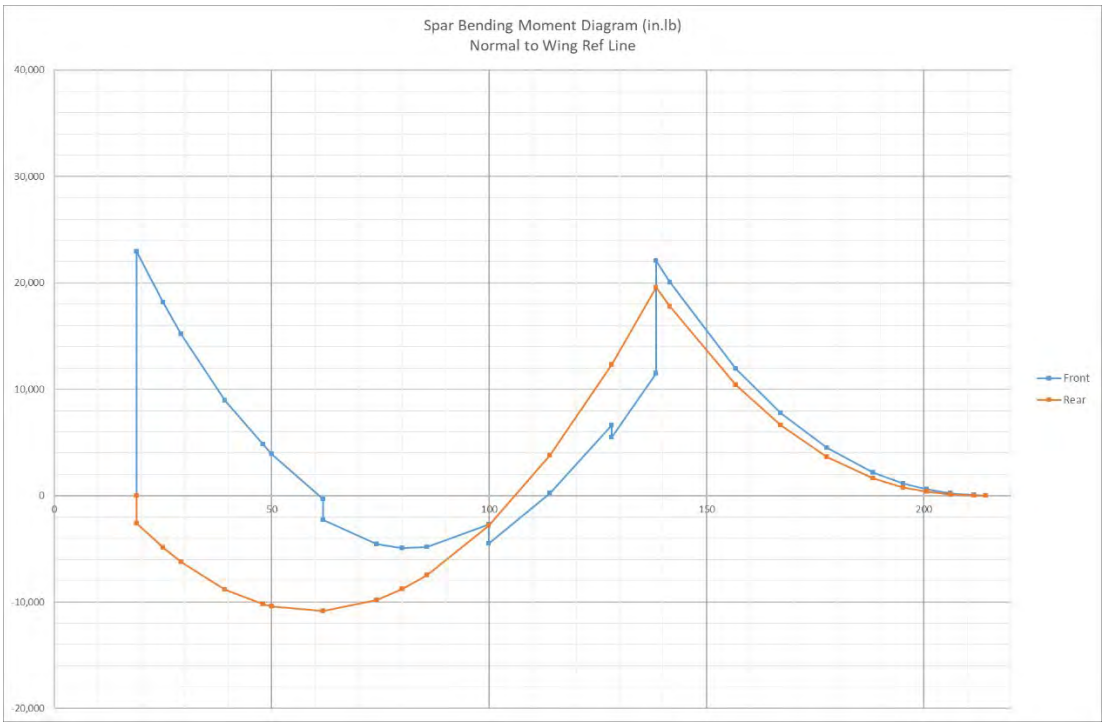

Figure 16-22 Spar Bending Moments for 2460 lb at 150 Knots and 3.8 g

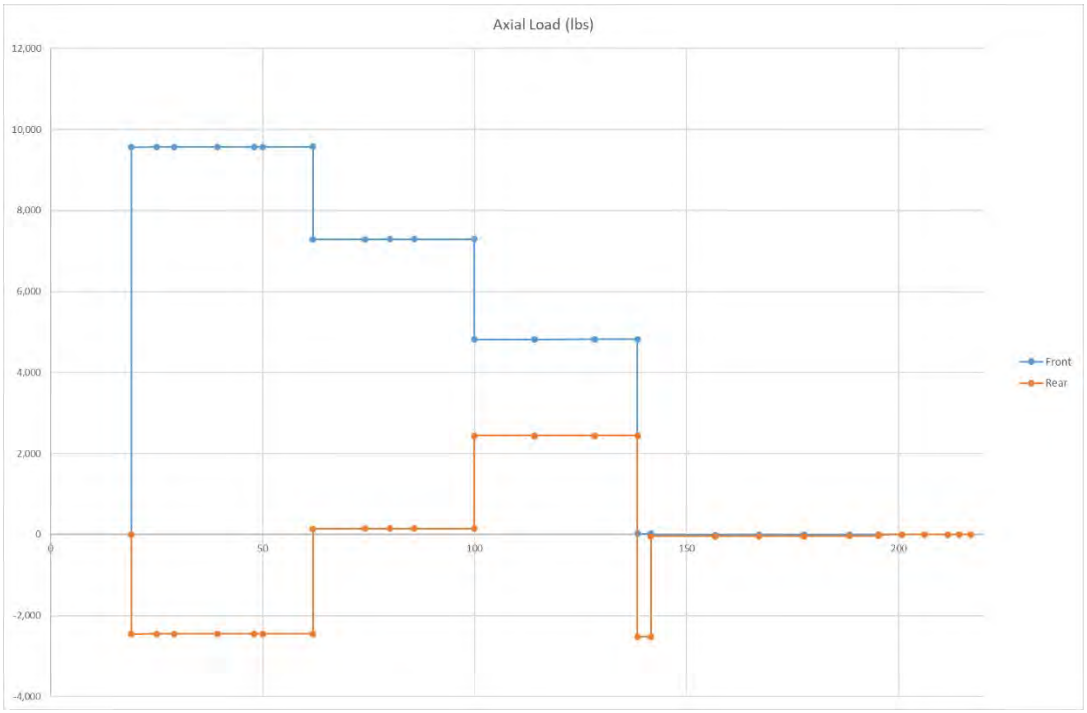

Figure 16-23 Spar Axial Loads for 2460 lb at 150 Knots and 3.8 g

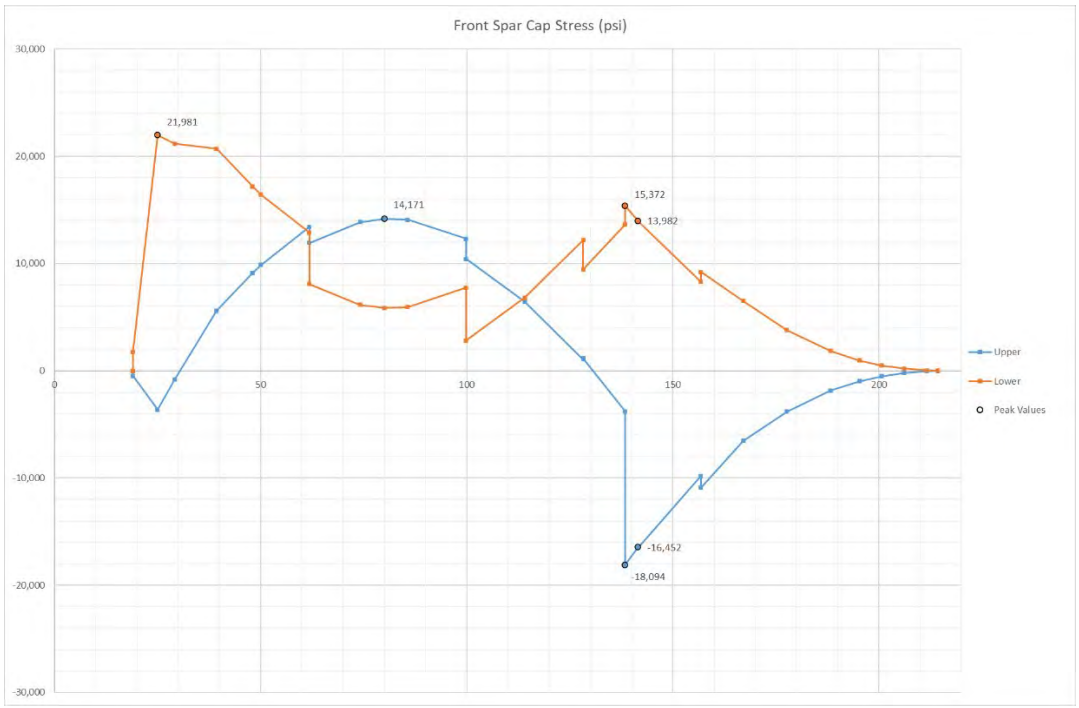

Figure 16-24 Front Spar Cap Stresses for 2260 lb at 150 Knots and 3.8 g

17. PAWNEE D RESULTS - AGRICULTURAL

17.1 **Load Case: 3205 lb at 127 kts and 3.8 g.** In comparison to the Pawnee B / C results, the bending moment at the strut connection is reduced but the bending moment mid span between the root and the strut connection is increased. The strut attachment stress in the lower cap is reduced from 25,331 psi to 21,389 psi. The mid span stress in the upper cap is increased from 24,196 psi to 25,611 psi.

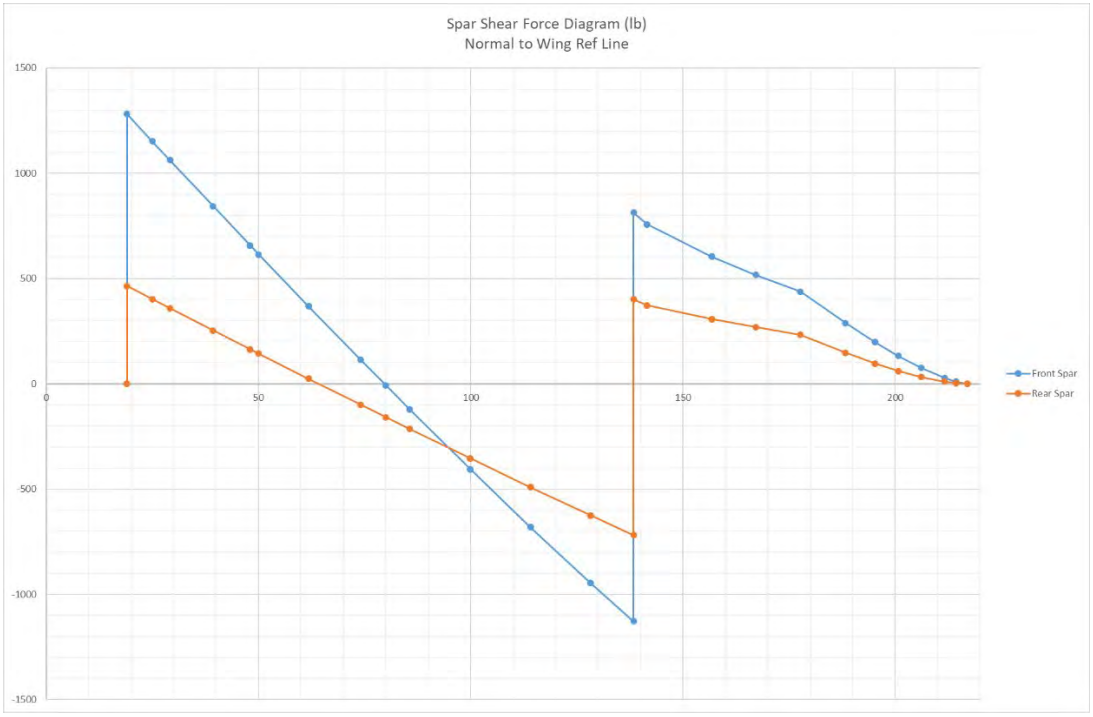

Figure 17-1 Pawnee D Spar Shear Force for 3205 lb at 127 Knots and 3.8 g

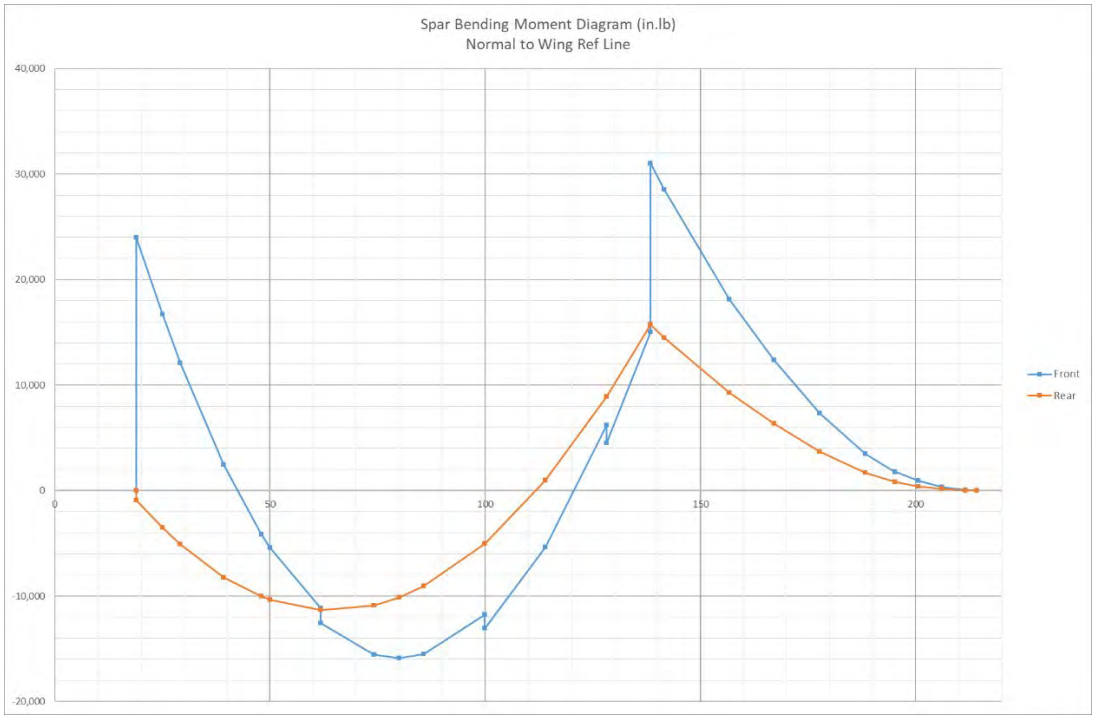

Figure 17-2 Pawnee D Spar Bending Moments for 3205 lb at 127 Knots and 3.8 g

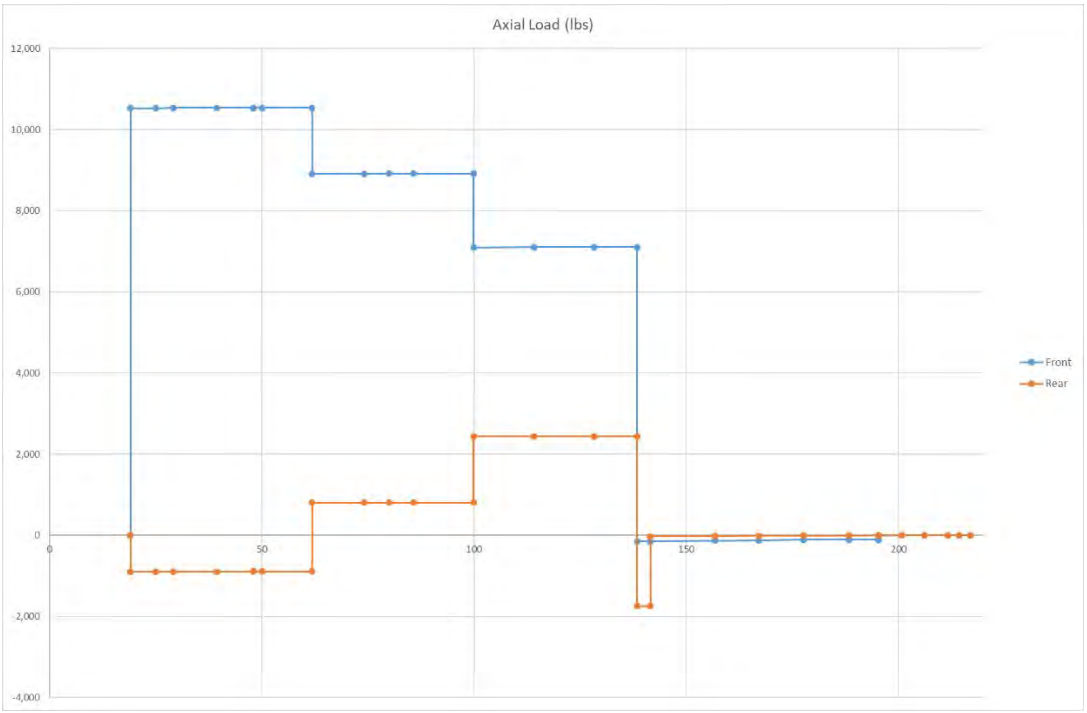

Figure 17-3 Pawnee D Axial Loads for 3205 lb at 127 Knots and 3.8 g

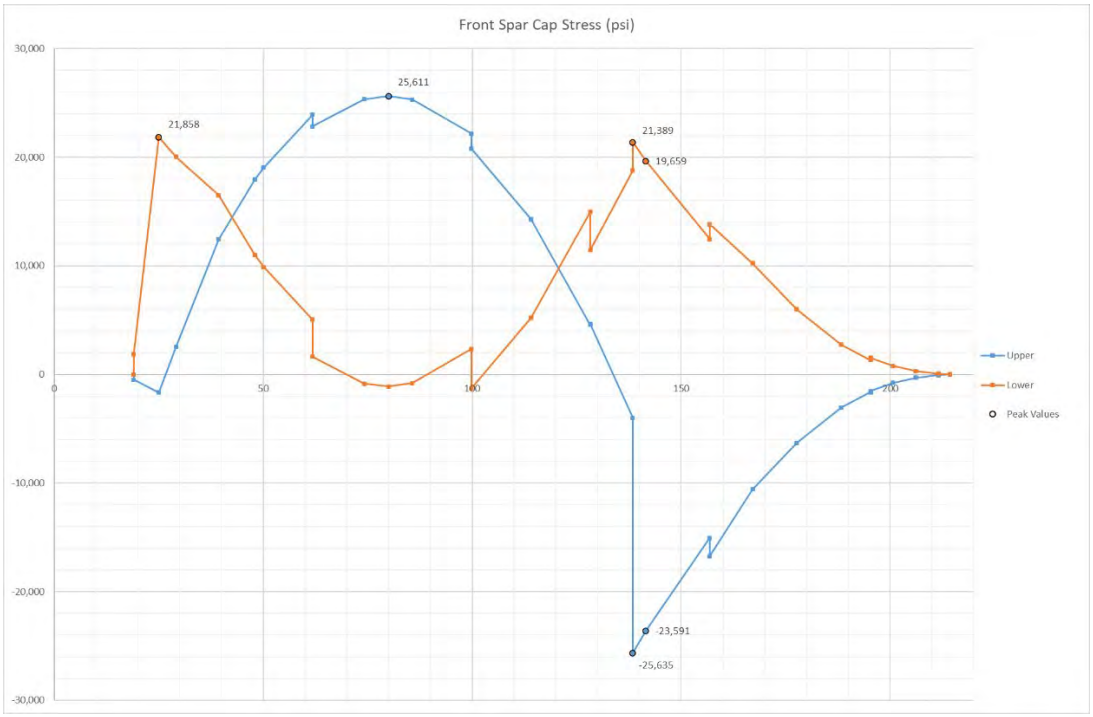

Figure 17-4 Pawnee D Front Spar Cap Stress for 3205 lb at 127 Knots and 3.8 g

17.2 **Load Case: 3205 lb at 150 knots and 3.8 g**. In comparison to the Pawnee B / C results, the bending moment at the strut connection is reduced but the bending moment mid span between the root and the strut connection is increased. The strut attachment in the lower cap is reduced from 23,062 psi to 19,102 psi. The mid span stress in the upper cap is increased from 21,770 psi to 23,152 psi.

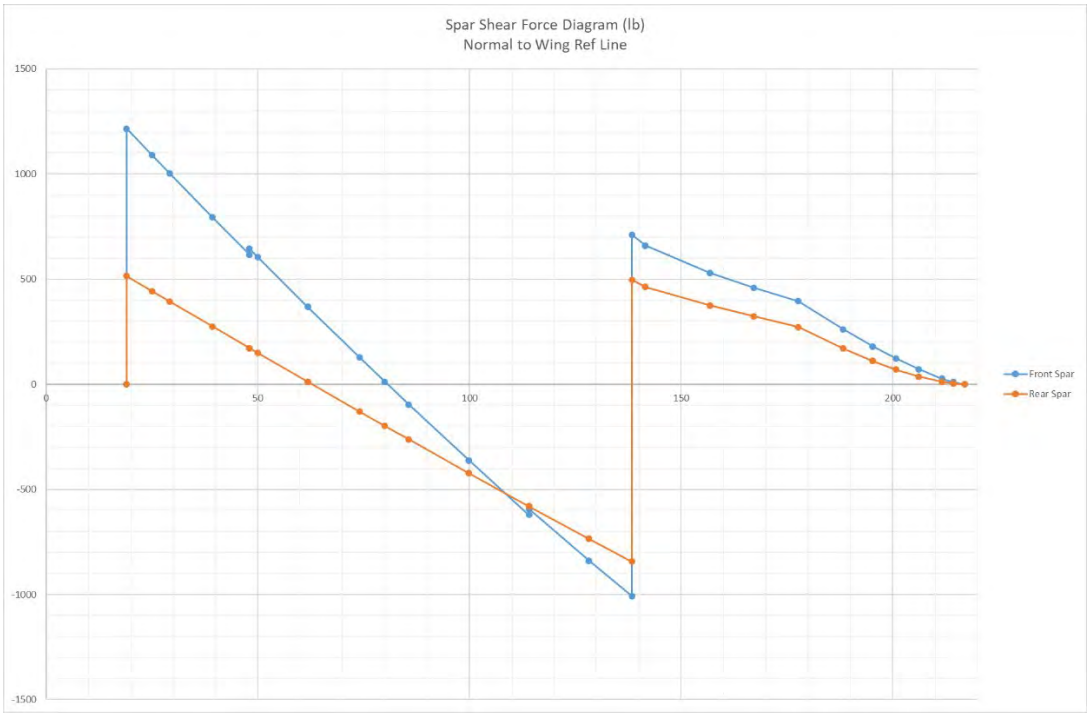

Figure 17-5 Pawnee D Spar Shear Force for 3205 lb at 150 Knots and 3.8 g

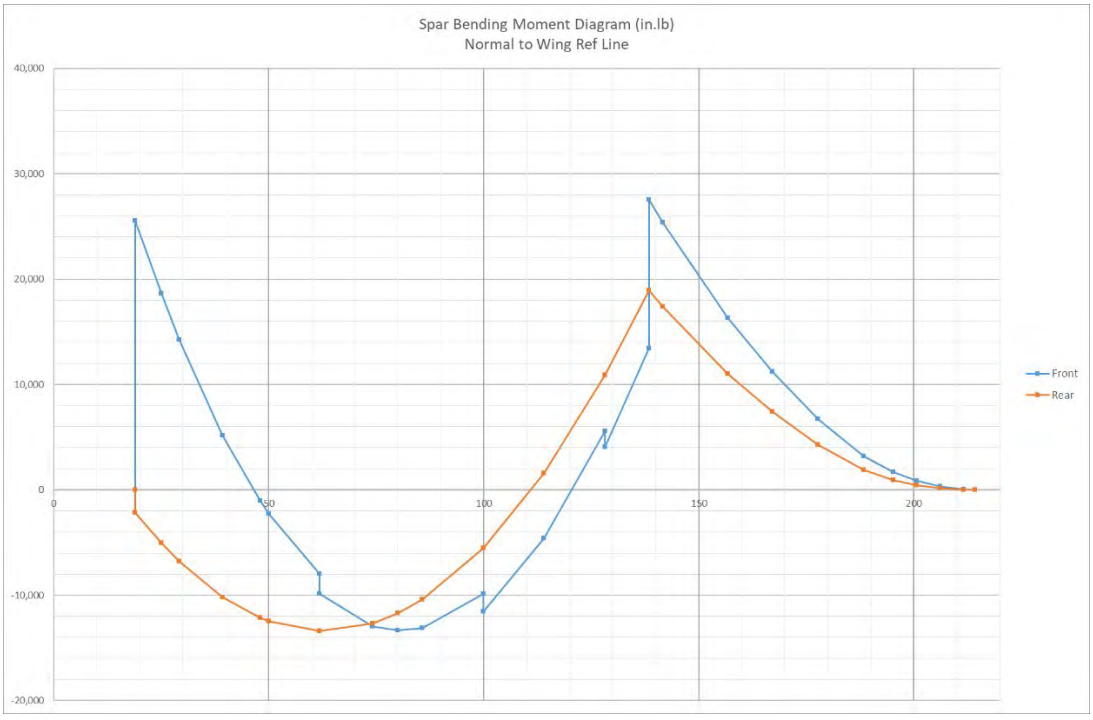

Figure 17-6 Pawnee D Spar Bending Moments for 3205 lb at 150 Knots and 3.8 g

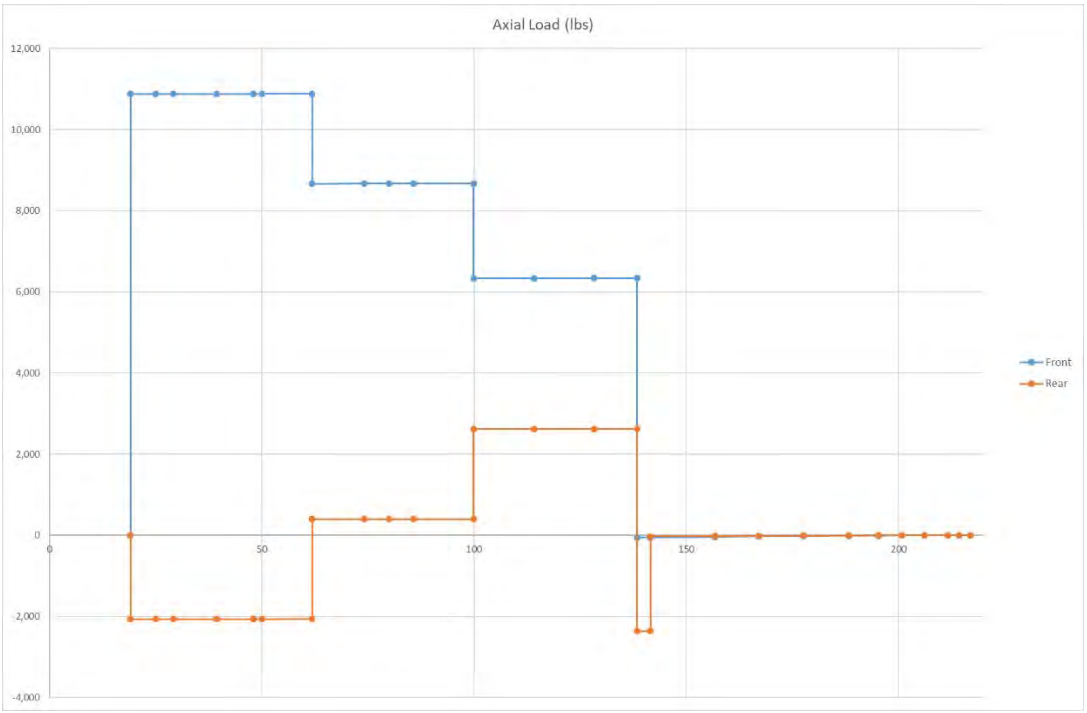

Figure 17-7 Pawnee D Axial Loads for 3205 lb at 150 Knots and 3.8 g

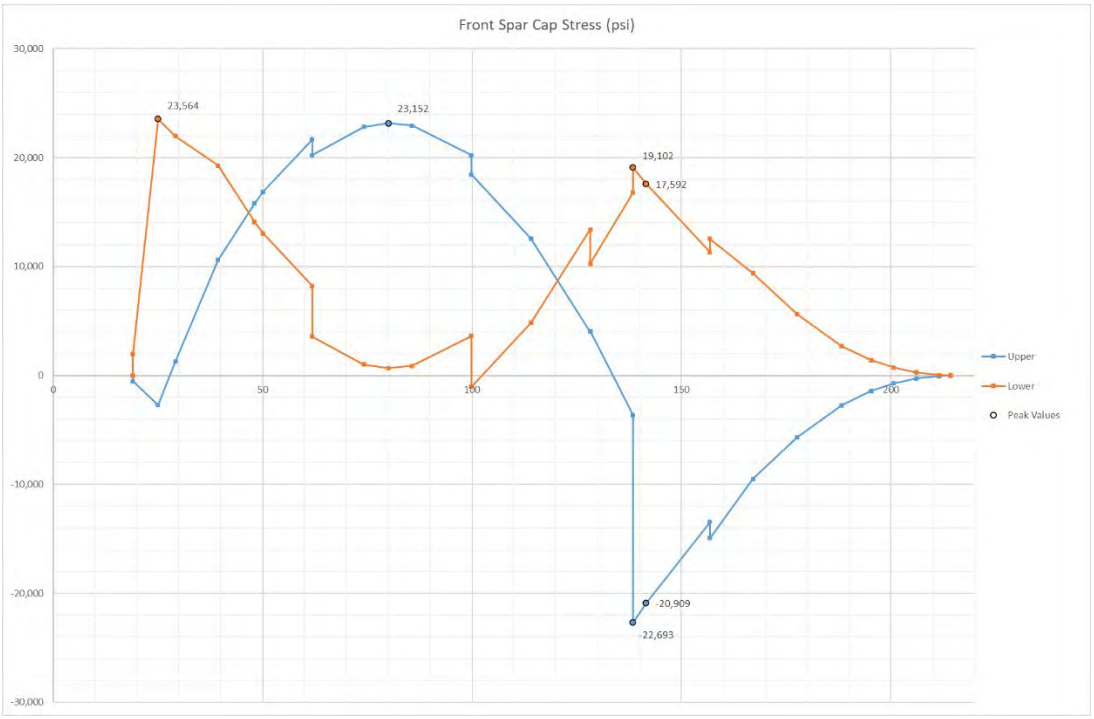

Figure 17-8 Pawnee D Front Spar Cap Stress for 3205 lb at 150 Knots and 3.8 g

17.3 **Load Case: 2900 lb at 121 knots and 3.8 g**. In comparison to the Pawnee B / C results, the bending moment at the strut connection is reduced but the bending moment mid span between the root and the strut connection is increased. The strut attachment stress in the lower cap is reduced from 22,772 psi to 18,831 psi. The mid span stress in the upper cap is increased from 21,701 psi to 23,120 psi.

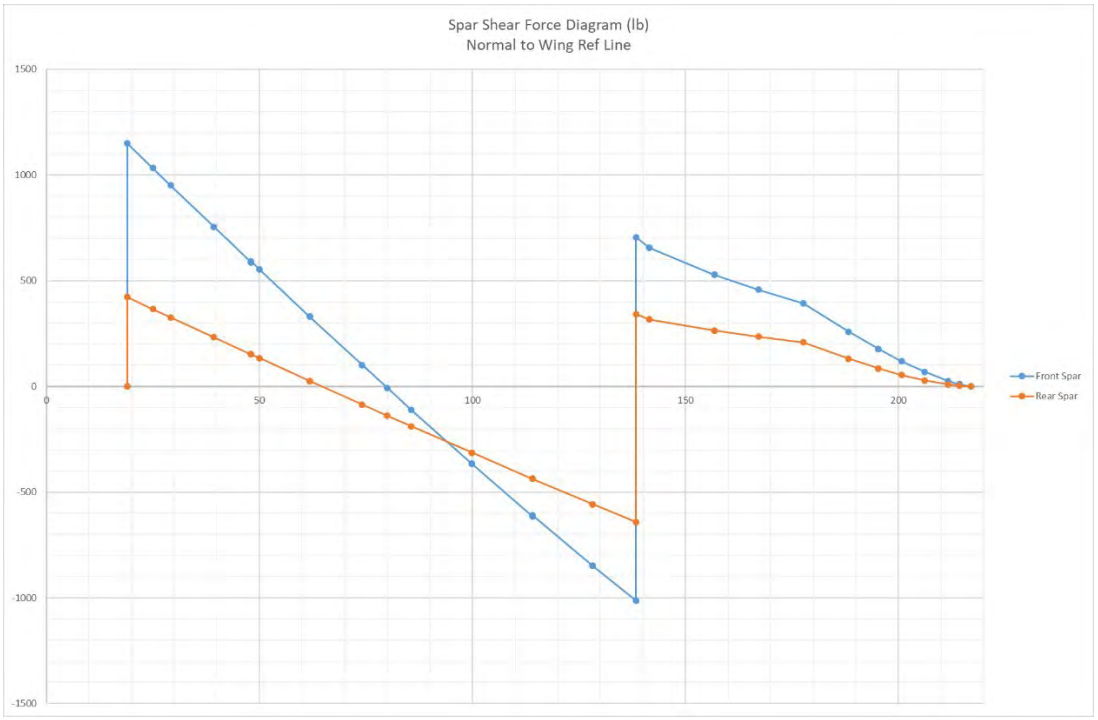

Figure 17-9 Pawnee D Spar Shear Force for 2900 lb at 121 Knots and 3.8 g

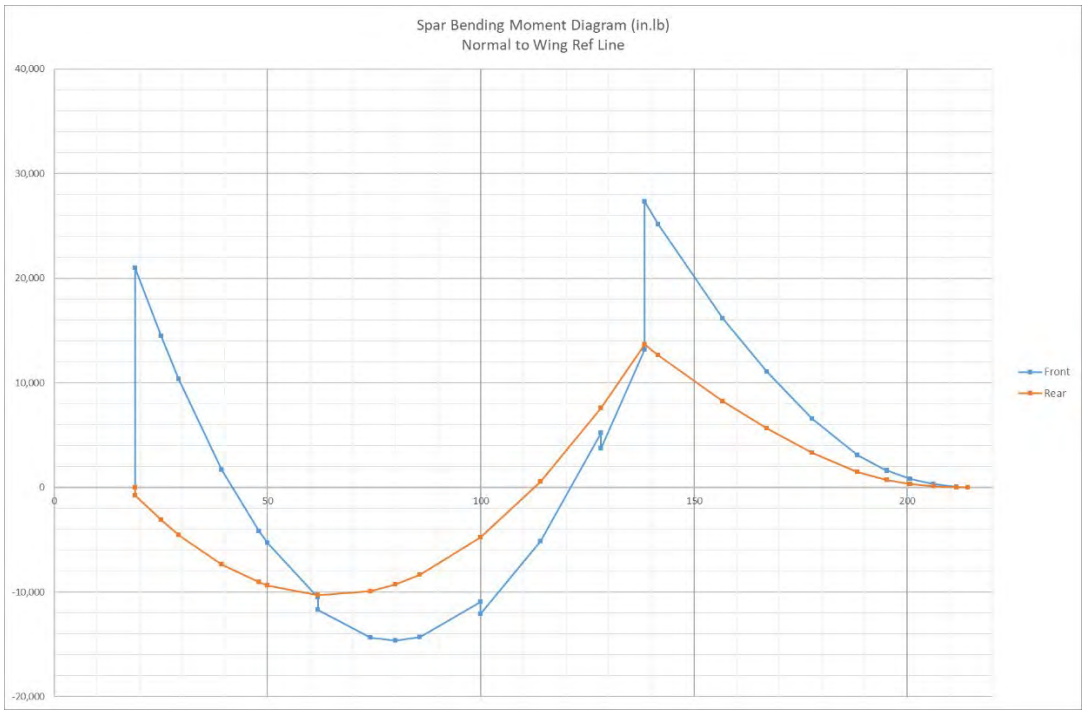

Figure 17-10 Pawnee D Spar Bending for 2900 lb at 121 Knots and 3.8 g

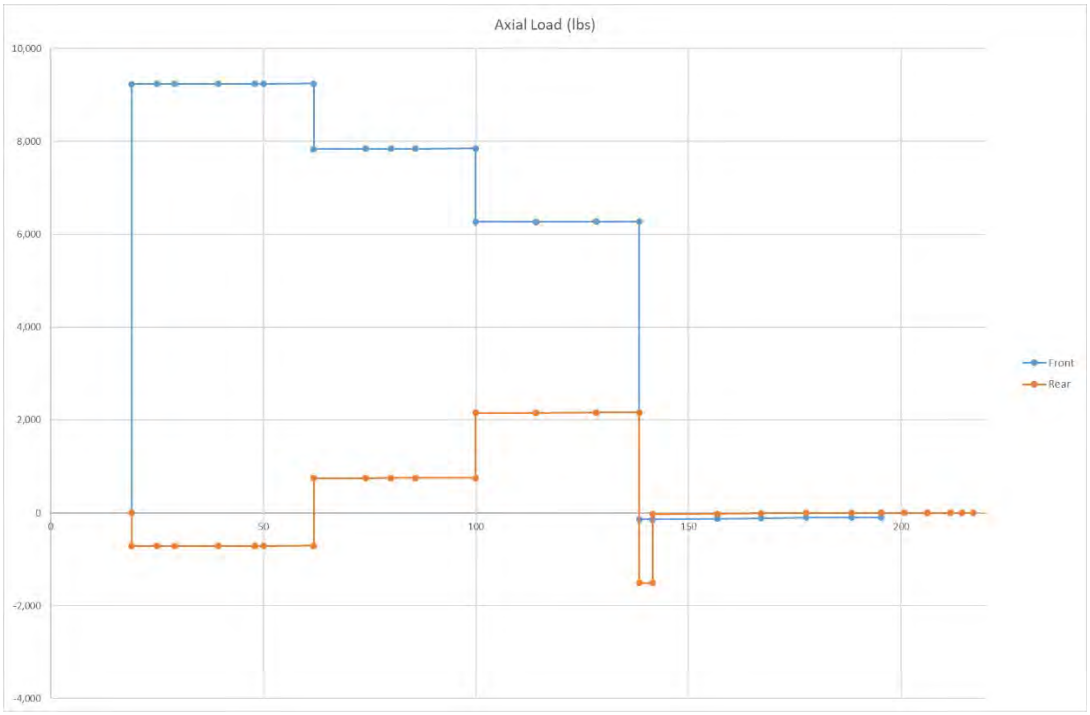

Figure 17-11 Pawnee D Spar Axial Load for 2900 lb at 121 Knots and 3.8 g

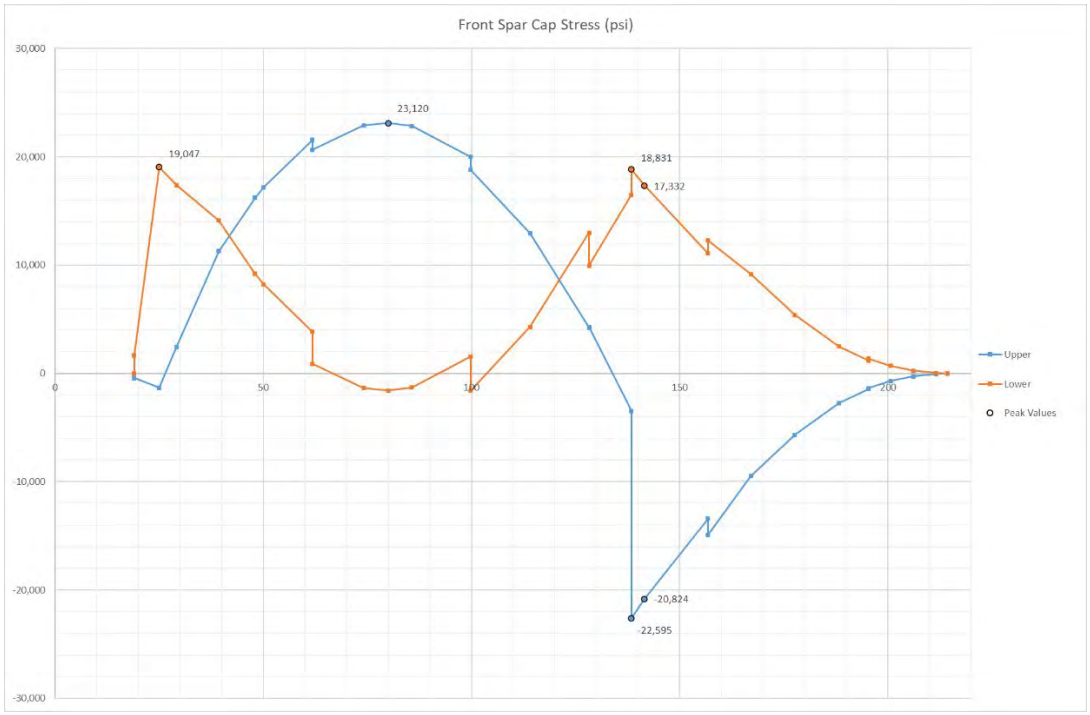

Figure 17-12 Pawnee D Front Spar Cap Stress for 2900 lb at 121 Knots and 3.8 g

17.4 **Load Case: 2900 lb at 150 knots and 3.8 g**. In comparison to the Pawnee B / C results, the bending moment at the strut connection is reduced but the bending moment mid span between the root and the strut connection is increased. The strut attachment stress in the lower cap is reduced from 19,939 psi to 15,983 psi. The mid span stress in the upper cap is increased from 18,672 psi to 20,045 psi.

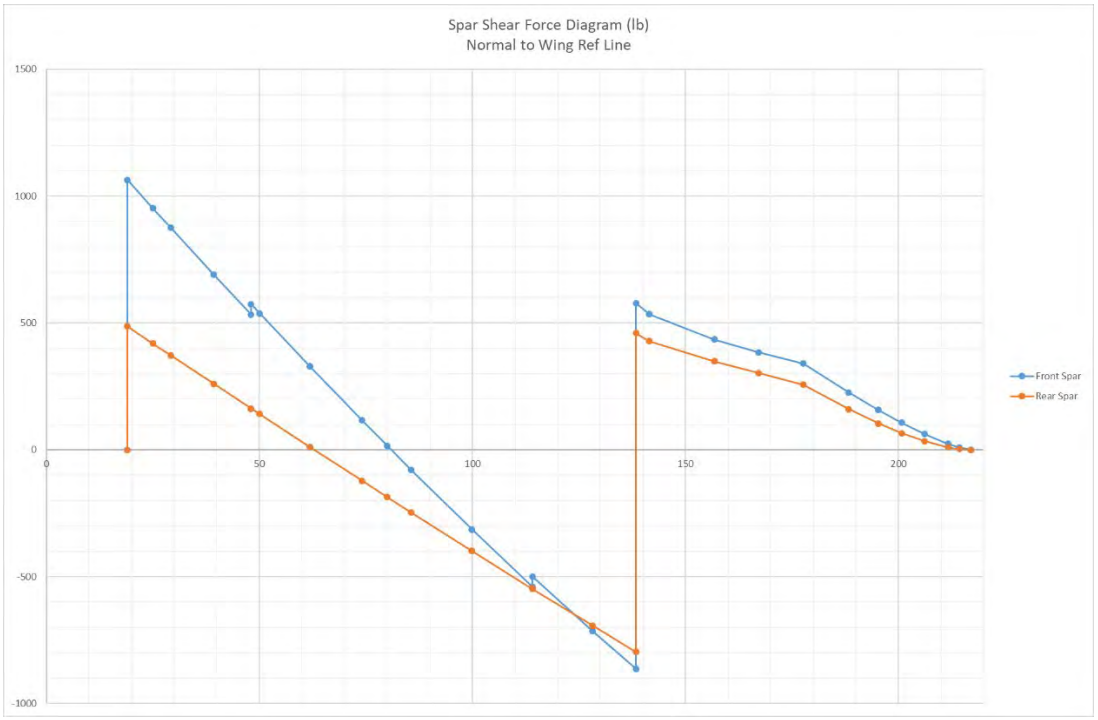

Figure 17-13 Pawnee D Spar Shear Force for 2900 lb at 150 Knots and 3.8 g

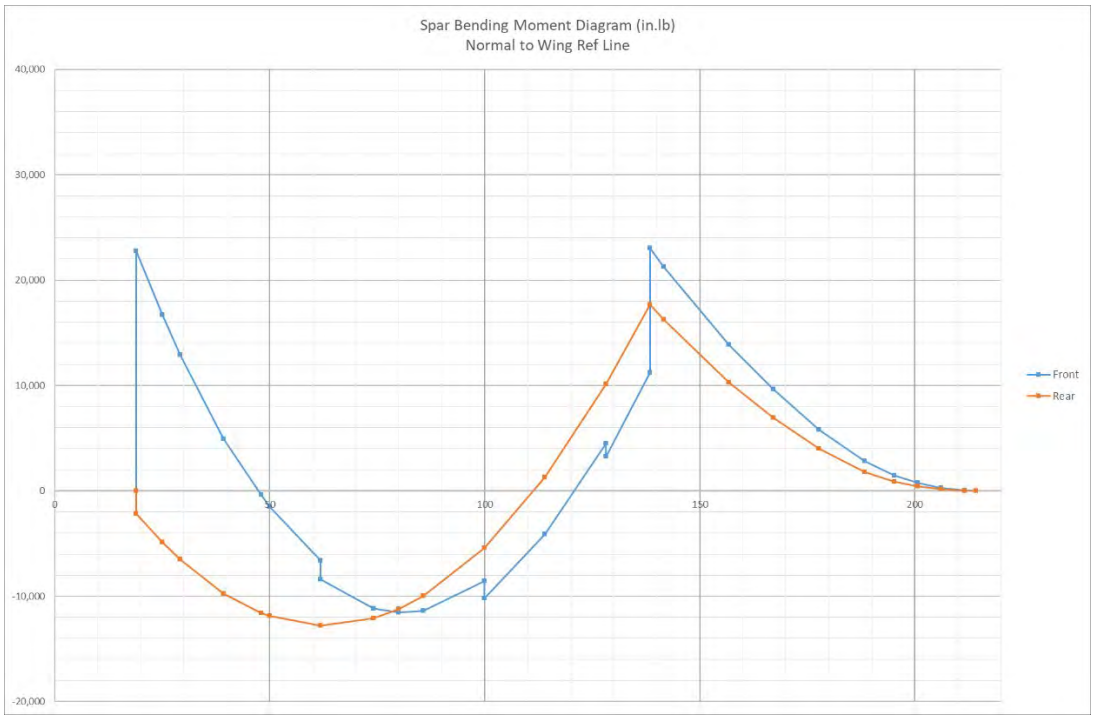

Figure 17-14 Pawnee D Spar Bending Moments for 2900 lb at 150 Knots and 3.8 g

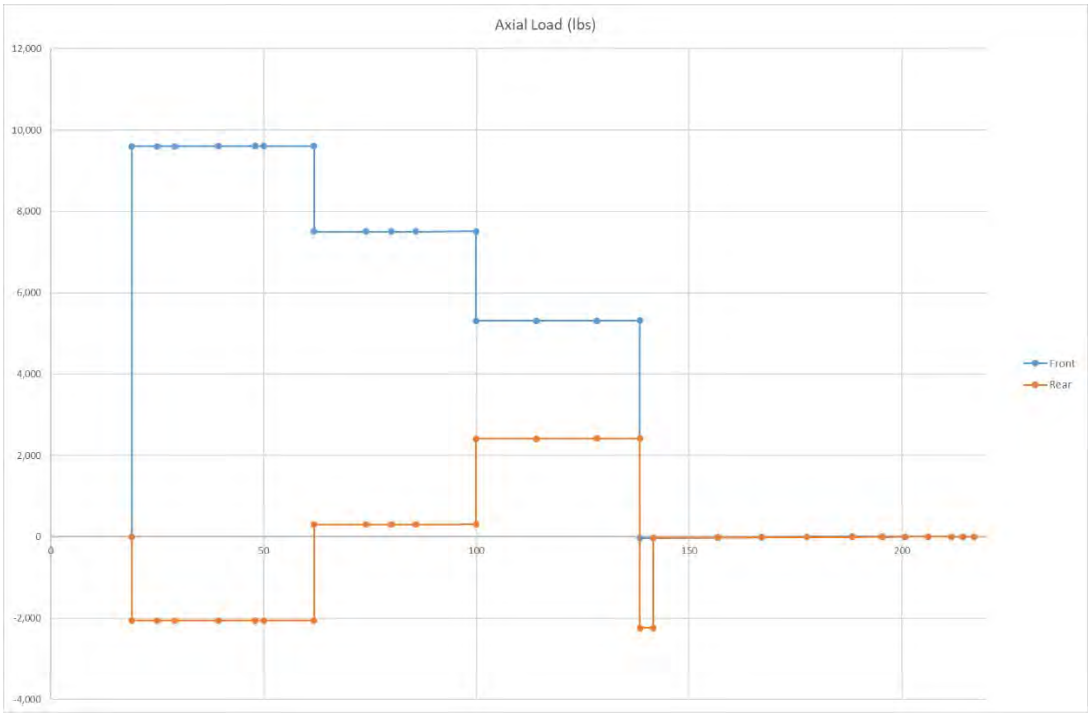

Figure 17-15 Pawnee D Spar Axial Loads for 2900 lb at 150 Knots and 3.8 g

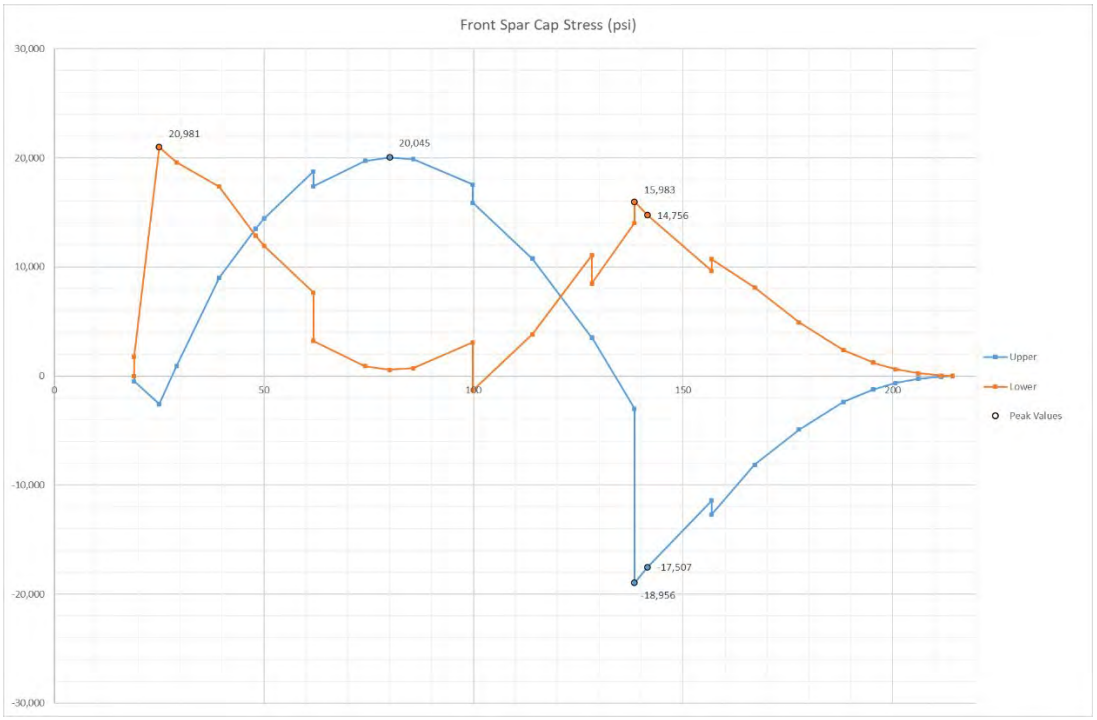

Figure 17-16 Pawnee D Front Spar Cap Stress for 2900 lb at 150 Knots and 3.8 g

17.5 **Load Case: 2005 lb at 101 knots and 3.8 g**. In comparison to the Pawnee B / C results, the bending moment at the strut connection is reduced but the bending moment mid span between the root and the strut connection is increased.

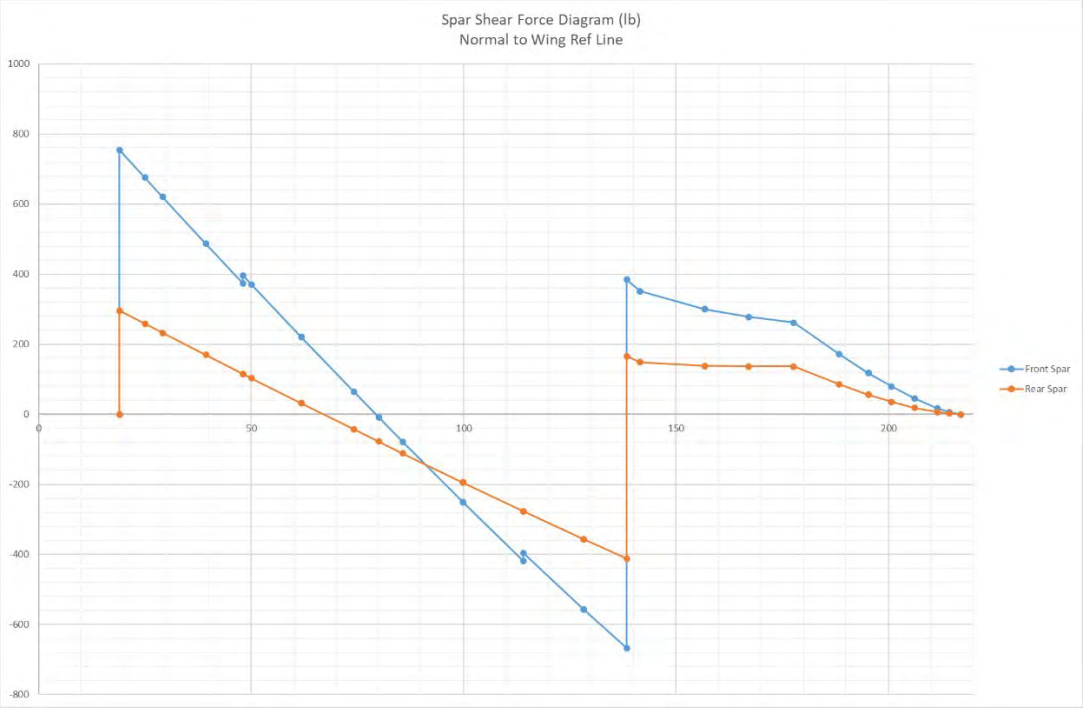

Figure 17-17 Pawnee D Spar Shear Force for 2005 lb at 101 Knots and 3.8 g

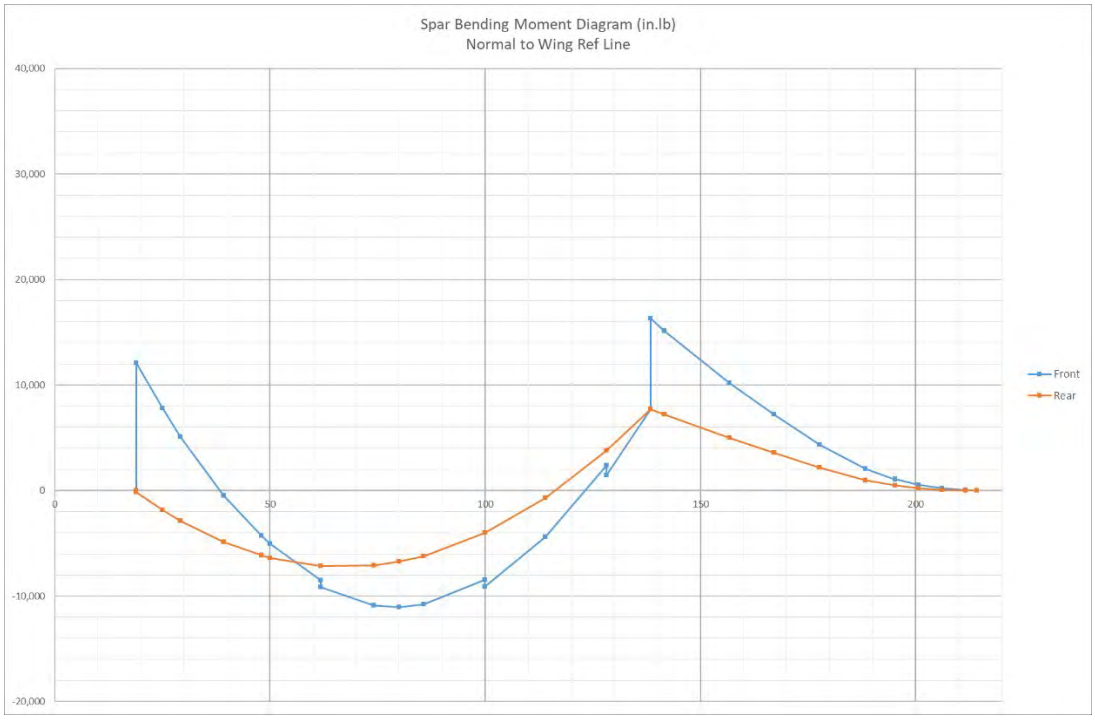

Figure 17-18 Pawnee D Spar Bending Moment for 2005 lb at 101 Knots and 3.8 g

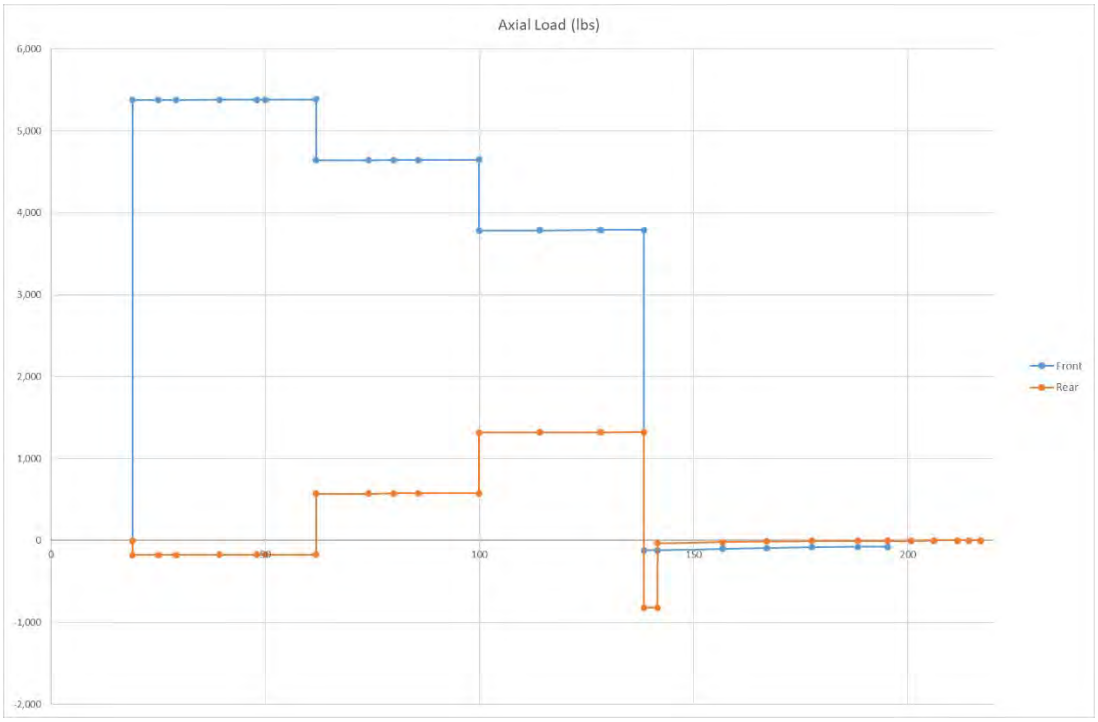

Figure 17-19 Pawnee D Spar Axial Loads for 2005 lb at 101 Knots and 3.8 g

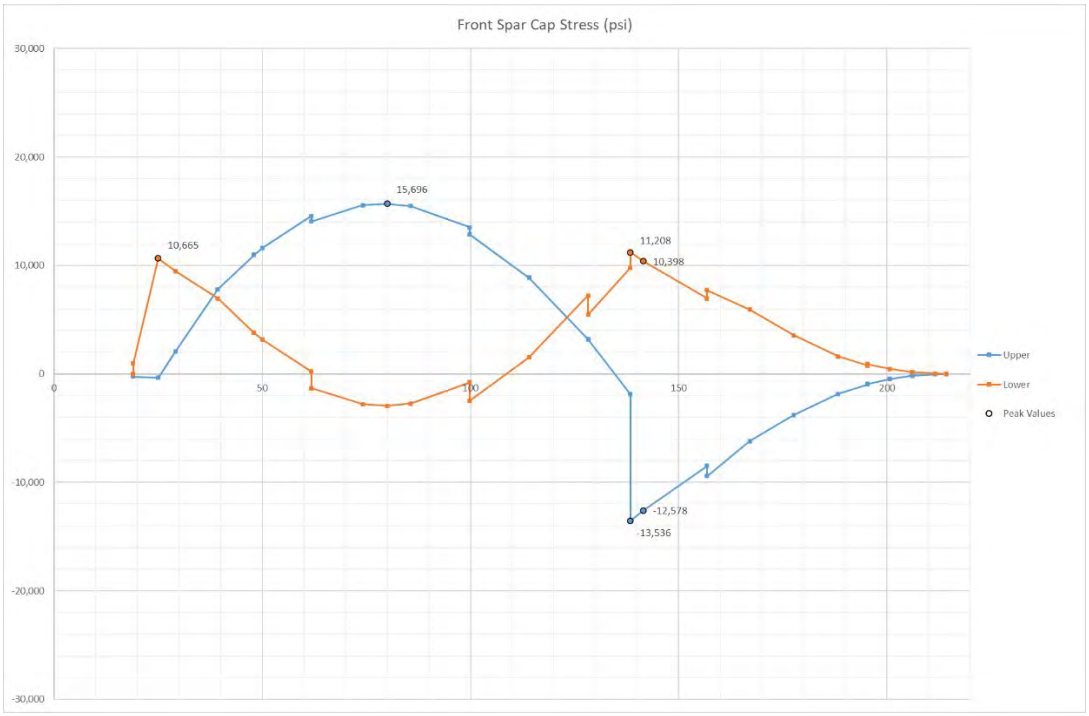

Figure 17-20 Pawnee D Front Spar Cap Stress for 2005 lb at 101 Knots and 3.8 g

17.6 **Load Case: 2005 lb at 113 knots and 27.7 ft/sec gust**. In comparison to the Pawnee B / C results, the bending moment at the strut connection is reduced but the bending moment mid span between the root and the strut connection is increased.

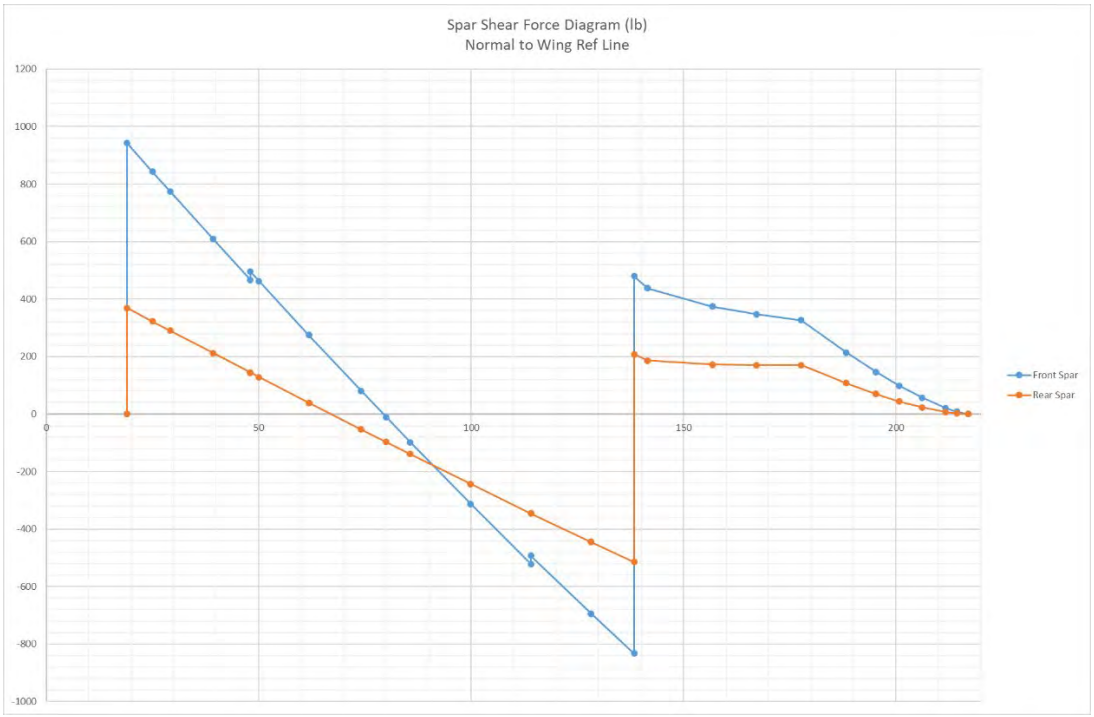

Figure 17-21 Pawnee D Spar Shear Force for 2005 lb at 113 Knots and 27.7 ft/sec gust

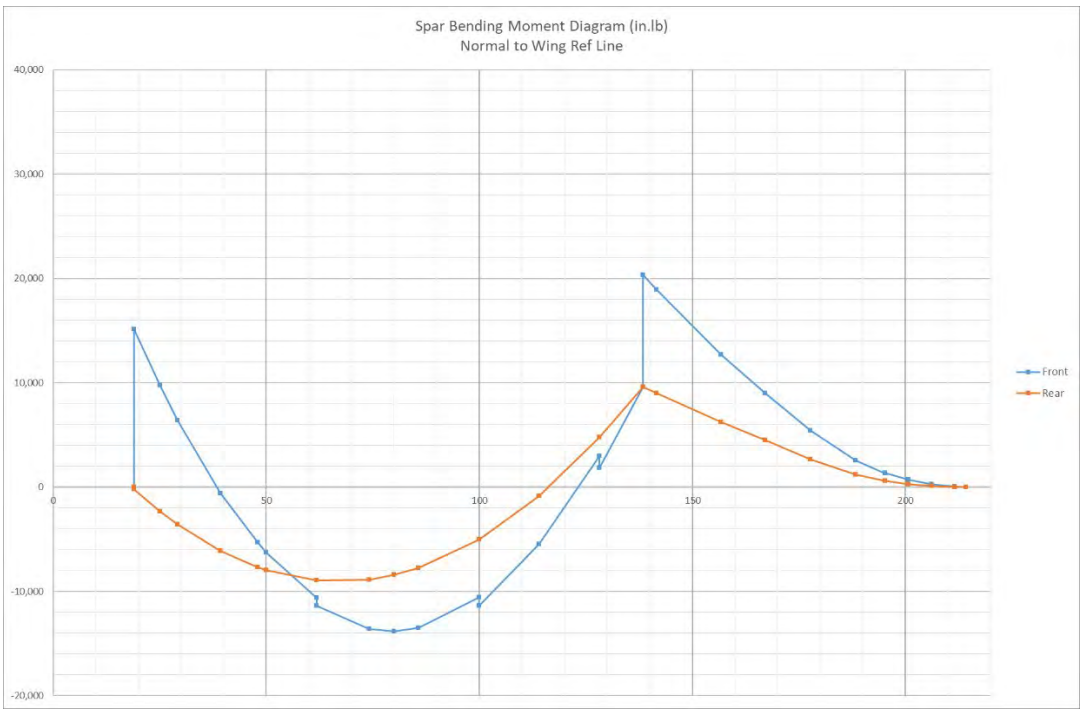

Figure 17-22 Pawnee D Spar Bending Moment for 2005 lb at 113 Knots and 27.7 ft/sec gust

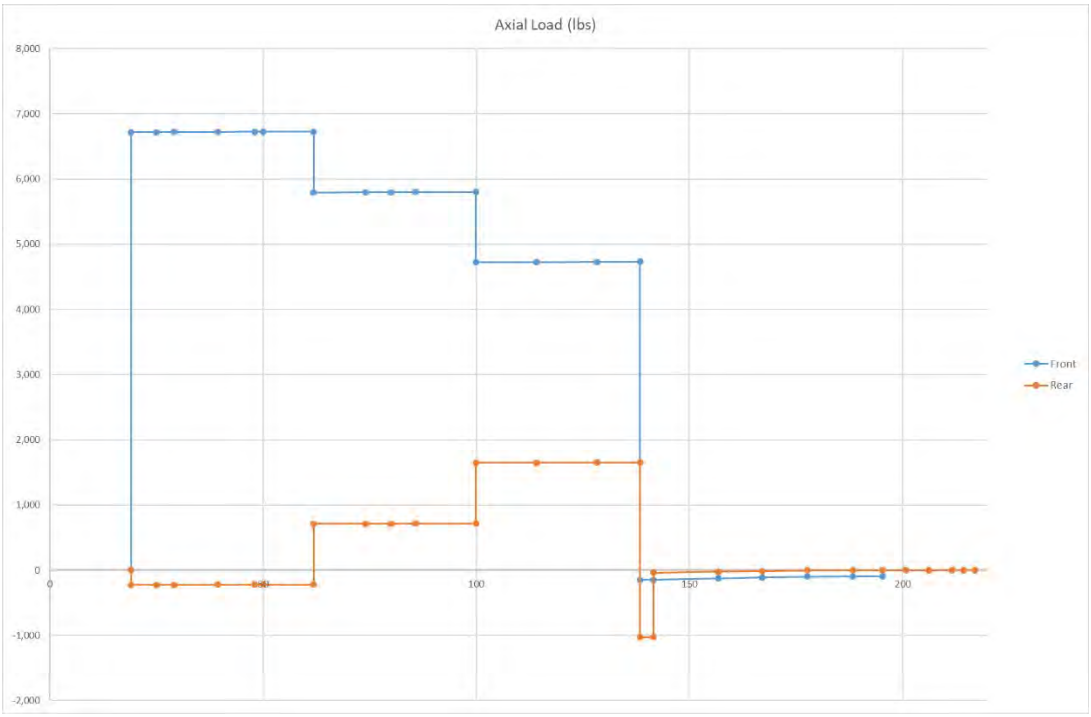

Figure 17-23 Pawnee D Spar Axial Load for 2005 lb at 113 Knots and 27.7 ft/sec gust

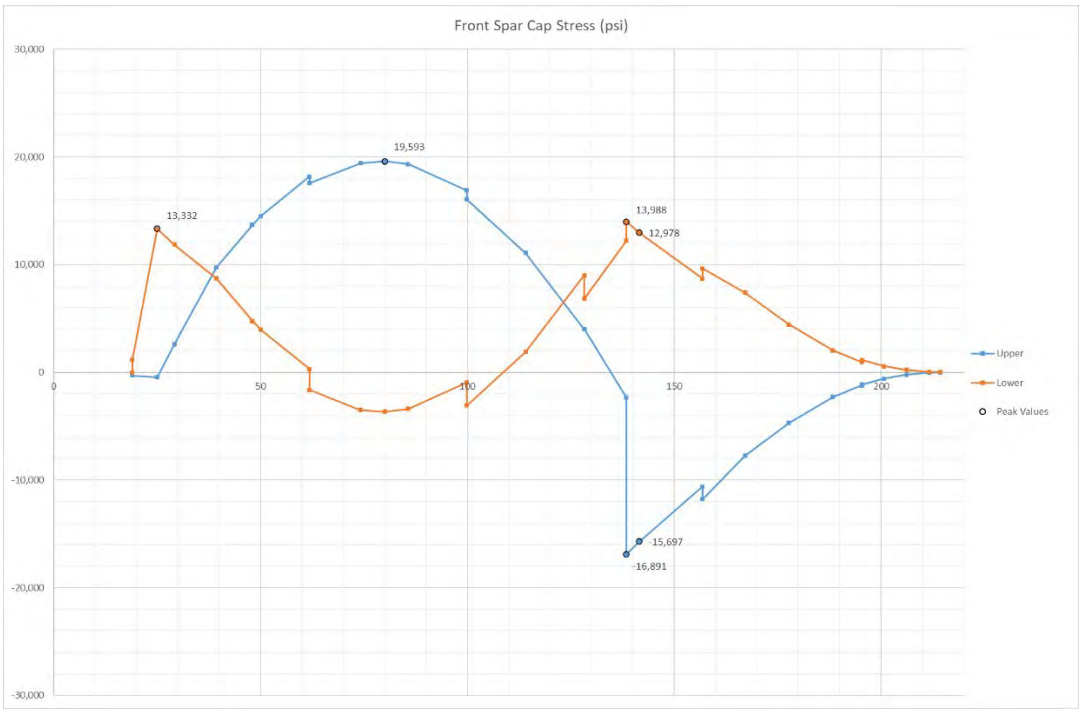

Figure 17-24 Pawnee D Front Spar Cap Stress for 2005 lb at 113 Knots and 27.7 ft/sec gust

17.7 **Load Case: 2005 lb at 150 knots and 3.8 g**. In comparison to the Pawnee B / C results, the bending moment at the strut connection is reduced but the bending moment mid span between the root and the strut connection is increased.

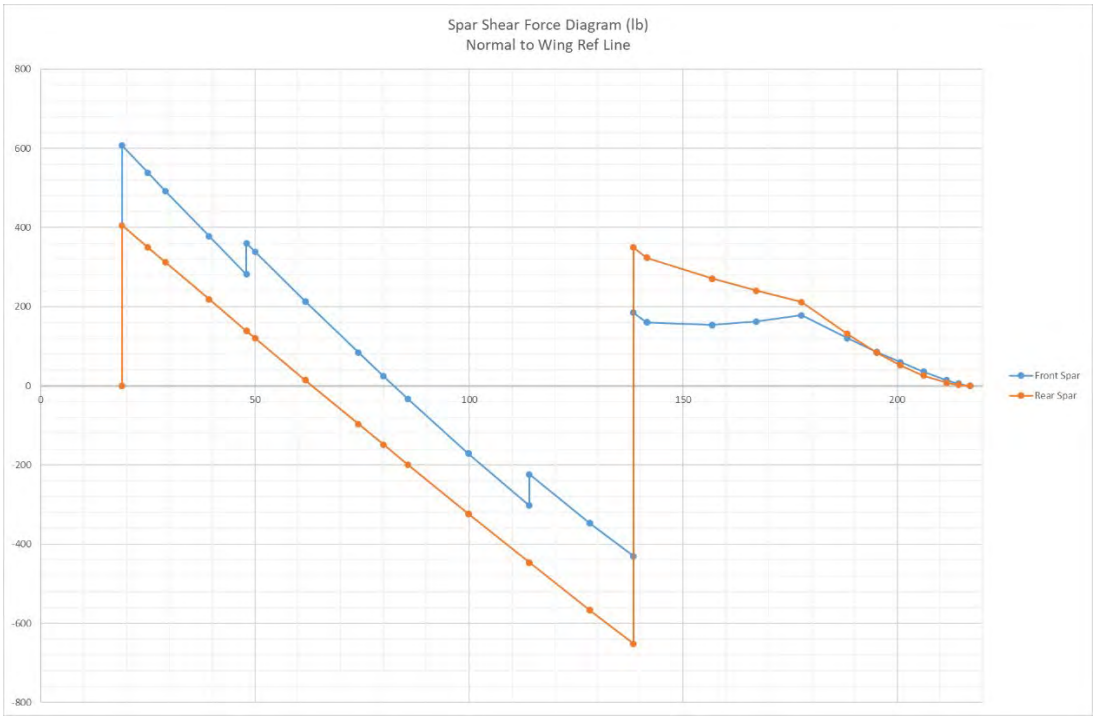

Figure 17-25 Pawnee D Spar Shear Force for 2005 lb at 150 Knots and 3.8 g

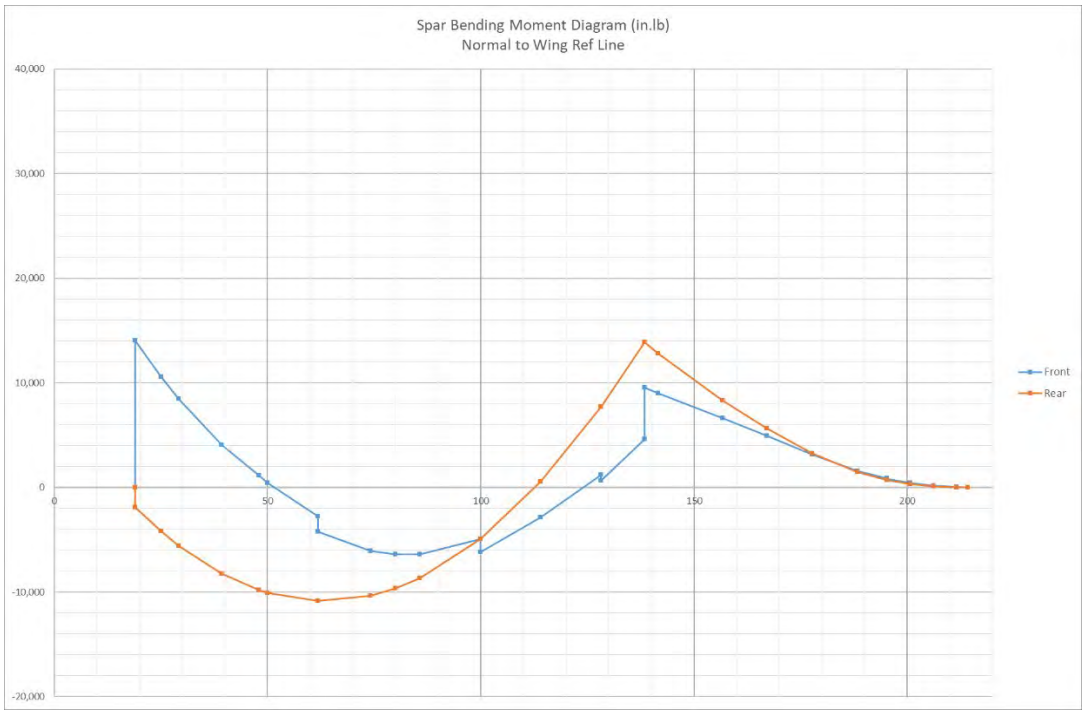

Figure 17-26 Pawnee D Spar Bending Moment for 2005 lb at 150 Knots and 3.8 g

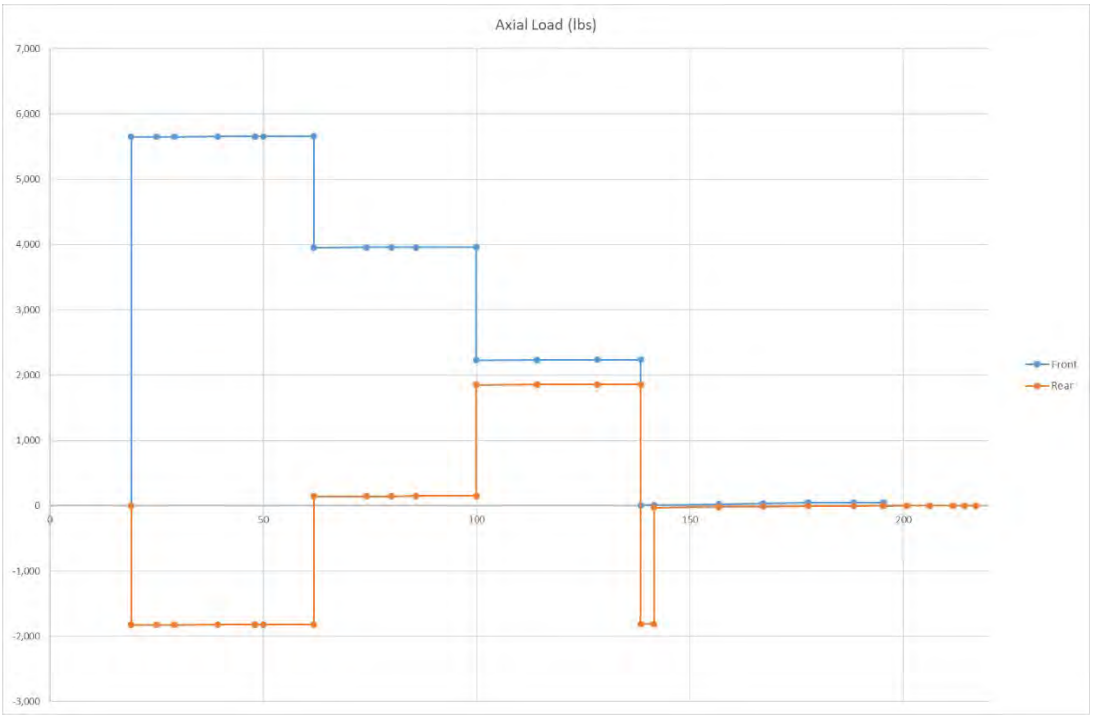

Figure 17-27 Pawnee D Spar Axial Load for 2005 lb at 150 Knots and 3.8 g

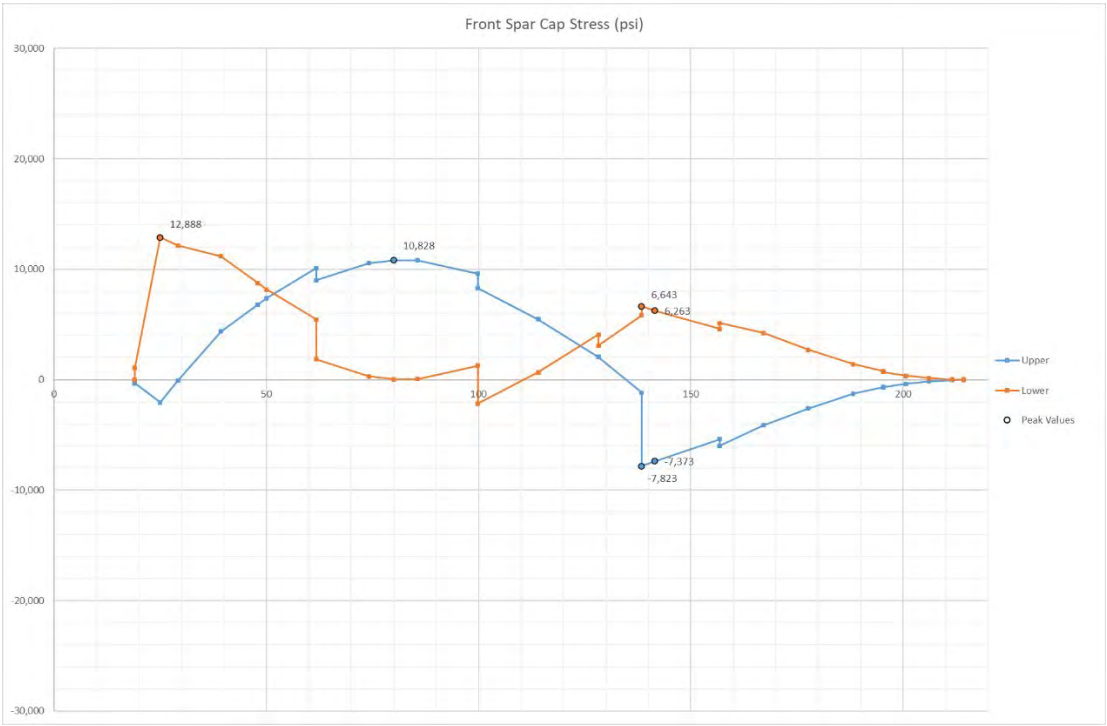

Figure 17-28 Pawnee D Front Spar Cap Stress for 2005 lb at 150 Knots and 3.8 g

18. PAWNEE D RESULTS – GLIDER TOWING

18.1 **Load Case: 2205 lb at 106 knots and 3.8g**. This is the single seat glider towing comparative case to the agricultural 2900 lb at 121 kts and 3.8 g.

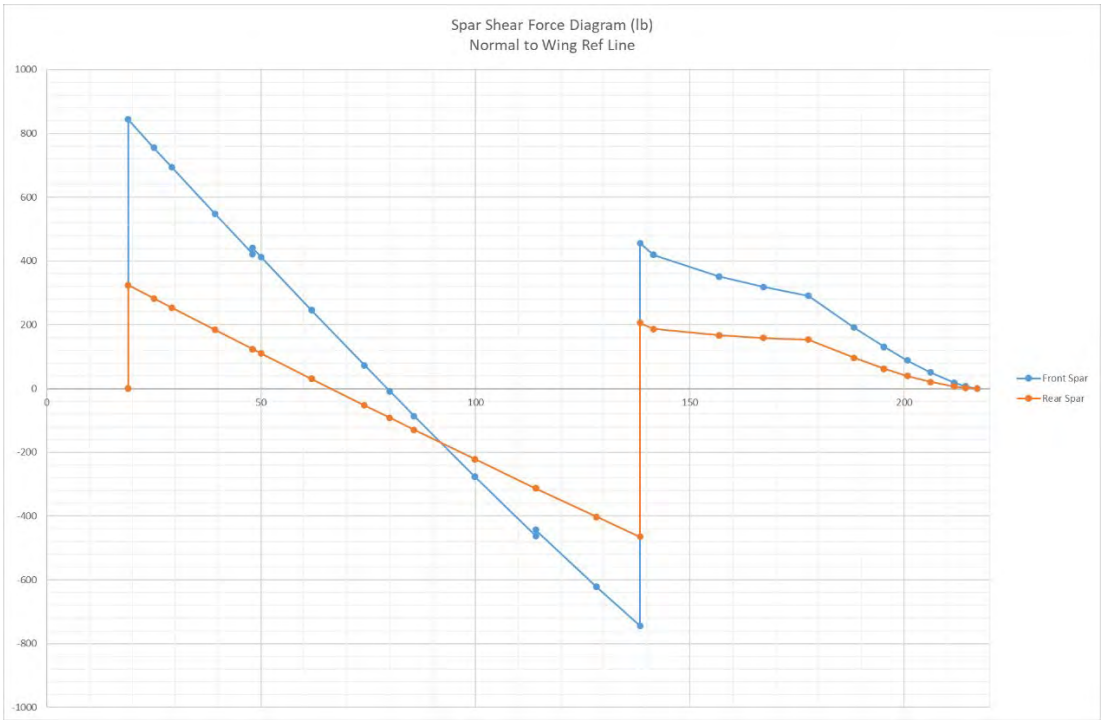

Figure 18-1 Spar Shear Force for 2205 lb at 106 Knots and 3.8 g

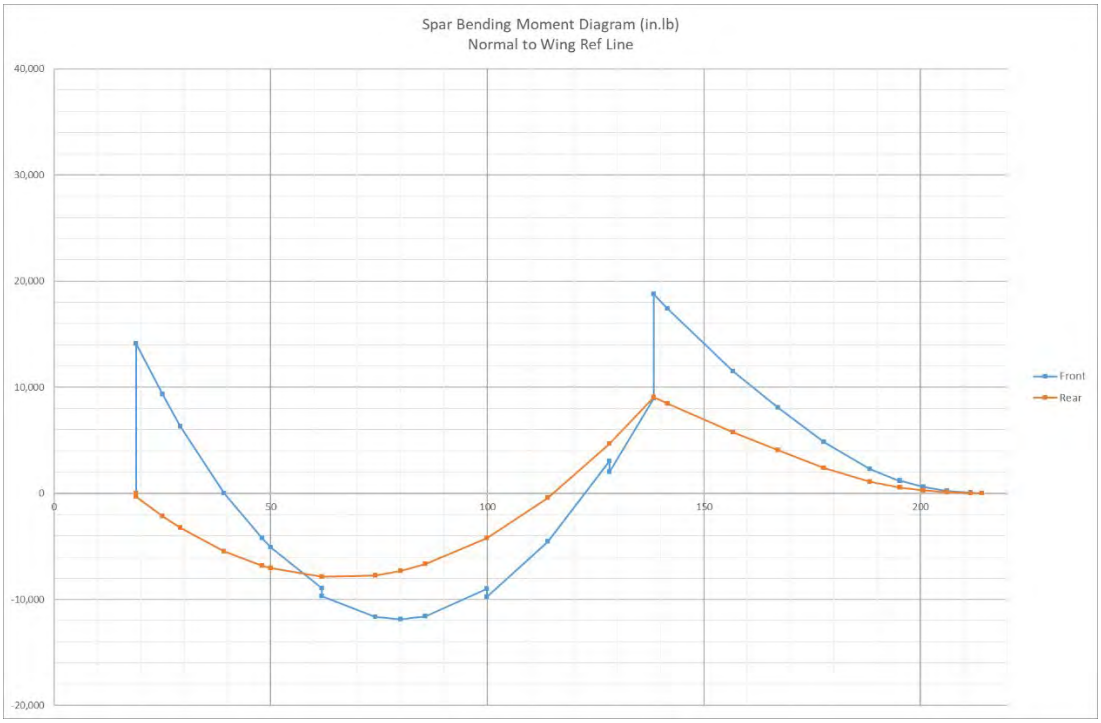

Figure 18-2 Spar Bending for 2205 lb at 106 Knots and 3.8 g

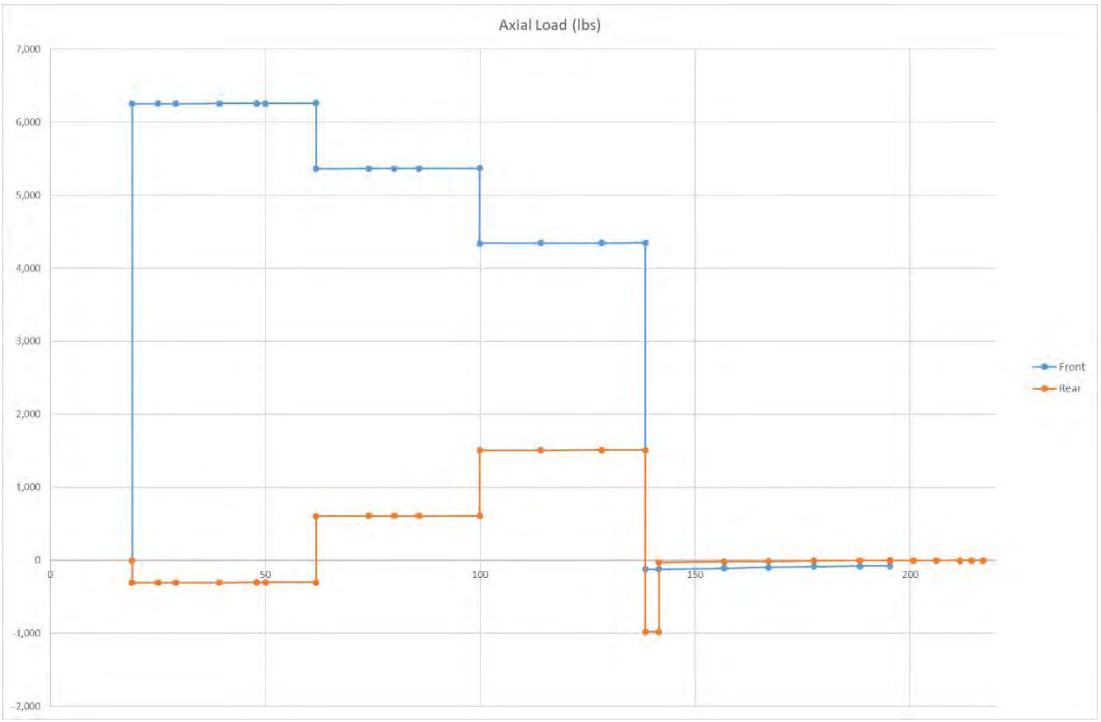

Figure 18-3 Spar Axial Loads for 2206 lb at 106 Knots and 3.8 g

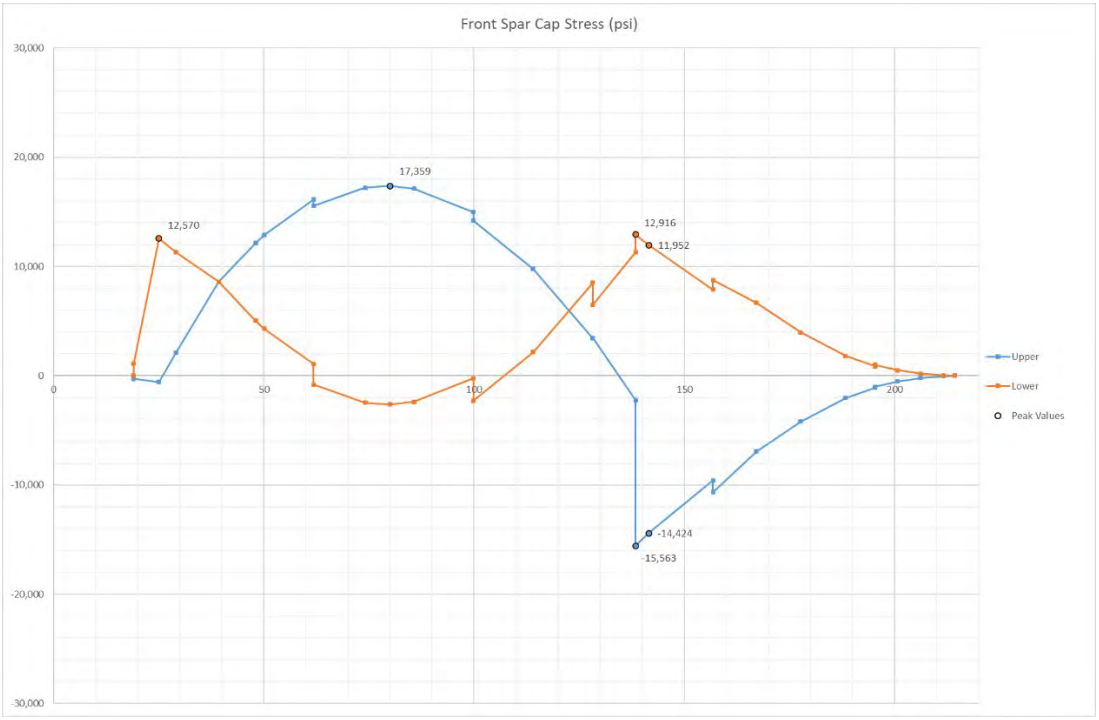

Figure 18-4 Front Spar Cap Stress for 2205 lb at 106 Knots and 3.8 g

18.2 **Load Case: 2205 lb at 114 knots and 27.1 ft/sec gust**. This is the single seat glider towing comparative gust case.

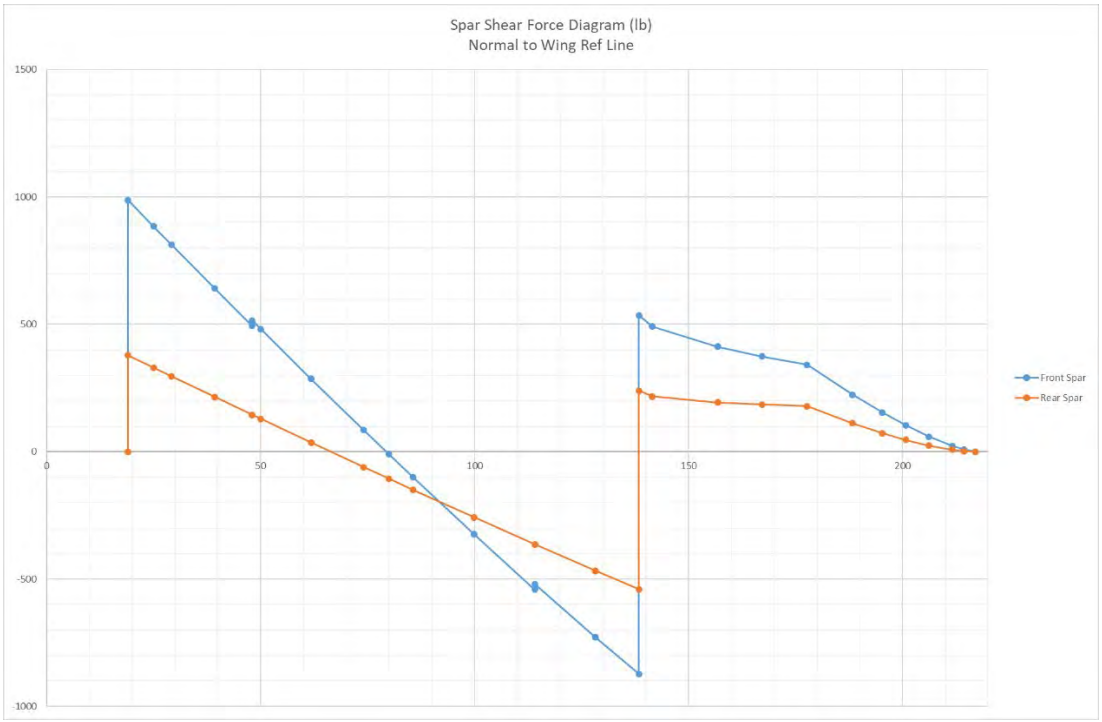

Figure 18-5 Spar Shear Force for 2205 lb at 114 knots and 27.1 ft/sec gust

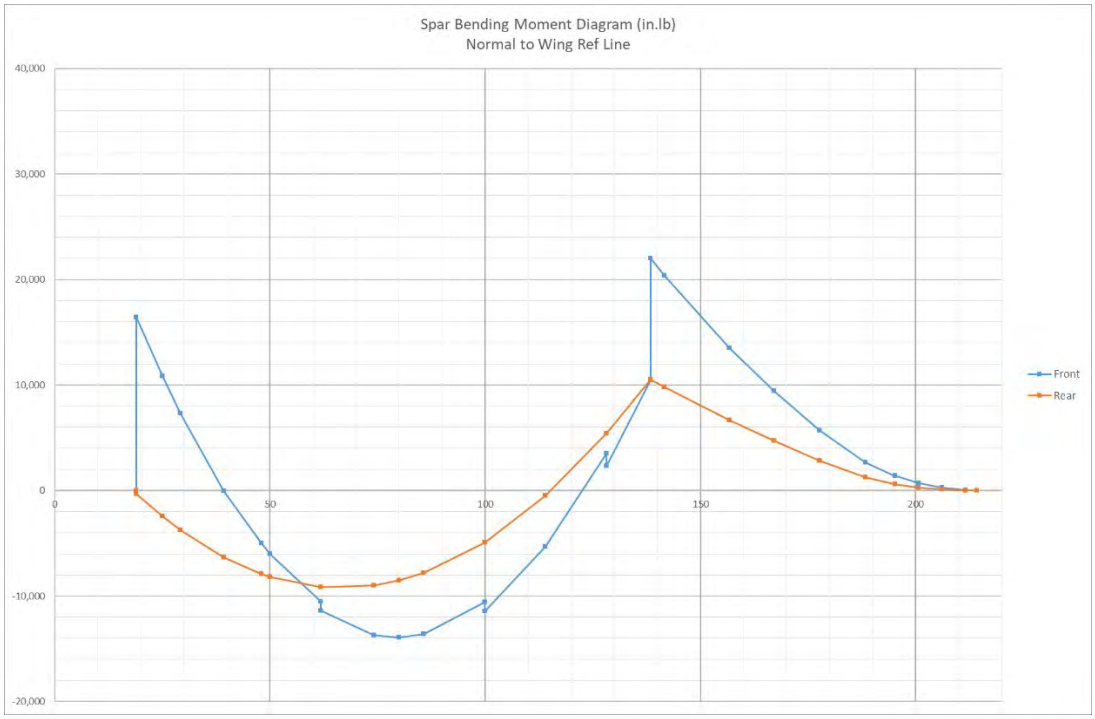

Figure 18-6 Spar Bending for 2205 lb at 114 knots and 27.1 ft/sec gust

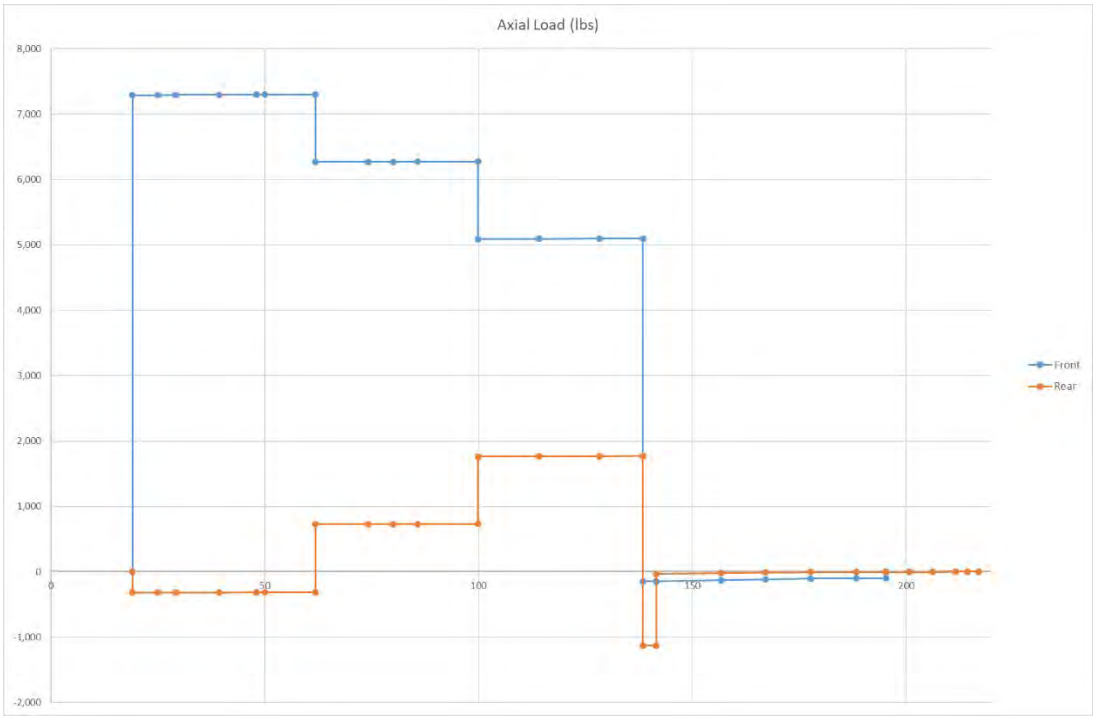

Figure 18-7 Spar Axial Loads for 2205 lb at 114 knots and 27.1 ft/sec gust g

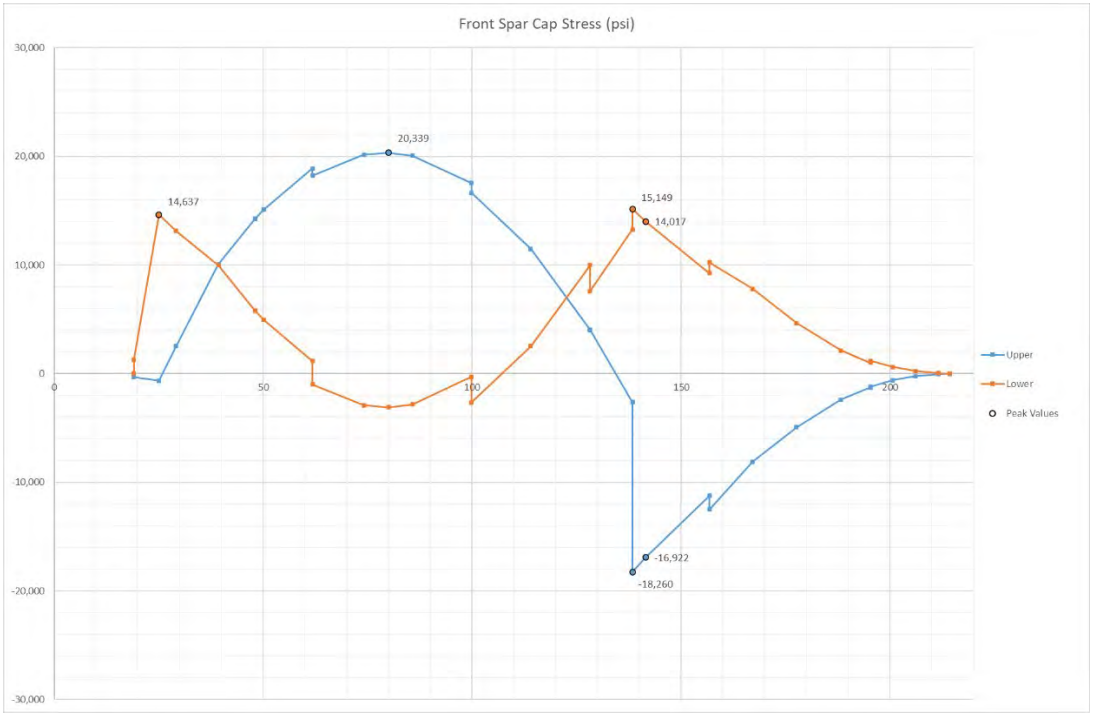

Figure 18-8 Front Spar Cap Stress for 2205 lb at 114 knots and 27.1 ft/sec gust

18.3 **Load Case: 2205 lb at 150 knots and 3.8 g**. This is the single seat glider towing comparative case to the agricultural 2900 lb at 150 kts and 3.8 g.

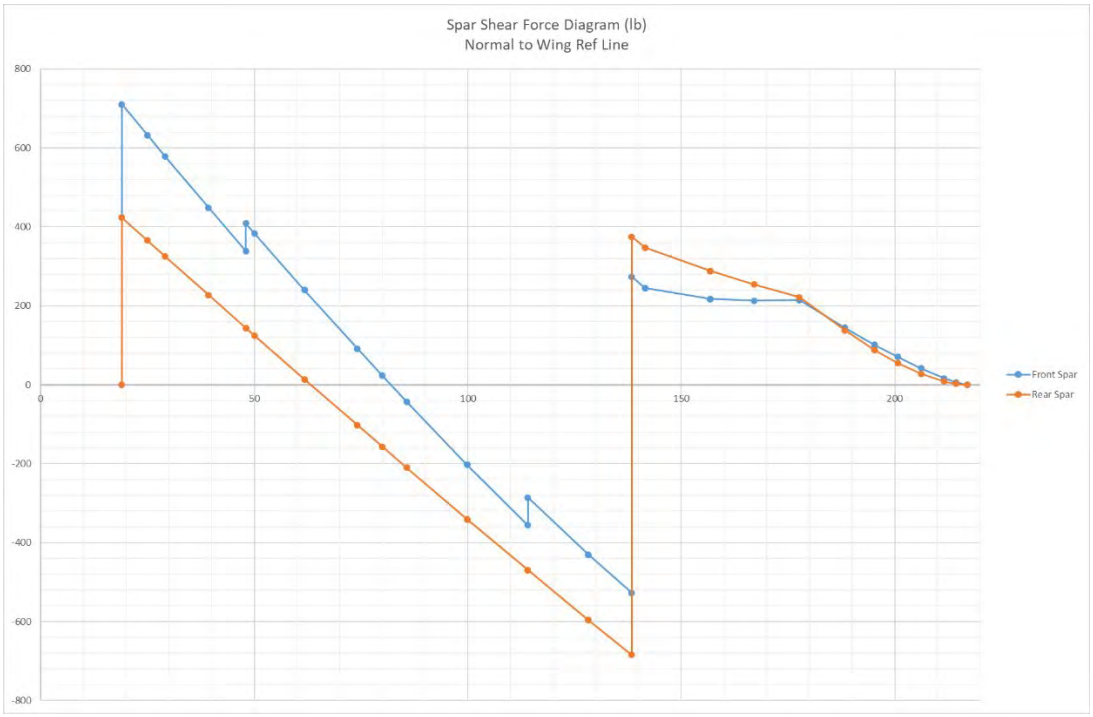

Figure 18-9 Spar Shear Force for 2205 lb at 150 Knots and 3.8 g

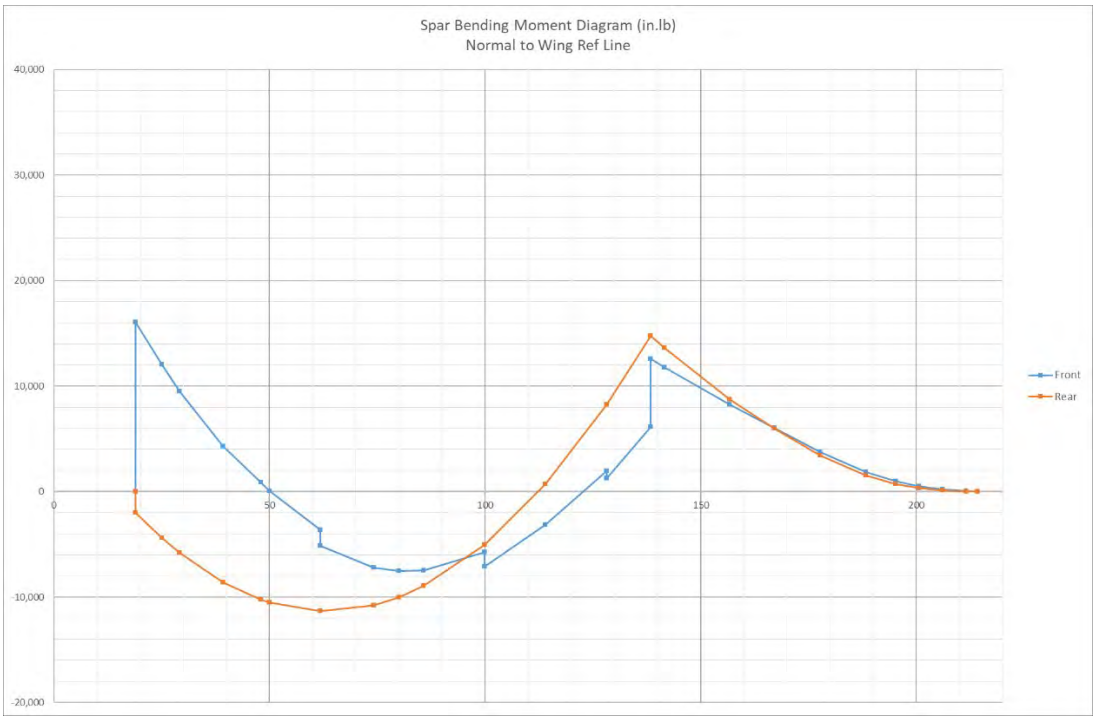

Figure 18-10 Spar Bending for 2205 lb at 150 Knots and 3.8 g

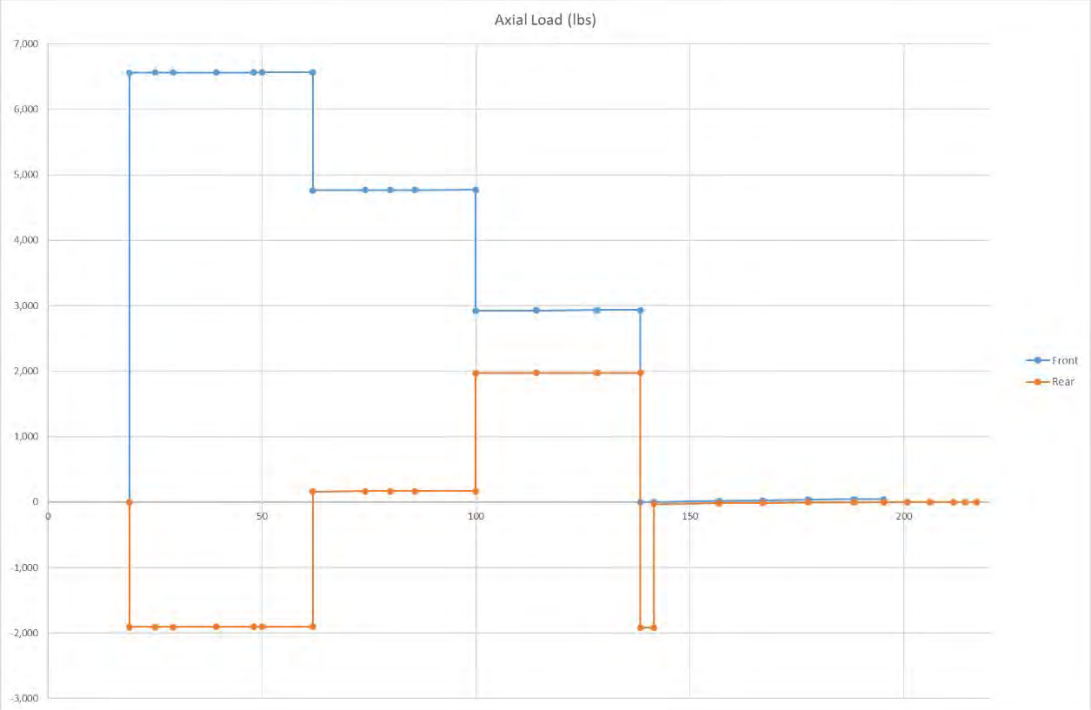

Figure 18-11 Spar Axial Loads for 2205 lb at 150 Knots and 3.8 g

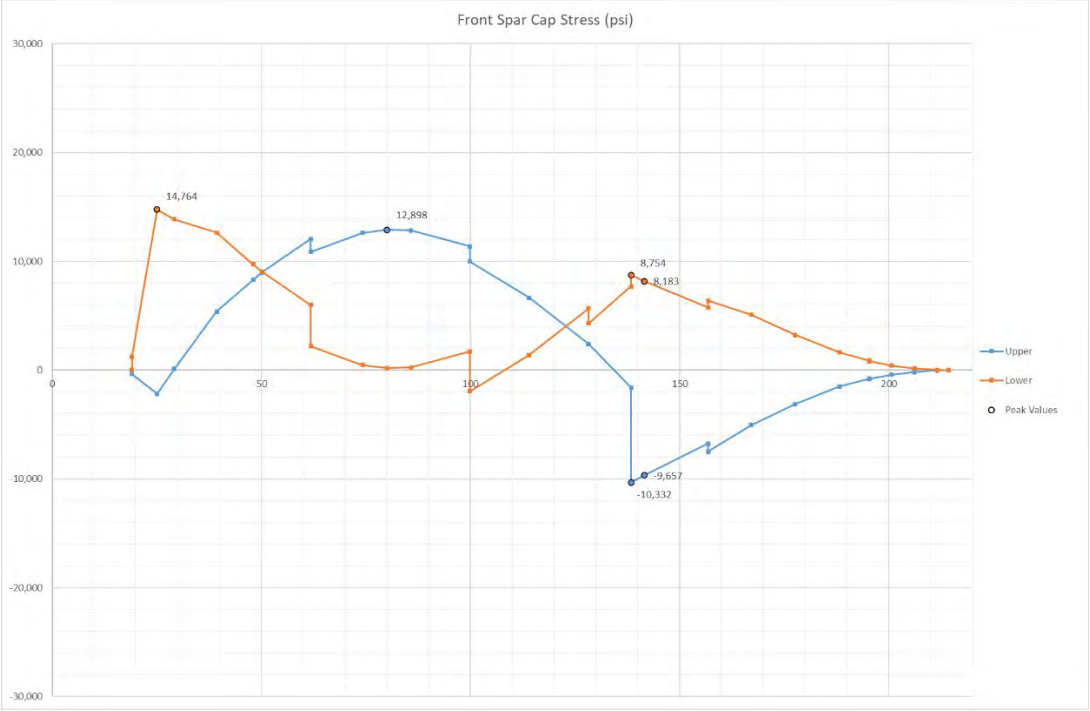

Figure 18-12 Front Spar Cap Stress for 2205 lb at 150 Knots and 3.8 g

18.4 **Load Case: 2460 lb at 112 knots and 3.8 g**. This is the dual seat aerotow comparative case to the agricultural 2900 lb at 121 kts and 3.8 g.

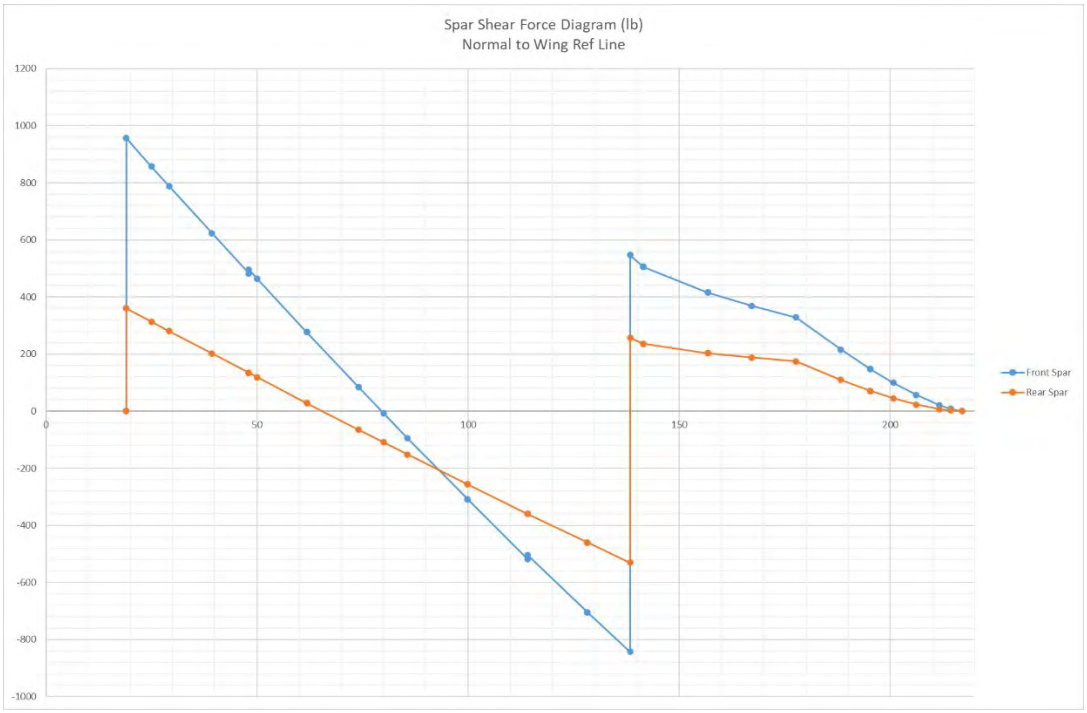

Figure 18-13 Spar Shear Force for 2460 lb at 112 Knots and 3.8 g

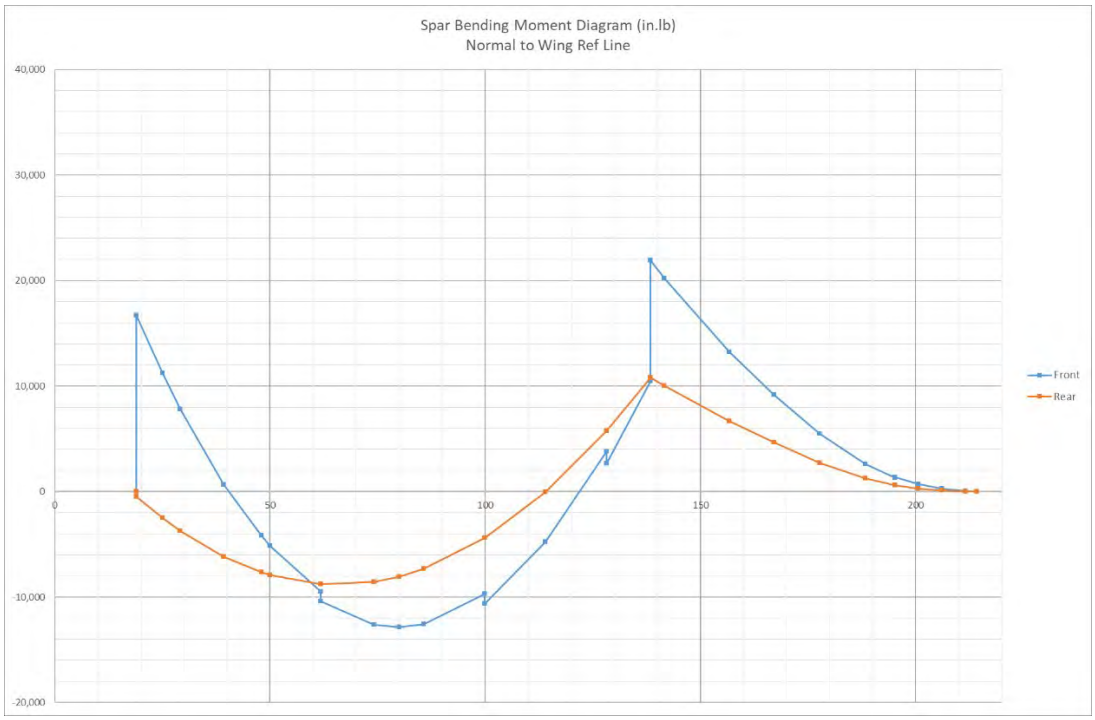

Figure 18-14 Spar Bending for 2460 lb at 112 Knots and 3.8 g

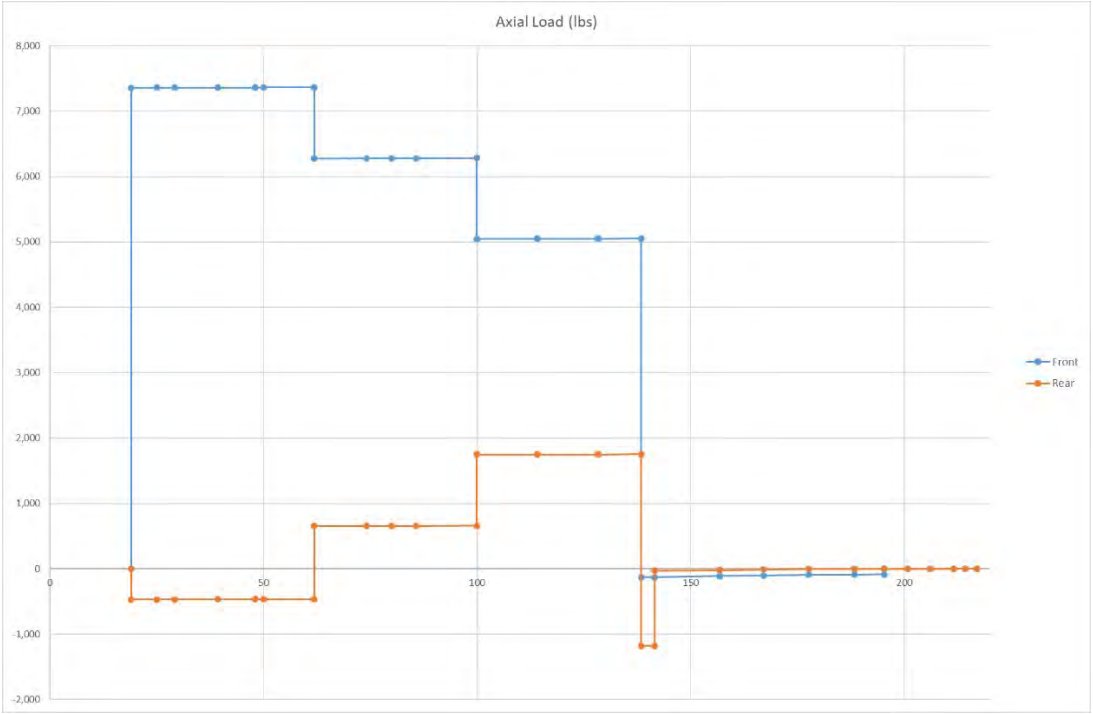

Figure 18-15 Spar Axial Loads for 2460 lb at 112 Knots and 3.8 g

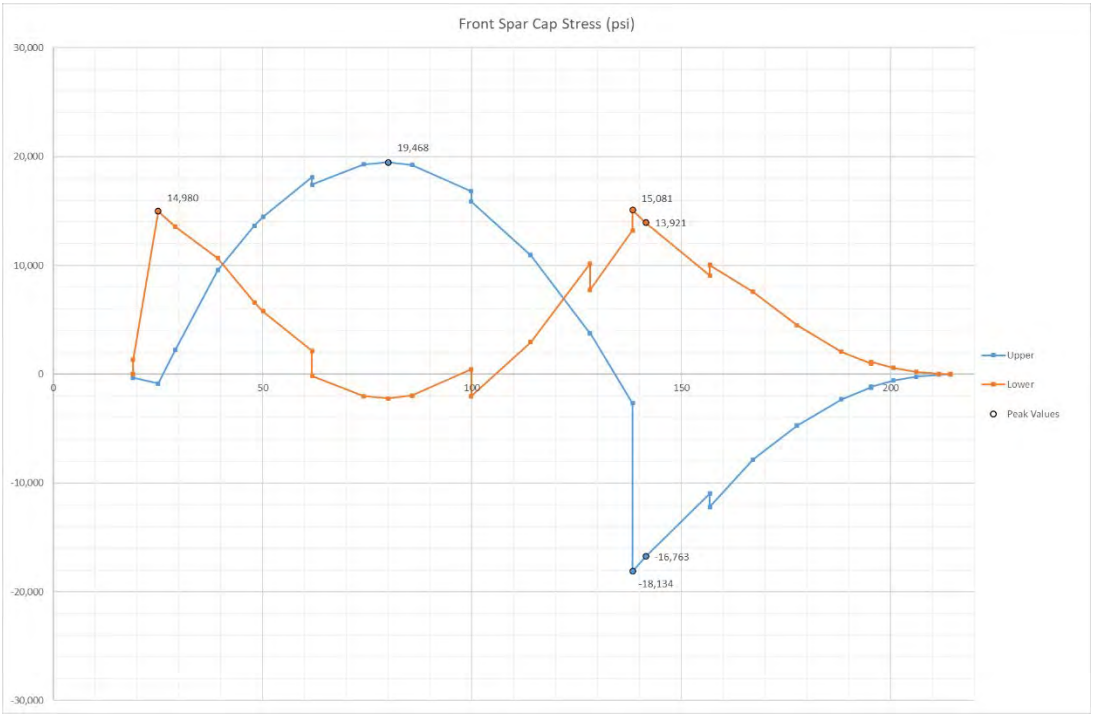

Figure 18-16 Front Spar Cap Stress for 2460 lb at 112 Knots and 3.8 g

18.5 **Load Case: 2460 lb at 116 knots and 26.2 ft/sec gust**. This is the dual seat aerotow comparative gust case.

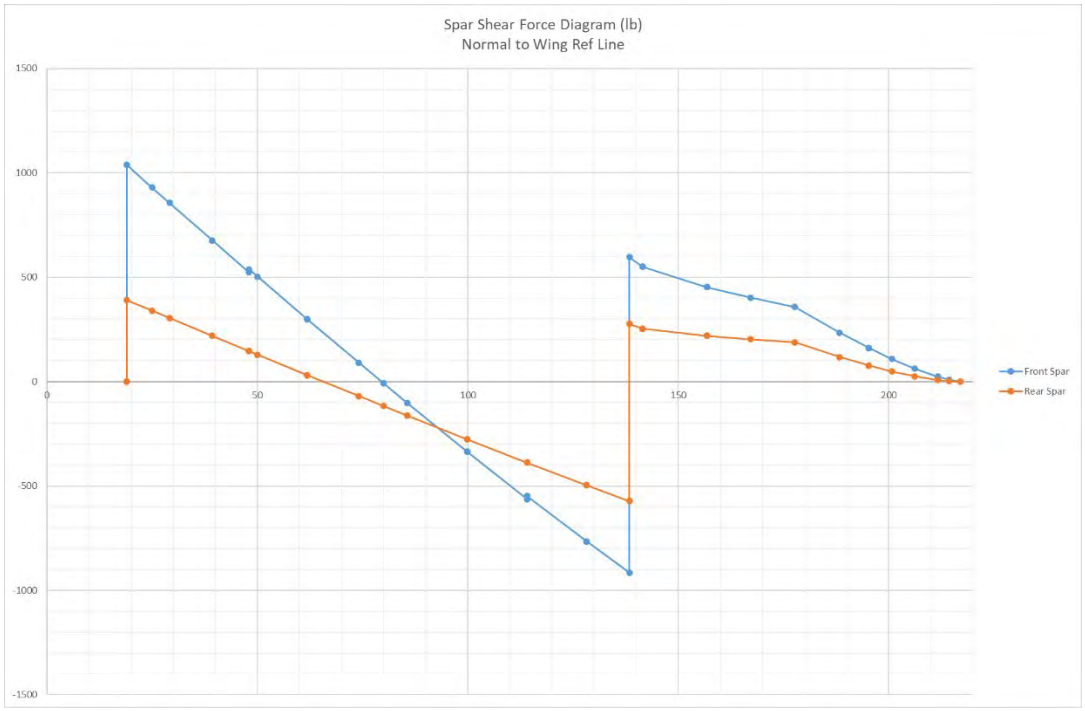

Figure 18-17 Spar Shear Force for 2460 lb at 116 Knots and 26.2 ft/sec gust

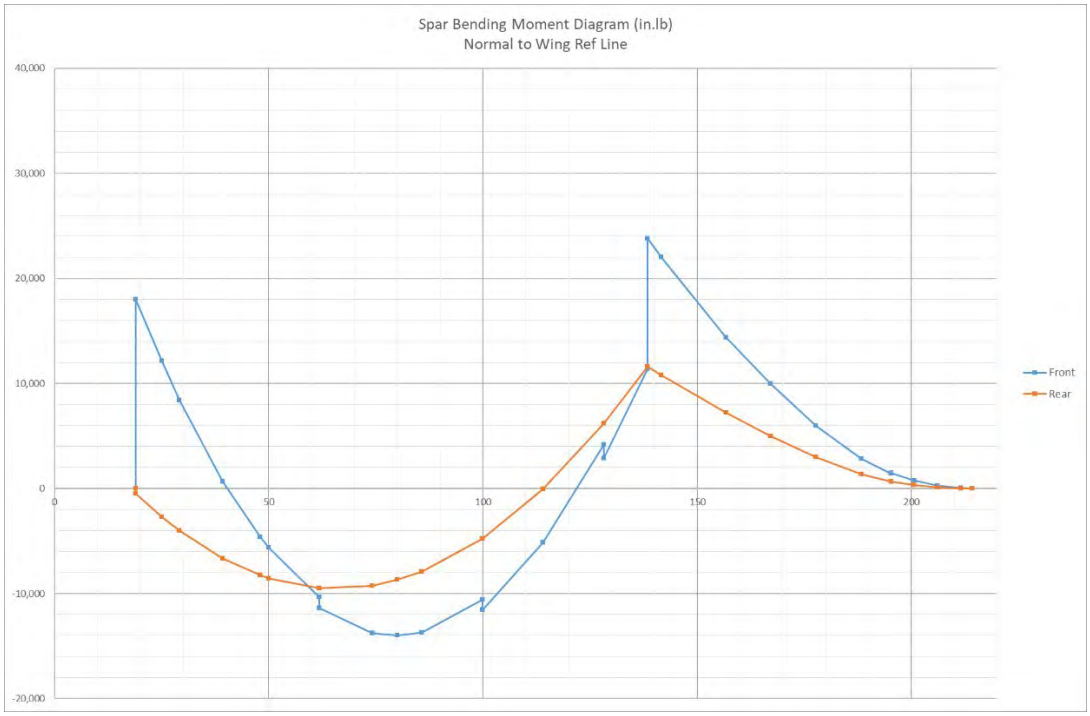

Figure 18-18 Spar Bending Moment for 2460 lb at 116 Knots and 26.2 ft/sec gust

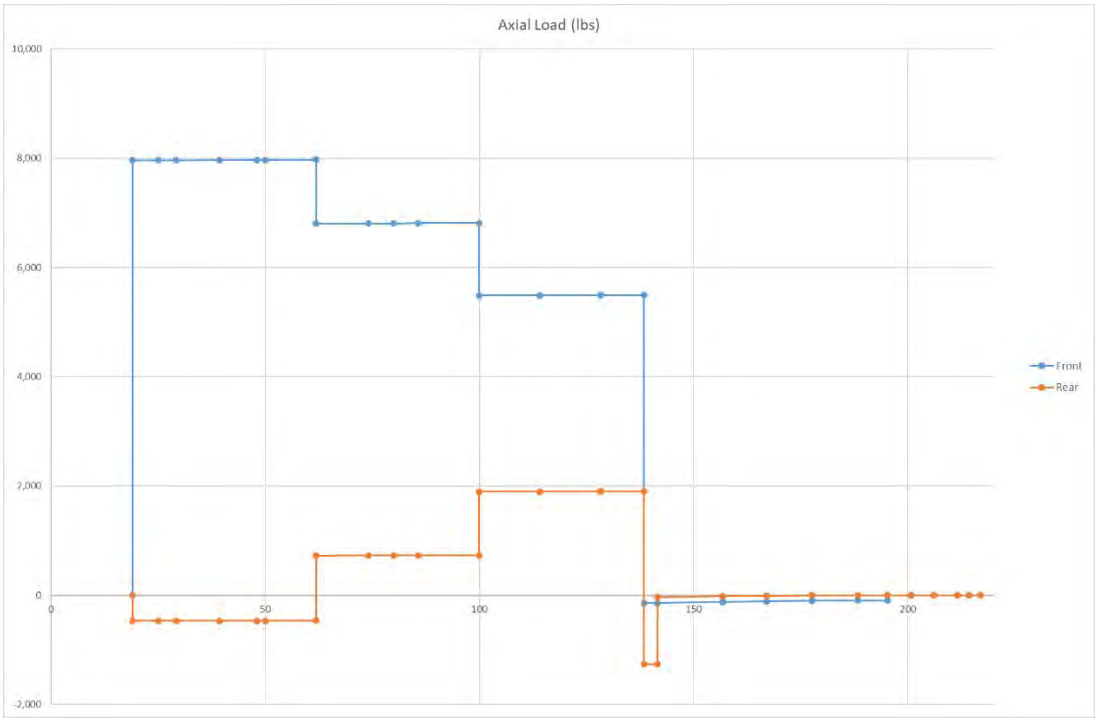

Figure 18-19 Spar Axial Loads for 2460 lb at 116 Knots and 26.2 ft/sec gust

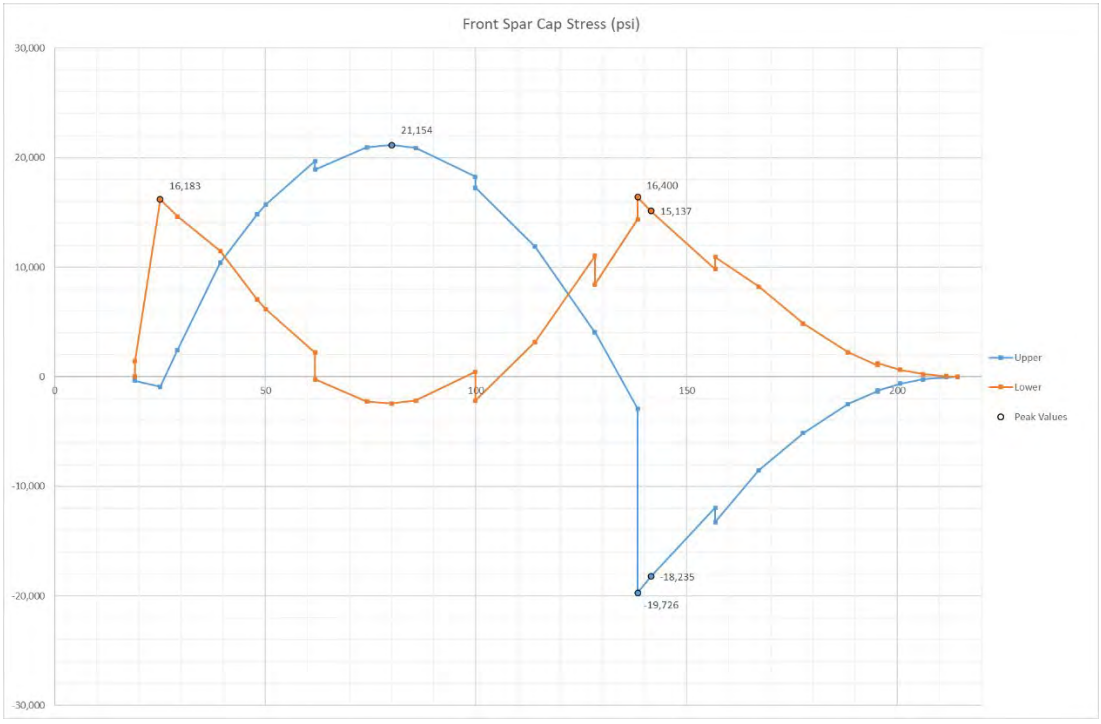

Figure 18-20 Front Spar Cap Stress for 2260 lb at 115 Knots and 26.8 ft/sec gust

18.6 **Load Case: 2460 lb at 150 knots and 3.8 g**. This is the dual seat aerotow comparative case to the agricultural 2900 lb at 121 kts and 3.8 g.

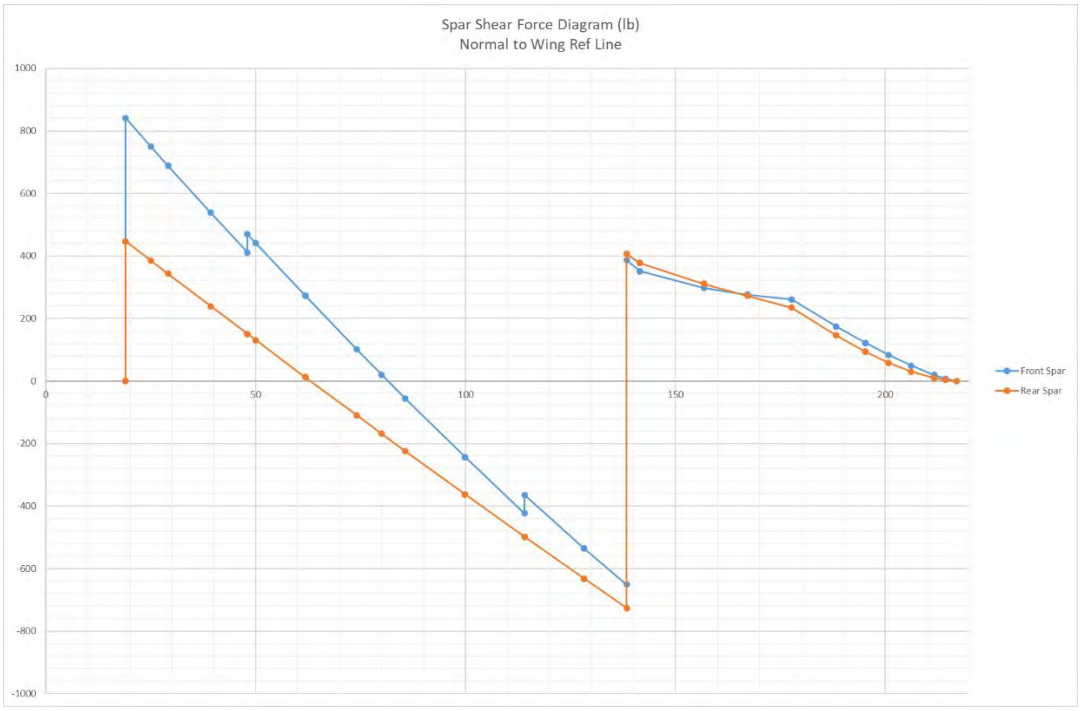

Figure 18-21 Spar Shear Force for 2460 lb at 150 Knots and 3.8 g

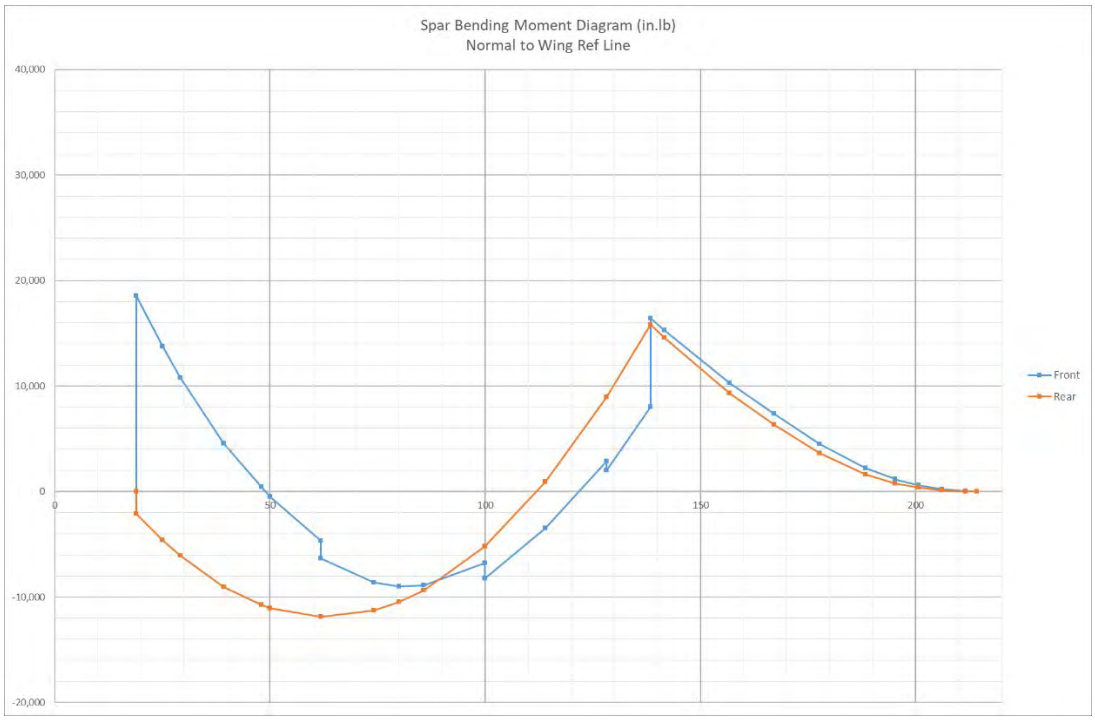

Figure 18-22 Spar Bending Moments for 2460 lb at 150 Knots and 3.8 g

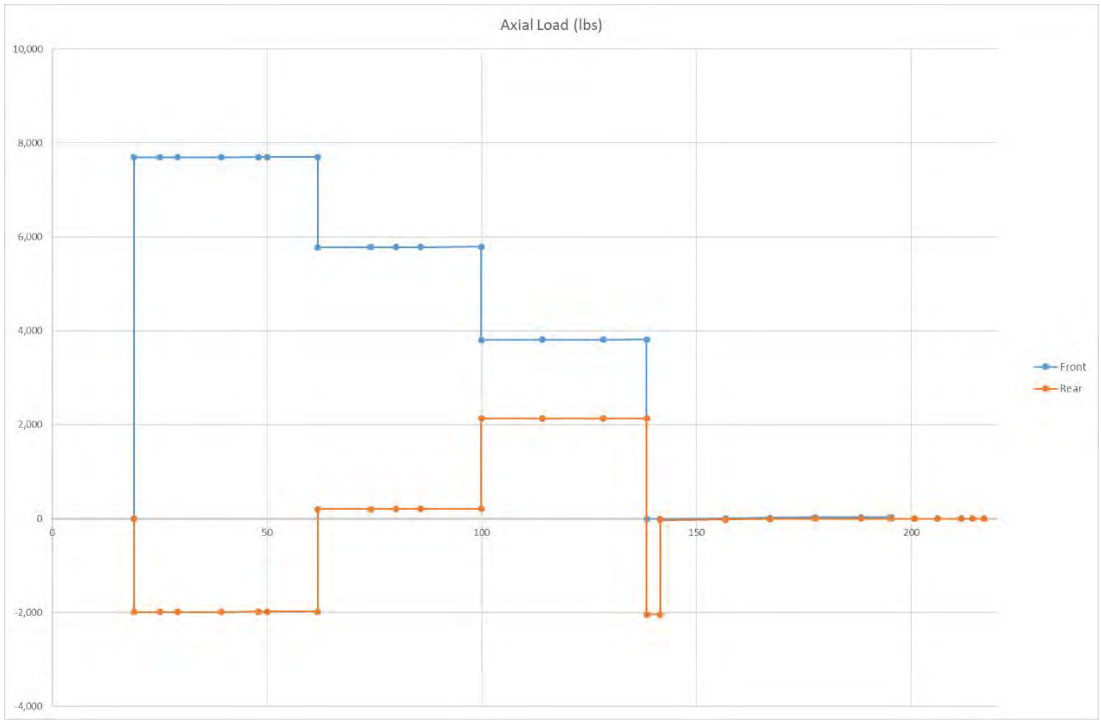

Figure 18-23 Spar Axial Loads for 2460 lb at 150 Knots and 3.8 g

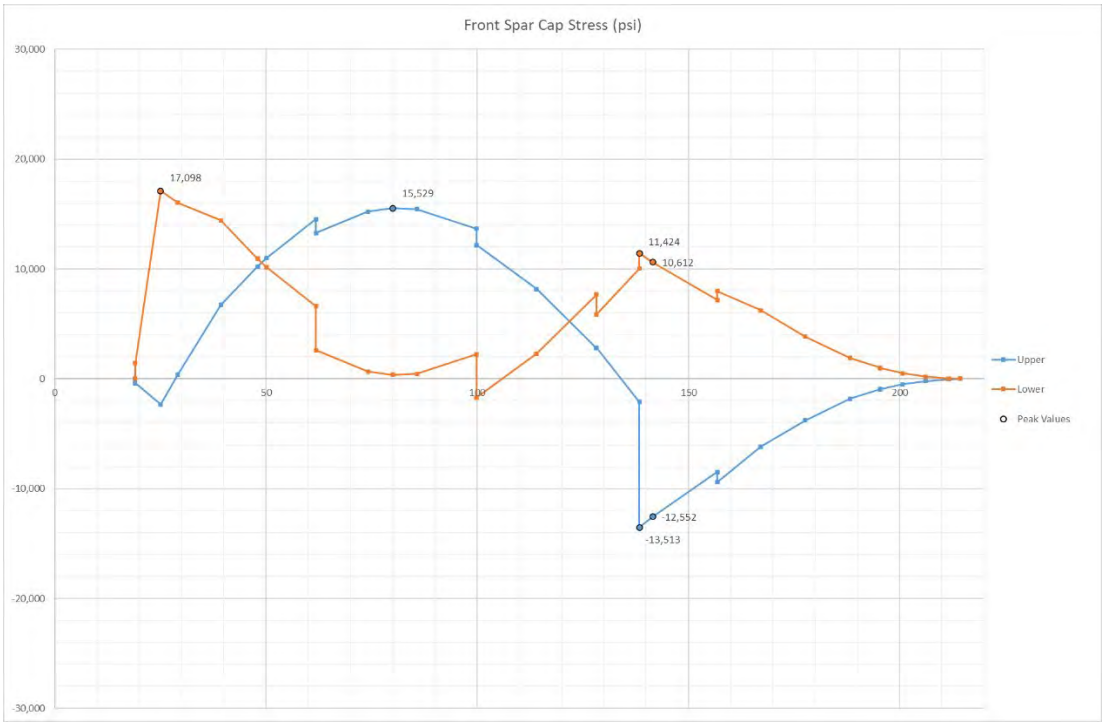

Figure 18-24 Front Spar Cap Stresses for 2260 lb at 150 Knots and 3.8 g